



**US Army Corps
of Engineers**
Waterways Experiment
Station

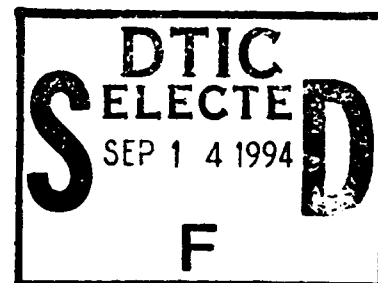
Contract Report HL-94-2
August 1994

AD-A284 394



Three-Dimensional Numerical Simulation of Mobile-Bed Hydrodynamics

*by Miodrag Spasojevic, Forrest M. Holly, Jr.,
Iowa Institute of Hydraulic Research*



Approved For Public Release; Distribution Is Unlimited

1670x

94-29807



DTIC QUALITY INSPECTED 3

94 9 13 098

Prepared for U.S. Army Engineer District, New Orleans

Three-Dimensional Numerical Simulation of Mobile-Bed Hydrodynamics

by Miodrag Spasojevic, Forrest M. Holly, Jr.

Iowa Institute of Hydraulic Research
The University of Iowa
Iowa City, IA 52242

Accession For	
NTIS CRA&I	<input checked="" type="checkbox"/>
DTIC TAB	<input type="checkbox"/>
Unannounced	<input type="checkbox"/>
Justification	
By	
Distribution /	
Availability Codes	
Dist	Avail and/or Special
A-1	

Final report

Approved for public release; distribution is unlimited

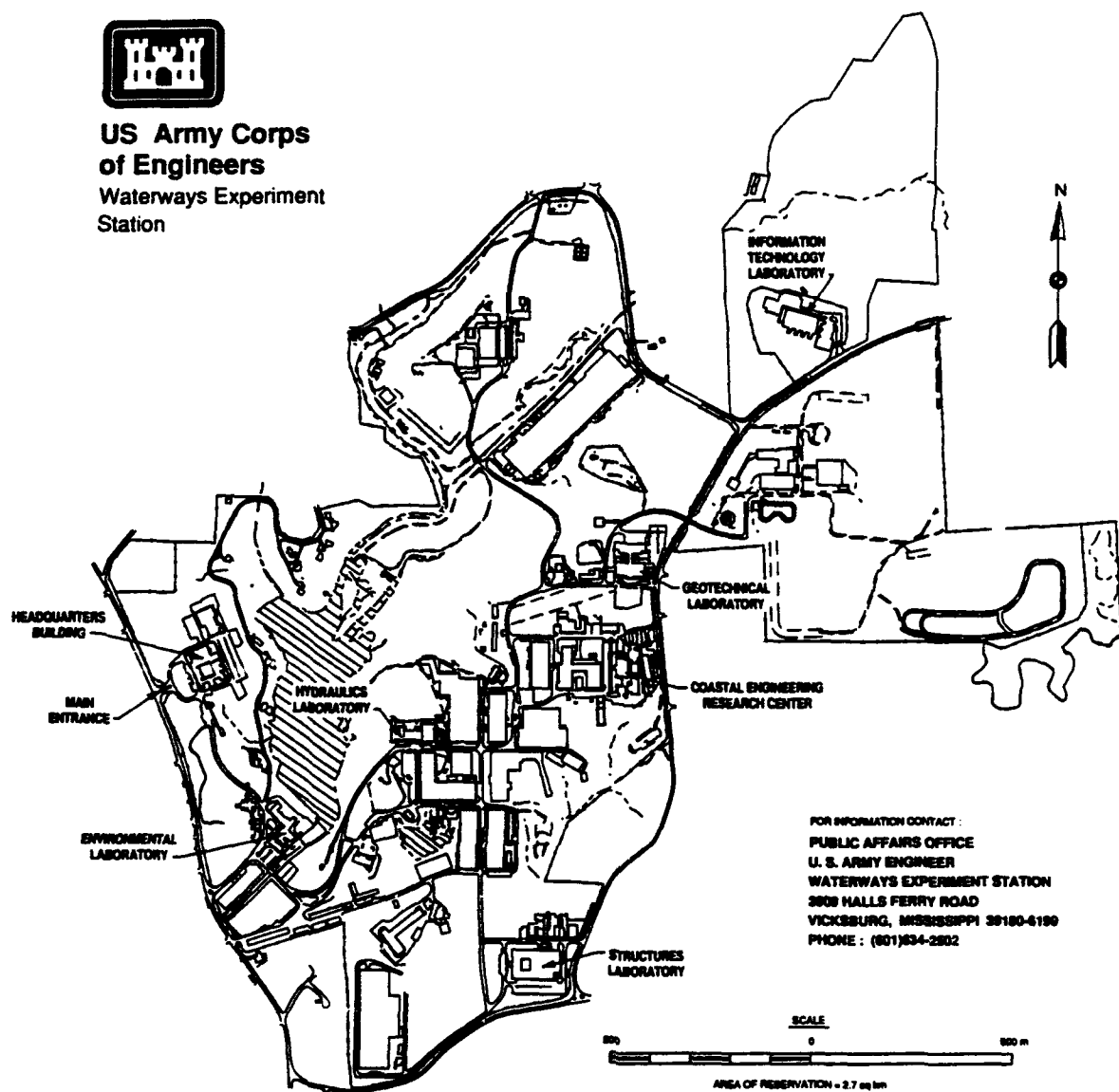
DTIC QUALITY INSPECTED 3

Prepared for U.S. Army Engineer District, New Orleans
P.O. Box 60267
New Orleans, LA 70160-0267

Monitored by U.S. Army Engineer Waterways Experiment Station
3909 Halls Ferry Road
Vicksburg, MS 39180-6199



**US Army Corps
of Engineers**
Waterways Experiment
Station



Waterways Experiment Station Cataloging-in-Publication Data

Spasojevic, Miodrag.

Three-dimensional numerical simulation of mobile-bed hydrodynamics/by Miodrag Spasojevic, Forrest M. Holly, Jr. ; prepared for U.S. Army Engineer District, New Orleans ; monitored by U.S. Army Engineer Waterways Experiment Station.

163 p. : ill. ; 28 cm. -- (Contract report ; HL-94-2)

Includes bibliographical references.

1. Sediment transport -- Mathematical models. 2. Bed load -- Measurement -- Simulation methods. 3. Suspended sediments -- Mathematical models -- Data processing. 4. CH3D-WES (Computer program) I. Holly, Forrest M. II. United States. Army. Corps of Engineers. New Orleans District. III. U.S. Army Engineer Waterways Experiment Station. IV. Hydraulics Laboratory (U.S.) V. Title. VI. Series: Contract report (U.S. Army Engineer Waterways Experiment Station) ; HL-94-2. TA7 W34c no.HL-94-2

Contents

Preface	v
Chapter I: Introduction	1
Chapter II: Governing Equations	4
Chapter III: Numerical Solution	19
Chapter IV: Description of the Sediment-Operations Program Module	40
Chapter V: Tests	56
Chapter VI: Conclusions and Suggestions for Further Development	69
References	71
Appendix A: Quickest Method	73
Appendix B: Discretized Mass-Conservation Equation for Suspended Sediment	89
Appendix C: Coefficients in Discretized Global Mass-Conservation Equation for Bed Sediment and Mass-Conservation Equations for Active-Layer Sediment	133
Appendix D: CH3D Input Data Guide (May 1992)	135
Appendix E: Model of the Mississippi River at the Old River Sample Input-Data Set	156

SF 298

List of Figures

Figure 1.	Schematic representation of bed-material finite elemental volume	4
Figure 2.	Stratum control volumes below active-layer elemental volume	6
Figure 3.	Coordinate transformations	14
Figure 4.	Computational grid	22
Figure 5.	Summary block diagram of sediment-operations program module	41
Figure 6.	Mississippi River at the Old River Control Structure complex: location map	58
Figure 7.	The model domain and computational grid	60
Figure 8.	Vertical concentration profiles for size class 2 at the model upstream boundary	62

Preface

This project was sponsored by the U.S. Army Engineer District, New Orleans, under Contract No. DACW39-91-K-0025. The study was conducted from August 1991 to December 1993 at the Iowa Institute of Hydraulic Research (IIHR), University of Iowa, Iowa City. The contract was monitored by the Hydraulics Laboratory (HL), U.S. Army Engineer Waterways Experiment Station (WES). Contracting Officer's Representative was Mr. Brad R. Hall, Math Modeling Branch, Waterways Division, HL.

Principal investigators were Drs. Miodrag Spasojevic and Forrest M. Holly, Jr., IIHR. The project benefitted from close collaboration and consultation with many individuals at HL. The support of Messrs. Michael J. Trawle, David D. Abraham, Ronald E. Heath, and Mr. Hall, all of the Math Modeling Branch, Dr. Billy H. Johnson, HL, and Dr. Kue W. Kim, Estuarine Simulation Branch, Estuaries Division, HL, was particularly appreciated. Special thanks go to Mrs. Twila Meder, IIHR, for her conscientious entry of the many equations in this report. This report was written by Drs. Spasojevic and Holly.

This project was conducted under the general supervision of Messrs. Frank A. Herrmann, Jr., Director, HL; Richard A. Sager, Assistant Director, HL; Marden B. Boyd, Chief, Waterways Division; and Mr. Trawle, Chief, Math Modeling Branch.

At the time of publication of this report, Director of WES was Dr. Robert W. Whalin. Commander was COL Bruce K. Howard, EN.

The contents of this report are not to be used for advertising, publication, or promotional purposes. Citation of trade names does not constitute an official endorsement or approval of the use of such commercial products.

CHAPTER I

INTRODUCTION

The objective of this research is to generalize innovative two-dimensional mobile-bed modelling techniques, recently developed at the Iowa Institute of Hydraulic Research, and to merge these techniques with the CH3D three-dimensional hydrodynamic simulation code, thus generalizing CH3D to include mobile-bed processes (such as aggradation and scour, bed-material sorting, and movement of both bedload and suspended load of nonuniform sediment mixtures).¹

During the past several years research efforts at the Iowa Institute of Hydraulic Research (IIHR) have been devoted to development of a new generation of two-dimensional mobile-bed modelling. The distinguishing technical features of this new generation include the following features:

1. - The fact that the same sediment particle can move either in suspension or as bedload, depending on local flow conditions, is explicitly recognized. This removes the need to assume any specific transport mode in advance.
2. - Criteria for distinguishing between bedload and suspended-sediment transport, as well as mechanisms defining exchange between the two, are incorporated.
3. - A sediment mixture in a natural watercourse is represented through a suitable number of size classes (with most mathematical relations for sediment written for a particular size class).
4. - The global set of sediment equations for all size classes, taken as a whole and solved simultaneously, describes the behavior of a nonuniform sediment, including natural phenomena such as differential settling, armoring and hydraulic sorting.
5. - The governing sediment equations have a clear analytical form which provides for the possibility to analyze their mathematical character and choose proper boundary conditions as well as the most appropriate numerical solution for each of them.
6. - The procedure directly accounts for the effects of change in the sediment size distribution at the bed surface, and change in bed elevation, on the flow field through iterative coupling of the water and sediment equations.

¹ The numerical model referred to in this report as CH3D was developed from the CH3D-WES numerical model developed at the U.S. Army Engineer Waterways Experiment Station as described in Johnson, B. H., et al. (1991). "User's guide for a three-dimensional numerical hydrodynamic, salinity, and temperature model of Chesapeake Bay," Technical Report HL-91-20, U.S. Army Engineer Waterways Experiment Station, Vicksburg, MS.

7. - The tensor form of the governing water and sediment equations is written for an orthogonal curvilinear system, permitting ready representation of the boundaries of natural watercourses.
8. - The new concept of sediment-transport and bed-evolution processes is inspired by current qualitative understanding of particular aspects of sediment-flow interaction. The derived sediment equations contain several so-called auxiliary relations - terms that need to be evaluated by using empirical relations. However, the global concept and its associated numerical solution are structured so as to avoid use of any particular empirical relation until the very end of the derivations. Therefore, the overall structure of the new computational procedures remains independent of particular empirical expressions used to evaluate the auxiliary relations.

These features, taken together, have made it possible to perform two-dimensional mobile-bed simulation which is not subject to many of the traditional limitations, and which incorporates a more realistic conceptualization of the governing physics than has heretofore been possible. The proven hydrodynamic framework of the CH3D code for unsteady, three-dimensional fixed-bed simulation provides an opportunity to implement the above mobile-bed concepts in the three-dimensional environment.

Generalization of the IHR two-dimensional mobile-bed modelling techniques, in preparation for their implementation in CH3D, means not only performing a three-dimensional generalization of the governing sediment equations, but also ensuring their compatibility with the overall CH3D environment. Generalization thus comprises the following specific tasks:

1. - Redefine the governing sediment equations in vector form and in standard Cartesian coordinates. For example, compatibility with the CH3D environment requires that the non-constant density of the water-sediment mixture be taken into account; that the three-dimensional suspended-sediment equation include a 'fall-velocity' term; that mechanisms for exchange between bed sediment and suspended sediment be redefined; and that several new auxiliary relations be introduced (e.g. mass-diffusion coefficient, density of a mixture containing water and suspended sediment); etc.
2. - Rederive the governing sediment equations in σ -stretched coordinates (partial coordinate transformation in the vertical direction).
3. - Nondimensionalize the governing sediment equations.
4. - Rederive the dimensionless sediment equations in general (nonorthogonal) horizontal curvilinear coordinates.

It does not appear to be necessary to anticipate direct coupling of the hydrodynamic and sediment processes in CH3D. The partial explicitness of CH3D precludes the use of large time steps at the present stage of development, so that the error involved in water-sediment uncoupling at the scale of one time step (the order of several minutes) is not judged to be serious. Furthermore, a small time step offers the possibility to couple suspended- and bed-sediment computations in an iterative manner.

One of the implications of short-term uncoupling of sediment and hydrodynamics operations is that a separate program module can be dedicated to the sediment operations. The implication of iterative coupling of the suspended-sediment and bed-sediment operations is that different numerical methods can be used for, and separate program submodules dedicated to, the suspended-sediment and bed-sediment computations.

Numerical solution of the suspended-sediment equations is based upon the QUICKEST numerical method (Leonard (1979)), in order to ensure compatibility with the existing CH3D salinity and temperature computations. The original QUICKEST method is generalized to accommodate the appropriate terms in the three-dimensional suspended-sediment equation in general curvilinear coordinates.

Numerical procedures for the bed-sediment equations are based on the previously-developed two-dimensional numerical-solution algorithm for sediment equations. This original IIHR two-dimensional solution was developed for both suspended- and bed-sediment operations (depth-averaged) expressed in dimensional equations in orthogonal curvilinear coordinates. The IIHR method is redefined herein to be used for bed-sediment operations only, in the context of dimensionless equations in general curvilinear coordinates.

Even though they are contained in a separate program module, the sediment-operations developed for CH3D fully communicate with the rest of the CH3D code. The hydrodynamics operations in CH3D provide all the necessary hydrodynamic input required by the sediment module (velocities, depths, etc.). The sediment module, in turn, communicates changes in bed elevations (i.e. depths), bed-surface size-distributions (i.e. friction coefficients) and density (due to the presence of suspended sediment) back to the CH3D hydrodynamics operations.

Detailed documentation of the coding and use of mobile-bed capability in CH3D is included herein, as well as results of tests performed on the Mississippi River near the Old River Control Structure complex.

CHAPTER II

GOVERNING EQUATIONS

Concept of Sediment Transport and Bed Evolution

The concept of sediment transport and bed evolution, and the appropriate mathematical formulation, described herein, accounts for the following important aspects of sediment-flow interaction in natural watercourses: suspended-sediment transport, bedload transport, and interaction between the two; bed level changes; differential settling; hydraulic sorting and armoring; interaction between the flow and changes in bed elevation and bed surface size distribution; and washload transport.

Bedload Transport and Bed Evolution

Since it is difficult to account for the exact position and size of each sediment particle being entrained from the bed or ending its trajectory at a certain spot on the bed surface (Fig. 1), a uniform size distribution is assumed inside a finite elemental area of bed surface. This elemental area must satisfy the condition that its dimension Δl is not less than the maximum average saltation length. If this requirement is satisfied, then the bedload flux (taken as parallel to the bed surface) represents bedload exchange between two neighboring elemental areas.

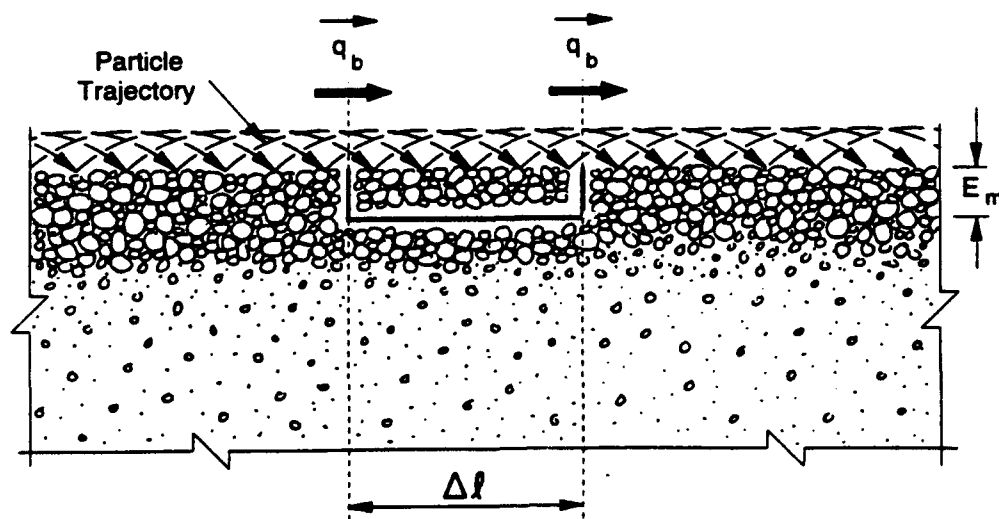


Figure 1. Schematic Representation of Bed-Material Finite Elemental Volume.

The notion of an active layer is introduced to obviate the need to account for the position and size of each sediment particle below the bed surface that may, during erosion, become exposed to the flow and become part of the bed surface. The active layer is defined as an upper layer of the bed, including the bed surface, having a uniform size distribution over its depth. It is assumed that all sediment particles of a given size class inside the active layer are equally exposed to the flow irrespective of their location in the layer.

A finite elemental volume ΔV is defined as having dimension Δl and a thickness E_m (Fig. 1). For a fixed active-layer floor elevation, the mass-conservation equation for one particular size class of sediment in the active-layer elemental volume is written as follows:

$$\rho_s(1-p) \frac{\partial(\beta E_m)}{\partial t} + \nabla \cdot \bar{q}_b + S_e - S_d = 0 \quad (1)$$

where p = porosity of the bed material, assumed to be constant; ρ_s = density of sediment, assumed to be constant; β = active-layer size fraction, defined as a ratio of the mass of particles of one particular size class inside the active-layer elemental volume ΔV to the mass $\rho_s(1-p)\Delta V$ of all sediment particles contained in ΔV ; S_e = suspended-sediment 'erosion' source, representing the entrainment of sediment particles from the bed into suspension; S_d = suspended-sediment 'deposition' source, representing gravitational settling of suspended sediment particles onto the bed.

Subsurface material below the active-layer elemental volume is discretized into a sequence of control volumes, one below the other, called herein stratum control volumes (Fig. 2). Each stratum control volume has the same dimension Δl as the active-layer elemental volume above it. The bed material inside one stratum control volume is assumed to have uniform size distribution.

The stratum control volume immediately below the active-layer elemental volume is called the active-stratum control volume. It is possible, indeed likely, that the active-layer elemental volume and active-stratum elemental volume have different size distributions. The active-layer floor, which is at the same time an active-stratum ceiling, descends or rises whenever the bed elevation changes due to deposition or erosion occurring in the active-layer elemental volume. If, for example, the active-layer floor descends, some of the material that belonged to the active-stratum control volume becomes part of the active-layer elemental volume, whose homogeneous size distribution thus may change.

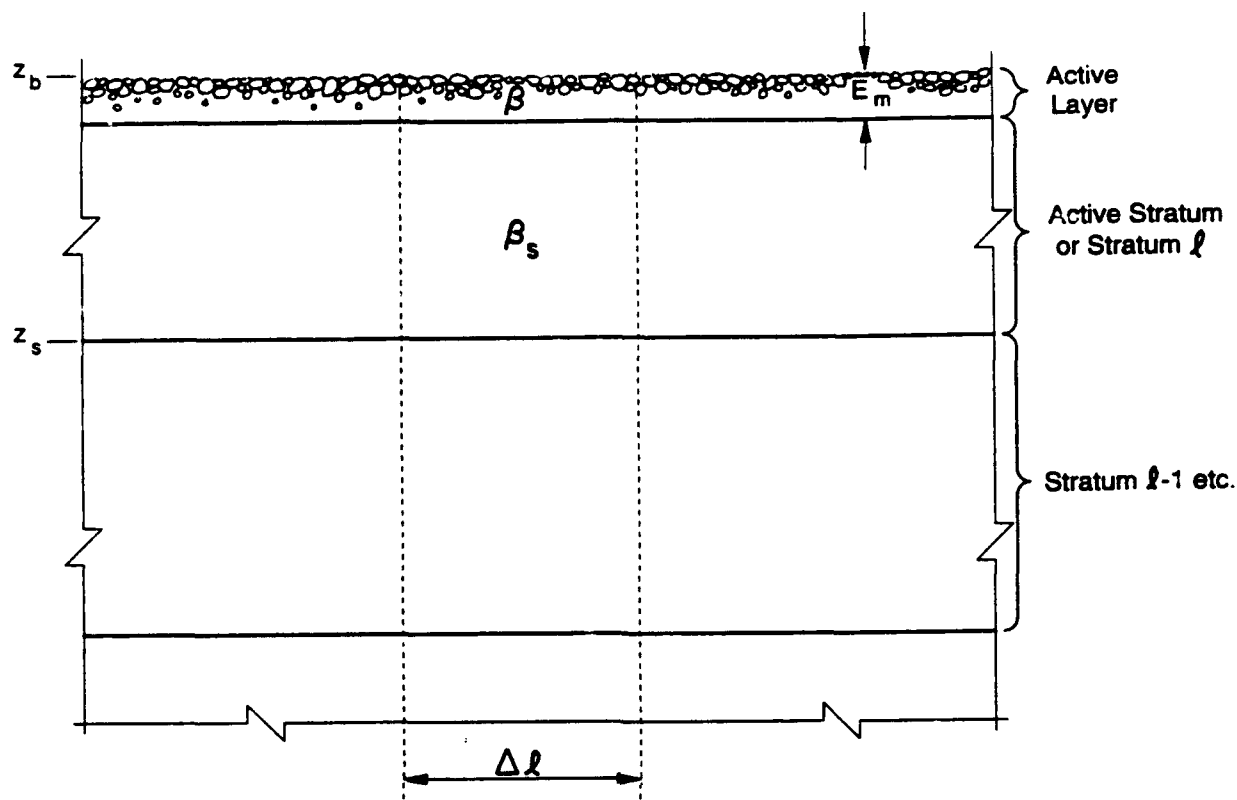


Figure 2. Stratum Control Volumes Below an Active-Layer Elemental Volume.

In order to represent the exchange of sediment particles between the active-layer elemental volume and the active-stratum control volume due to active-layer floor movement, another 'source' term is introduced, called herein the active-layer floor 'source' S_F , again specific to one particular size class of particles. The mass-conservation equation for a size class of sediment particles in the active-layer elemental volume then reads:

$$\rho_s(1-p)\frac{\partial(\beta E_m)}{\partial t} + \nabla \cdot \bar{q}_b + S_e - S_d - S_F = 0 \quad (2)$$

Since the bedload flux is a vector parallel to the bed surface, the vector Eq.(2) is essentially two-dimensional.

The mass of a particular size class in the active-stratum control volume may change only due to active-layer floor movement, i.e. due to exchange of material between the active layer and active stratum, while the active-stratum floor elevation remains unchanged. This is expressed by a mass-conservation equation written for each size class in the active-stratum control volume:

$$\rho_s(1-p) \frac{\partial}{\partial t} [\beta_s(z_b - E_m)] + S_F = 0 \quad (3)$$

where z_b = bed-surface level (bed elevation); β_s = active-stratum size fraction; and $(z_b - E_m)$ = active-layer floor elevation, i.e. active-stratum ceiling.

Summation of the mass-conservation equations for all size classes in the active-layer elemental volume and use of the basic constraint:

$$\Sigma \beta = 1 \quad (4)$$

where Σ represents summation over all size classes, leads to the global mass-conservation equation for the active-layer elemental volume:

$$\rho_s(1-p) \frac{\partial E_m}{\partial t} + \Sigma(\nabla \cdot \bar{q}_b + S_e - S_d - S_F) = 0 \quad (5)$$

A similar equation can be obtained for the active-stratum control volume:

$$\rho_s(1-p) \frac{\partial(z_b - E_m)}{\partial t} + \Sigma S_F = 0 \quad (6)$$

where again Eq.(4) is invoked. Summation of Eqs.(5) and (6) gives the global mass-conservation equation for bed sediment:

$$\rho_s(1-p) \frac{\partial Z_b}{\partial t} + \Sigma(\nabla \cdot \bar{q}_b + S_e - S_d) = 0 \quad (7)$$

which can be recognized as the familiar Exner equation with the addition of suspended-sediment source terms. This last equation is again essentially two-dimensional, for the bedload-flux vector is parallel to the bed surface.

When the overall bed slope is small, the mass-conservation equation for a particular size class of active-layer sediment and global mass-conservation equation for bed sediment, (Eqs.(2) and (7)), could be written in Cartesian coordinates as follows:

$$\rho_s(1-p) \frac{\partial(\beta E_m)}{\partial t} + \frac{\partial q_{bx}}{\partial x} + \frac{\partial q_{by}}{\partial y} + S_e - S_d - S_F = 0 \quad (8)$$

$$\rho_s(1-p)\frac{\partial z_b}{\partial t} + \Sigma\left(\frac{\partial q_{bx}}{\partial x} + \frac{\partial q_{by}}{\partial y} + S_e - S_d\right) = 0 \quad (9)$$

where q_{bx}, q_{by} = x- and y-direction components of the bedload flux.

Suspended-Sediment Transport

Under the assumption that the suspended sediment particles are advected essentially by the local water velocity, except for the downward gravitational settling expressed through the fall velocity, the mass-conservation equation for one particular size class of suspended sediment in the elemental volume has the following form in Cartesian coordinates:

$$\begin{aligned} & \frac{\partial(\rho C)}{\partial t} + \frac{\partial}{\partial x}(\rho Cu) + \frac{\partial}{\partial y}(\rho Cv) + \frac{\partial}{\partial z}(\rho Cw) - \frac{\partial}{\partial z}(\rho Cw_f) \\ & = \frac{\partial}{\partial x}\left(D_H \frac{\partial(\rho C)}{\partial x}\right) + \frac{\partial}{\partial y}\left(D_H \frac{\partial(\rho C)}{\partial y}\right) + \frac{\partial}{\partial z}\left(D_H \frac{\partial(\rho C)}{\partial z}\right) \end{aligned} \quad (10)$$

where ρ = density of a mixture of water and suspended sediment (all size classes); C = dimensionless concentration, i.e. ratio of the mass ρCdV of the particular size-class particles contained in elemental volume dV to the total mass of the elemental volume; w_f = fall velocity for suspended-sediment particles of a particular size class; u, v, w = water-velocity components; D_H = horizontal mass-diffusivity coefficient; D_v = vertical mass-diffusivity coefficient.

Suspended-Sediment Source Terms

The suspended-sediment 'erosion' source represents entrainment of active-layer and bedload sediment particles into suspension. It is generally accepted that the entrainment of near-bed sediment particles into suspension can be modeled as an upward near-bed mass diffusion flux modified by β to reflect the availability of the particular size class in the active-layer control volume:

$$S_e = -\beta \left(D_v \frac{\partial(\rho C)}{\partial z} \right)_a \quad (11)$$

Subscript 'a' denotes that the mass-diffusion flux is evaluated at a near-bed point some distance a above the bed surface.

The suspended-sediment 'erosion' source is further modeled as:

$$S_e = -\beta D_{v_a} \frac{(\rho C)_{a+\Delta a} - (\rho C)_a}{\Delta a} \quad (12)$$

where C_a is a near-bed concentration estimated in a way to reflect the action of near-bed flow on the active-layer and bedload particles at a certain bed-surface location. Concentration $C_{a+\Delta a}$ is a near-bed concentration extrapolated from the suspended-sediment computations.

The suspended-sediment 'deposition' source represents gravitational settling of sediment particles already in suspension, i.e. particles that have been entrained into suspension elsewhere, or entered the model through a boundary, and transported as suspended sediment until reaching the vicinity of a certain location on the bed surface. The suspended-sediment 'deposition' source is modeled as a downward near-bed fall velocity flux:

$$S_d = (w_f \rho C)_{a+\Delta a} \quad (13)$$

where concentration $C_{a+\Delta a}$ is extrapolated from the suspended-sediment computations. Subscript ' $a + \Delta a$ ' denotes that concentration $C_{a+\Delta a}$ is evaluated at some distance $a + \Delta a$ above the bed surface.

One should note that when Eq.(10) is integrated over the elemental volume next to the bed, it must contain the same terms as described by Eqs. (11)-(13), i.e. downward near-bed fall-velocity flux and upward near-bed mass diffusion flux modified by β .

Primary Sediment Unknowns and Auxiliary Relations

If the sediment mixture in a natural watercourse is represented by a total of KS sediment size classes, then the following sediment variables are considered primary sediment unknowns: (1) bed-surface level z_b and KS active-layer size fractions β for each

active-layer elemental volume; and (2) KS suspended-sediment concentrations C for each elemental volume containing a mixture of water and suspended sediment.

The near-bed concentration C_a , bedload flux q_b , active-layer thickness E_m , active-layer floor 'source' S_F , fall velocity w_f , mass-diffusion coefficient D , and density of mixture containing water and suspended sediment ρ are in general functions of flow variables and primary sediment unknowns and are treated as auxiliary relations.

The basic nature of the auxiliary relations is described next. Beforehand, it is worth mentioning that the present work establishes a reliable computational framework for solving the relevant conservation laws as correctly as possible, incorporating the best available empirical information, that may be even site-specific for a particular application. The numerical procedure for solution of the sediment equations is formulated without reference to the specific empirical relations that ultimately must be invoked to evaluate the auxiliary relations. This allows for use of any suitable empirical relation when evaluating a particular auxiliary relation, and renders the formal numerical procedure independent of any specific empirical relation. Details of empirical relations currently used to quantify the auxiliary relations are presented in Chapter III.

The near-bed concentration C_a (for a particular size class of sediment) generally depends on the near-bed flow characteristics and it is evaluated by using an appropriate empirical relation, for example that of van Rijn (1984a).

The net bedload flux is represented herein as:

$$q_b = (1 - \gamma)\zeta_h \beta q_b^t \quad (14)$$

where q_b^t = theoretical bedload capacity for a bed containing only sediment of the particular size class, evaluated using an appropriate bedload predictor such as proposed by van Rijn (1984a). This load is adjusted by ζ_h , a so called hiding factor accounting for the reduction or increase in a particular size class transport rate when it is part of a mixture. Empirical relations such as those proposed by Karim and Kennedy (1982) or Shen and Lu (1983) can be used to evaluate ζ_h . The adjusted load is modified by β to reflect the availability of the particular size class in the active-layer elemental volume. Finally, the load is modified by $(1 - \gamma)$ to reflect the fact that some fraction γ of the particular size-class particles is transported as suspended load.

The active-layer thickness E_m is evaluated by an appropriate empirical concept of the depth of bed material that supplies material for bedload transport and suspended-sedi-

ment entrainment. Examples are the concepts of Karim and Kennedy (1982), Bennet and Nordin (1977), or Borah et al. (1982).

The active-layer floor 'source' S_F for a particular size class of sediment is derived from the mass-conservation equation for that particular size class in the active-stratum control volume. When the active-layer floor (active-stratum ceiling) descends, then:

$$S_F = -\rho_s(1-p) \frac{\partial}{\partial t} [\beta_s(z_b - E_m)] \quad (15)$$

gives the mass of the particular size class, formerly comprising size fraction β_s of the active-stratum control volume, which becomes part of the active-layer elemental volume. When the active-layer floor (active-stratum ceiling) rises, then:

$$S_F = -\rho_s(1-p) \frac{\partial}{\partial t} [\beta(z_b - E_m)] \quad (16)$$

gives the mass of the particular size class, formerly comprising size fraction β of the active-layer elemental volume, which becomes part of the active stratum control volume.

Depending on sediment-particle size, different experimental relations can be used to compute particle fall velocity, as described by van Rijn (1984b).

The mass-diffusion coefficient D is obtained by modifying the momentum-diffusion coefficient A to reflect the difference in the diffusion of a discrete sediment particle and the diffusion of a fluid 'particle' (or small coherent fluid structure), and also to reflect the damping of the fluid turbulence by the sediment particles, as suggested by van Rijn (1984b).

The local density of water with suspended sediment is modified to reflect the influence of local suspended-sediment concentration by using an appropriate empirical relation such as proposed by Zhou and McCorquodale (1992) or Holly and Rahuel (1989).

Dimensional Equations in Cartesian Coordinates

The dimensional governing sediment equations in Cartesian coordinates are summarized below, for convenient reference:

mass-conservation equation for one particular size class of active-layer sediment:

$$\rho_s(1-p)\frac{\partial(\beta E_m)}{\partial t} + \frac{\partial q_{bx}}{\partial x} + \frac{\partial q_{by}}{\partial y} - \beta \left(D_v \frac{\partial(\rho C)}{\partial z} \right)_a - (w_f \rho C)_{a+\Delta a} - S_F = 0 \quad (17)$$

global mass-conservation equation for bed sediment:

$$\rho_s(1-p)\frac{\partial z_b}{\partial t} + \Sigma \left[\frac{\partial q_{bx}}{\partial x} + \frac{\partial q_{by}}{\partial y} - \beta \left(D_v \frac{\partial(\rho C)}{\partial z} \right)_a - (w_f \rho C)_{a+\Delta a} \right] = 0 \quad (18)$$

mass-conservation equation for a particular size class of suspended sediment:

$$\begin{aligned} \frac{\partial(\rho C)}{\partial t} + \frac{\partial}{\partial x}(\rho C u) + \frac{\partial}{\partial y}(\rho C v) + \frac{\partial}{\partial z}(\rho C w) - \frac{\partial}{\partial z}(\rho C w_f) \\ = \frac{\partial}{\partial x} \left(D_H \frac{\partial(\rho C)}{\partial x} \right) + \frac{\partial}{\partial y} \left(D_H \frac{\partial(\rho C)}{\partial y} \right) + \frac{\partial}{\partial z} \left(D_v \frac{\partial(\rho C)}{\partial z} \right) \end{aligned} \quad (19)$$

In order to maintain compatibility with the rest of the CH3D code, the governing sediment equations are further manipulated the same way as the governing flow, salinity and temperature equations of CH3D. First, the governing sediment equations are transformed from Cartesian x, y, z coordinates into so-called σ -stretched coordinates x', y', σ (from now on called Cartesian σ -stretched coordinates), then made dimensionless, and, finally, transformed from Cartesian σ -stretched coordinates x', y', σ into curvilinear σ -stretched coordinates ξ, η, σ with a complete transformation used for nonorthogonal curvilinear coordinates ξ, η while the σ coordinate remains unchanged.

Dimensional Equations in Cartesian σ -stretched Coordinates

Cartesian σ -stretched coordinates x', y', σ are defined as follows:

$$\begin{aligned} x' &= x \\ y' &= y \\ \sigma &= \frac{z - \zeta}{\zeta + h} = \frac{z - \zeta}{H} \end{aligned} \quad (20)$$

where ζ = free-surface elevation, i.e. free-surface displacement (Fig. 3); h = distance between bed elevation and reference level $z = 0$; $H = \zeta + h$ = water depth.

So-called σ -stretching is a partial transformation of the equations. Components of the position vector (independent variable) are easily transformed by using rules of partial transformation, and keep the same dimensions as in original equations, except for the dimensionless vertical coordinate σ . Vector components of dependent variables remain untransformed i.e. aligned with the Cartesian coordinate directions and keep the same dimensions as in original equations, except for the newly defined vertical velocity component $\omega = \frac{d\sigma}{dt}$. The physical domain in vertical plane (Fig. 3a) transforms into rectangular computational domain (Fig. 3b) with upper boundary $\sigma = 0$ (obtained from Eq. (20) for $z = \zeta$) and lower boundary $\sigma = -1$ (obtained from Eq. (20) for $z = -h$). More details on σ -stretching could be found in Sheng and Lick (1980) or Sheng (1983).

The dimensional equations in σ -stretched coordinates read:

mass-conservation equation for one particular size class of active-layer sediment:

$$\rho_s(1-p) \frac{\partial(\beta E_m)}{\partial t} + \frac{\partial q_{bx}}{\partial x} + \frac{\partial q_{by}}{\partial y} - \frac{\beta}{H} \left(D_v \frac{\partial(\rho C)}{\partial \sigma} \right)_{\sigma_a} - (w_f \rho C)_{\sigma_a + \Delta a} - S_F = 0 \quad (21)$$

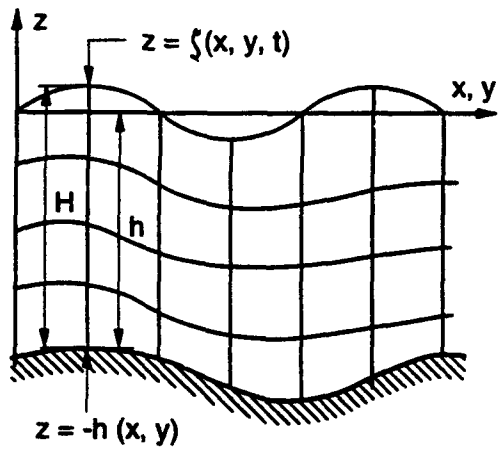
global mass-conservation equation for bed sediment:

$$\rho_s(1-p) \frac{\partial z_b}{\partial t} + \Sigma \left[\frac{\partial q_{bx}}{\partial x} + \frac{\partial q_{by}}{\partial y} - \frac{\beta}{H} \left(D_v \frac{\partial(\rho C)}{\partial \sigma} \right)_{\sigma_a} - (w_f \rho C)_{\sigma_a + \Delta a} \right] = 0 \quad (22)$$

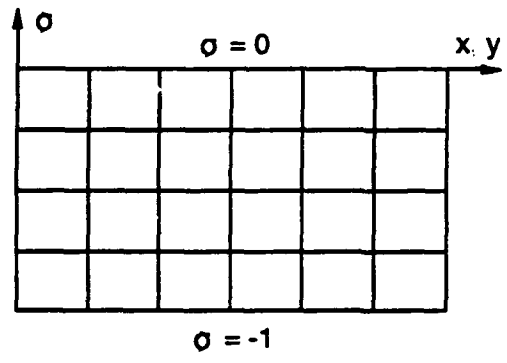
mass-conservation equation for a particular size class of suspended sediment:

$$\begin{aligned} & \frac{1}{H} \frac{\partial}{\partial t} (H\rho C) + \frac{1}{H} \left[\frac{\partial}{\partial x} (H\rho C u) + \frac{\partial}{\partial y} (H\rho C v) + \frac{\partial}{\partial \sigma} (H\rho C \omega) + \text{H.O.T.} - \frac{\partial}{\partial \sigma} (\rho C w_f) \right] \\ & = \frac{\partial}{\partial x} \left(D_H \frac{\partial(\rho C)}{\partial x} \right) + \frac{\partial}{\partial y} \left(D_H \frac{\partial(\rho C)}{\partial y} \right) + \text{H.O.T.} + \frac{1}{H^2} \frac{\partial}{\partial \sigma} \left(D_v \frac{\partial(\rho C)}{\partial \sigma} \right) \end{aligned} \quad (23)$$

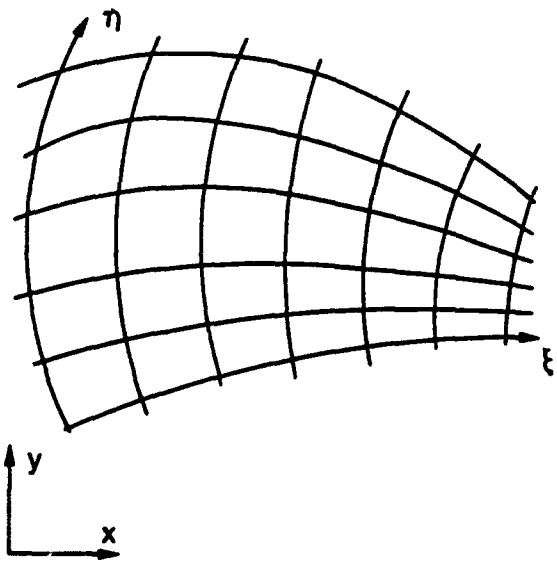
where H.O.T. are the higher order terms that will be dropped in all that follows.



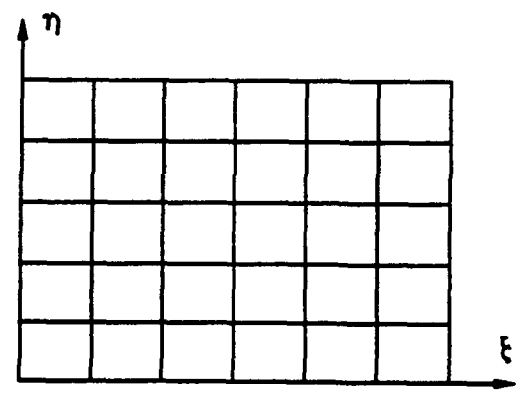
(a)



(b)



(c)



(d)

Figure 3. Coordinate Transformations.

Dimensionless Equations in σ -stretched Coordinates

In order to non-dimensionalize the equations, first a set of reference variables is defined, then the sediment variables are made dimensionless, and dimensionless numbers are defined.

Reference Variables:

f	=	frequency
x_r	=	reference length
z_r	=	reference depth
u_r	=	reference water velocity,
D_{H_r}	=	reference lateral mass-diffusivity coefficient,
D_{v_r}	=	reference vertical mass-diffusivity coefficient,
A_{H_r}	=	reference lateral momentum-diffusivity coefficient,
A_{v_r}	=	reference vertical momentum-diffusivity coefficient
w_{f_r}	=	reference fall velocity (computed with maximum sediment-particle diameter and reference water velocity),
ρ_r	=	reference density of water-sediment mixture,

Dimensionless Variables

$t^* = t \cdot f$	=	time
$x^* = \frac{x}{x_r}$	=	x coordinate
$y^* = \frac{y}{x_r}$	=	y coordinate
$\sigma^* = \sigma$	=	σ coordinate
$u^* = \frac{u}{u_r}$	=	x-direction velocity component
$v^* = \frac{v}{u_r}$	=	y-direction velocity component
$w^* = \frac{w \cdot x_r}{u_r}$	=	σ -direction velocity component
$H^* = \frac{H}{z_r}$	=	depth
$D_{H}^* = \frac{D_H}{D_{H_r}}$	=	lateral mass-diffusivity coefficient

$$D_v^* = \frac{D_v}{D_{v_r}} \quad = \text{vertical mass-diffusivity coefficient}$$

$$z_b^* = \frac{z_b}{z_r} \quad = \text{bed elevation}$$

$$\beta^* = \beta \quad = \text{active-layer size fraction}$$

$$C^* = C \quad = \text{suspended-sediment concentration}$$

$$\rho_s^* = \frac{\rho_s}{\rho_r} \quad = \text{sediment-particle density}$$

$$p^* = p \quad = \text{bed-material porosity}$$

$$E_m^* = \frac{E_m}{z_r} \quad = \text{active-layer thickness}$$

$$q_b^* = \frac{q_b}{\rho_r z_r x_r f} \quad = \text{bedload flux}$$

$$S_F^* = \frac{S_F}{\rho_r z_r f} \quad = \text{active-layer floor 'source'}$$

$$\rho^* = \frac{\rho}{\rho_r} \quad = \text{density of water-sediment mixture}$$

$$w_f^* = \frac{w_f}{w_{f_r}} \quad = \text{fall velocity}$$

Dimensionless Numbers

$$R_o = \frac{u_r}{f x_r} \quad = \text{Rossby number}$$

$$R_{of} = \frac{w_{f_r}}{f z_r} \quad = \text{fall-velocity Rossby number}$$

$$E_{KH} = \frac{A_{H_r}}{f x_r^2} \quad = \text{lateral Ekman number}$$

$$E_{Kv} = \frac{A_{v_r}}{f z_r^2} \quad = \text{vertical Ekman number}$$

$$S_{CH} = \frac{A_{H_r}}{D_{H_r}} \quad = \text{lateral Schmidt number}$$

$$S_{Cv} = \frac{A_{v_r}}{D_{v_r}} \quad = \text{vertical Schmidt number}$$

Dimensionless Equations

When the '*' is omitted, the dimensionless equations read:

mass-conservation equation for one particular size class of active-layer sediment:

$$\rho_s(1-p)\frac{\partial(\beta E_m)}{\partial t} + \frac{\partial q_{bx}}{\partial x} + \frac{\partial q_{by}}{\partial y} - \frac{E_{kv}}{S_{cv}} \frac{\beta}{H} \left(D_v \frac{\partial(\rho C)}{\partial \sigma} \right)_{\sigma_a} - R_{of}(w_f \rho C)_{\sigma_a+\Delta\sigma} - S_F = 0 \quad (24)$$

global mass-conservation equation for bed sediment:

$$\rho_s(1-p)\frac{\partial z_b}{\partial t} + \Sigma \left[\frac{\partial q_{bx}}{\partial x} + \frac{\partial q_{by}}{\partial y} - \frac{E_{kv}}{S_{cv}} \frac{\beta}{H} \left(D_v \frac{\partial(\rho C)}{\partial \sigma} \right)_{\sigma_a} - R_{of}(w_f \rho C)_{\sigma_a+\Delta\sigma} \right] = 0 \quad (25)$$

mass-conservation equation for a particular size class of suspended sediment:

$$\begin{aligned} & \frac{1}{H} \frac{\partial}{\partial t} (H\rho C) + \frac{R_o}{H} \left[\frac{\partial}{\partial x} (H\rho C u) + \frac{\partial}{\partial y} (H\rho C v) + \frac{\partial}{\partial \sigma} (H\rho C \omega) \right] - \frac{R_{of}}{H} \frac{\partial}{\partial \sigma} (\rho C w_f) \\ & = \frac{E_{kH}}{S_{cH}} \left[\frac{\partial}{\partial x} \left(D_H \frac{\partial(\rho C)}{\partial x} \right) + \frac{\partial}{\partial y} \left(D_H \frac{\partial(\rho C)}{\partial y} \right) \right] + \frac{E_{kv}}{S_{cv}} \frac{1}{H^2} \frac{\partial}{\partial \sigma} \left(D_v \frac{\partial(\rho C)}{\partial \sigma} \right) \end{aligned} \quad (26)$$

Dimensionless Equations in Curvilinear σ -stretched Coordinates

As previously stated, the governing sediment equations are transformed from Cartesian σ -stretched coordinates x', y', σ into curvilinear σ -stretched coordinates ξ, η, σ with a complete transformation used for the nonorthogonal curvilinear coordinates ξ, η while the σ coordinate remains unchanged. A complete transformation means that all vector components, not only those representing independent variables, but also those representing dependent variables, formerly aligned with Cartesian coordinate directions x, y , are now aligned with base vectors tangential to curvilinear coordinate lines ξ and η . The physical domain in (x, y) plane (Fig. 3c) transforms into a rectangular computational domain with a unit-square grid (Fig. 3d). Vector components aligned with the vertical σ direction remain unchanged.

Starting from a Cartesian tensor form of the governing equations, one can easily write general curvilinear tensor equations. The general curvilinear tensor form of the equa-

tions looks like a generalization of the Cartesian tensor form with partial derivatives replaced by general covariant derivatives, velocity expressed as a contravariant vector, and other vectors respecting the appropriate covariant/contravariant order. Finally, the working form of the governing sediment equations is obtained by expanding the tensor equations. The expanded form of the dimensionless sediment equations in curvilinear σ -stretched coordinates reads:

mass-conservation equation for one particular size class of active-layer sediment:

$$\begin{aligned} \rho_s(1-p) \frac{\partial(\beta E_m)}{\partial t} + \frac{1}{J} \left[\frac{\partial}{\partial \xi} (J q_{b\xi}) + \frac{\partial}{\partial \eta} (J q_{b\eta}) \right] - \frac{E_{k_v}}{S_{c_v}} \frac{\beta}{H} \left(D_v \frac{\partial(\rho C)}{\partial \sigma} \right)_{\sigma_a} \\ - R_{of} (w_f \rho C)_{\sigma_a + \Delta a} - S_F = 0 \end{aligned} \quad (27)$$

global mass-conservation equation for bed sediment:

$$\begin{aligned} \rho_s(1-p) \frac{\partial z_b}{\partial t} + \Sigma \left[\frac{1}{J} \frac{\partial}{\partial \xi} (J q_{b\xi}) + \frac{1}{J} \frac{\partial}{\partial \eta} (J q_{b\eta}) - \frac{E_{k_v}}{S_{c_v}} \frac{\beta}{H} \left(D_v \frac{\partial(\rho C)}{\partial \sigma} \right)_{\sigma_a} \right. \\ \left. - R_{of} (w_f \rho C)_{\sigma_a + \Delta a} \right] = 0 \end{aligned} \quad (28)$$

mass-conservation equation for a particular size class of suspended sediment:

$$\begin{aligned} \frac{1}{H} \frac{\partial}{\partial t} (H \rho C) + \frac{R_o}{H} \left[\frac{1}{J} \frac{\partial}{\partial \xi} (J H \rho C u) + \frac{1}{J} \frac{\partial}{\partial \eta} (J H \rho C v) + \frac{\partial}{\partial \sigma} (J H \rho C \omega) \right] \\ - \frac{R_{of}}{H} \frac{\partial}{\partial \sigma} (\rho C w_f) = \frac{E_{k_H}}{S_{c_H}} \frac{1}{J} \left[\frac{\partial}{\partial \xi} \left(\frac{D_H}{J} g_{22} \frac{\partial(\rho C)}{\partial \xi} \right) - \frac{\partial}{\partial \xi} \left(\frac{D_H}{J} g_{12} \frac{\partial(\rho C)}{\partial \eta} \right) \right. \\ \left. - \frac{\partial}{\partial \eta} \left(\frac{D_H}{J} g_{12} \frac{\partial(\rho C)}{\partial \xi} \right) + \frac{\partial}{\partial \eta} \left(\frac{D_H}{J} g_{11} \frac{\partial(\rho C)}{\partial \eta} \right) \right] \\ + \frac{E_{k_v}}{S_{c_v}} \frac{1}{H^2} \frac{\partial}{\partial \sigma} \left(D_v \frac{\partial(\rho C)}{\partial \sigma} \right) \end{aligned} \quad (29)$$

where $q_{b\xi}, q_{b\eta}$ = contravariant bedload-flux components in ξ and η directions, respectively; u, v, ω = contravariant velocity components in ξ, η and σ directions, respectively;

g_{11} , g_{12} , g_{22} = metric coefficients, and J = square root of the appropriate Jacobian-matrix determinant:

$$\begin{aligned}
 g_{11} &= \left(\frac{\partial x}{\partial \xi}\right)^2 + \left(\frac{\partial y}{\partial \xi}\right)^2 \\
 g_{12} &= \frac{\partial x}{\partial \xi} \frac{\partial x}{\partial \eta} + \frac{\partial y}{\partial \xi} \frac{\partial y}{\partial \eta} \\
 g_{22} &= \left(\frac{\partial x}{\partial \eta}\right)^2 + \left(\frac{\partial y}{\partial \eta}\right)^2 \\
 J &= \sqrt{g_{11}g_{22} - g_{12}^2} = \frac{\partial x}{\partial \xi} \frac{\partial y}{\partial \eta} - \frac{\partial x}{\partial \eta} \frac{\partial y}{\partial \xi}
 \end{aligned} \tag{30}$$

The principles of complete transformation of the basic fluid mechanics equations in general curvilinear coordinates are presented by Sokolnikoff (1951), Aris (1962) or, more recently, by Richmond et al. (1986). More details on sediment equations in curvilinear coordinates can be found in Spasojevic (1988).

CHAPTER III

NUMERICAL SOLUTION

Strategy for Approximate Solution

Fluid flow, sediment transport and bed evolution are elements of a coupled process. Sediment particles are being entrained, moving, and being deposited due to the action of fluid flow, causing bed evolution which is a direct consequence of sediment transport. On the other hand, change of the bed-surface level changes the flow domain, and thus the flow. Also, change in the size distribution of sediment particles at the bed surface changes the roughness of the bed surface, which in turn directly influences the bed shear stress. The suspended sediment changes the density of the water-sediment mixture.

On the other hand, one should note that fluid flow and sediment processes have quite different time scales. Bed-sediment transport and bed evolution are defined without following each sediment particle separately, but by considering sediment transport 'en masse'. It is impossible, therefore, to account for the changes at the bed due to movement

of a single sediment particle, changes that have the same time scale as the flow process. Instead, one focusses on global changes in bed level and bed-surface size distribution, with their much larger time scale. Changes in bed level during a time step appropriate for flow computations are usually too small to change the flow domain and flow field significantly. Similarly, changes in bed-surface size distribution i.e. roughness or friction, during a time step appropriate for flow computations, are insufficient to influence the flow field significantly. Only suspended-sediment transport has the same time scale as fluid flow. However, in most cases suspended-sediment concentrations in natural watercourses do not change abruptly with time, which suggests that changes in the density of the water and sediment mixture during a time step appropriate for flow computations, are also generally insufficient to influence the flow field significantly.

Given the above discussion, it would appear possible to uncouple water and sediment computations at the scale of one time step.

Furthermore, the small time step required by the numerical techniques of CH3D, offers the possibility to couple suspended- and bed-sediment computations in an iterative manner, as described below.

The suspended-sediment source terms are the link relating suspended and bed sediment computations. The suspended-sediment 'deposition' source term depends on the suspended-sediment concentrations, while the suspended-sediment 'erosion' source term depends both on the suspended-sediment concentrations and on the active-layer size fractions. The mass-conservation equations for each size class of active-layer sediment and the global mass-conservation equation for bed sediment, with the appropriate suspended-sediment source terms, are solved in a coupled manner, for one iteration of one computational time step, by assuming the suspended-sediment concentrations to be known from the previous iteration. An improved estimate of active-layer size fractions and the bed-surface elevation is thus obtained. The mass-conservation equations for each size fraction of suspended sediment are then solved for the same computational time step, by assuming the active-layer size fractions to be known from the bed-sediment computations. The whole procedure is repeated iteratively until a convergence criterion is satisfied.

However, in the present work a single global iteration is employed in each time step, in recognition of the fact that numerical techniques of CH3D code require time step of order of minutes and that changes in bed level, bed surface composition, and the density of the water-sediment mixture are generally small during such a small time step, although changes may accumulate to significant amounts over several time steps.

Numerical Method for the Mass-Conservation Equation for Active-Layer Sediment and the Global Mass-Conservation Equation for Bed Sediment

Figure 4 shows a portion of the computational domain. P denotes a computational point under consideration at the bed, while C denotes a suspended-sediment computational point under consideration. Computational points neighboring C (i.e. P) in the ξ direction are denoted as E (east), FE (far east), W (west) and FW (far west). Computational points neighboring C in the η direction are denoted as N (north), FN (far north), S (south) and FS (far south). Computational points neighboring C (i.e. P) in the σ direction are denoted as T (top) and B (bottom). Similarly, faces of control volume built around C are denoted as e (east), w (west), n (north), s (south), t (top), and b (bottom). Indexes i,j,k denote computational points along the ξ - η - and σ -direction coordinate lines, respectively.

As previously stated, $C_{\sigma_a+\Delta a}$ is a near-bed concentration extrapolated from the suspended sediment computations. A simple linear extrapolation gives:

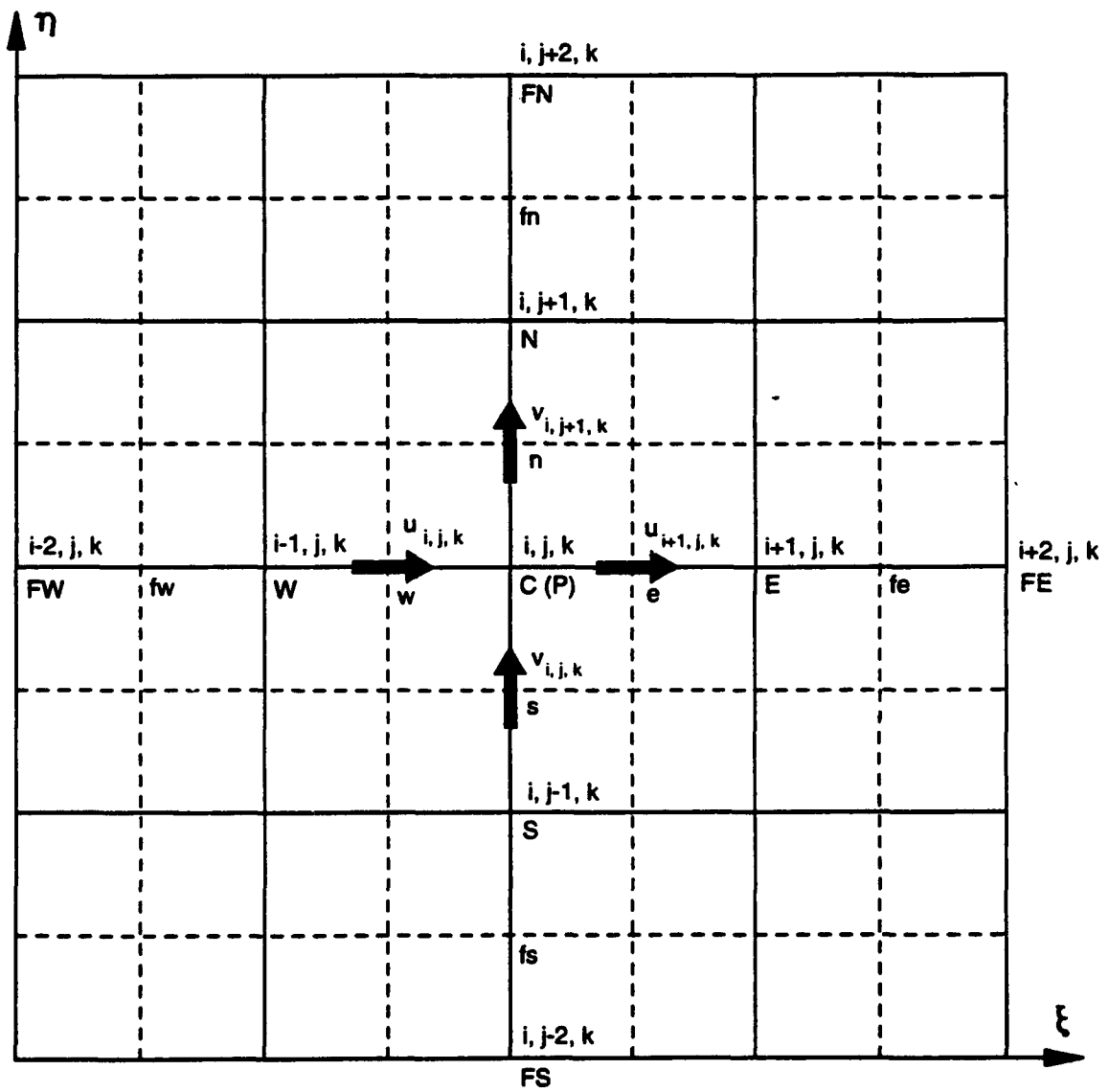
$$(\rho C)_{\sigma_a+\Delta a} = (1-c)(\rho C)_{k=2} + c(\rho C)_{k=1} \quad (31)$$

where c = extrapolation coefficient; subscript k defines computational points along the vertical σ -direction line (Fig. 4b i.e. 4c).

Taking into account Eq. (12) and (31), Eqs. (27) and (28) are discretized by integrating them over the time step and the control volume built around a main computational point P (Fig. 4a):

global mass-conservation equation for bed-sediment

$$\begin{aligned} & \rho_s(1-p)J_p \frac{(z_b)_p^{n+1} - (z_b)_p^n}{\Delta t} + \\ & + \sum \left\{ \theta \frac{J_e(q_{b_\xi})_e^{n+1} - J_w(q_{b_\xi})_w^{n+1}}{\Delta \xi} + (1-\theta) \frac{J_e(q_{b_\xi})_e^n - J_w(q_{b_\xi})_w^n}{\Delta \xi} \right. \\ & \left. + \theta \frac{J_n(q_{b_\eta})_n^{n+1} - J_s(q_{b_\eta})_s^{n+1}}{\Delta \eta} + (1-\theta) \frac{J_n(q_{b_\eta})_n^n - J_s(q_{b_\eta})_s^n}{\Delta \eta} \right. \\ & \left. - \frac{E_{k_v}}{S_{c_v}} J_p \theta \frac{\beta_p^{n+1}}{H_p^{n+1}} D_{v_a}^n \frac{(1-c)(\rho C)_{k=2}^{n+1} + c(\rho C)_{k=1}^{n+1} - (\rho C)_{\sigma_a}^{n+1}}{\Delta \sigma_{\Delta a}} \right. \end{aligned}$$



(a)

Figure 4. Computational Grid.

$$\begin{aligned}
& -\frac{E_{k_v}}{S_{c_v}} J_p (1-\theta) \frac{\beta_p^n}{H_p^n} D_{v_a}^n \frac{(1-c)(\rho C)_{k=2}^n + c(\rho C)_{k=1}^n - (\rho C)_{\sigma_a}^n}{\Delta \sigma_{\Delta a}} \\
& -J_p R o_f w_f \theta \left[(1-c)(\rho C)_{k=2}^{n+1} + c(\rho C)_{k=1}^{n+1} \right] \\
& -J_p R o_f w_f (1-\theta) \left[(1-c)(\rho C)_{k=2}^n + c(\rho C)_{k=1}^n \right] \Big\} = 0
\end{aligned} \tag{32}$$

mass-conservation equation for a particular size class of active-layer sediment

$$\begin{aligned}
& \rho_s (1-p) J_p \frac{(\beta E_m)_p^{n+1} - (\beta E_m)_p^n}{\Delta t} + \\
& + \theta \frac{J_e (q_{b_\xi})_e^{n+1} - J_w (q_{b_\xi})_w^{n+1}}{\Delta \xi} + (1-\theta) \frac{J_e (q_{b_\xi})_e^n - J_w (q_{b_\xi})_w^n}{\Delta \xi} \\
& + \theta \frac{J_n (q_{b_\eta})_n^{n+1} - J_s (q_{b_\eta})_s^{n+1}}{\Delta \eta} + (1-\theta) \frac{J_n (q_{b_\eta})_n^n - J_s (q_{b_\eta})_s^n}{\Delta \eta} \\
& - \frac{E_{k_v}}{S_{c_v}} J_p \theta \frac{\beta_p^{n+1}}{H_p^{n+1}} D_{v_a}^{n+1} \frac{(1-c)(\rho C)_{k=2}^{n+1} + c(\rho C)_{k=1}^{n+1} - (\rho C)_{\sigma_a}^{n+1}}{\Delta \sigma_{\Delta a}} \\
& - \frac{E_{k_v}}{S_{c_v}} J_p (1-\theta) \frac{\beta_p^n}{H_p^n} D_{v_a}^n \frac{(1-c)(\rho C)_{k=2}^n + c(\rho C)_{k=1}^n - (\rho C)_{\sigma_a}^n}{\Delta \sigma_{\Delta a}} \\
& -J_p R o_f w_f \theta \left[(1-c)(\rho C)_{k=2}^{n+1} + c(\rho C)_{k=1}^{n+1} \right] \\
& -J_p R o_f w_f (1-\theta) \left[(1-c)(\rho C)_{k=2}^n + c(\rho C)_{k=1}^n \right] - J_c S_F = 0
\end{aligned} \tag{33}$$

where subscripts e,w,n,s denote east, west, north and south control-volume faces in the (ξ, η) plane, respectively (Fig. 4a); subscript P denotes a main, i.e. cell-centered, computational point; superscript n denotes the time level; and θ = weighting (implication) factor.

Further treatment of the bedload fluxes is inspired by their physical character. Bedload flux acting through a control-volume face is governed by the staggered velocity component perpendicular to the particular control-volume face. A control volume is assumed to have a uniform size distribution of sediment particles at the bed. Consequently it is appropriate to suppose that the fluid flowing through a control-volume face transports bedload-sediment particles contained in the control volume on the upstream side. The bedload flux through a control-volume face knows nothing about the active-layer size frac-

tions in the control volume towards which it is heading, but carries the full legacy of the control volume from which it is coming. This treatment of bedload flux resembles the 'tank-and-tube' model of Gosman et al (1969), used for heat-transfer problems, and is also the essence of an upwind scheme.

The bedload flux at time level (n+1) is evaluated by using flow variables at time level (n+1), obtained from the flow computations and related to the control-volume face. The sediment variables (primarily the active-layer size fraction) needed to evaluate the bedload flux, are related to the 'upwind' control volume and expressed explicitly (using their values at time level n).

Evaluation of the bedload flux in the manner described above means that all bedload-flux components are expressed explicitly in terms of bed elevation and active-layer size fractions. Also, due to iterative coupling of the bed (i.e. active-layer sediment) computations and suspended-sediment computations, suspended-sediment source terms are expressed explicitly in terms of suspended-sediment concentrations. It is useful to point out those elements of the discretized equations that are expressed explicitly in terms of sediment variables by introducing a special notation for them.

The discretized global mass-conservation equation for bed sediment (Eq. (32)) can be written as:

$$\begin{aligned}
 & \rho_s(1-p)J_p \frac{(z_b)_p^{n+1} - (z_b)_p^n}{\Delta t} \\
 & + \Sigma \left[\theta(\text{div}q_b)_p^{n+1} + (1-\theta)(\text{div}q_b)_p^n \right. \\
 & + \theta\beta_p^{n+1}(S_e^t)_p^{n+1} + (1-\theta)(S_e)_p^n \\
 & \left. - \theta(S_d)_p^{n+1} - (1-\theta)(S_d)_p^n \right] = 0
 \end{aligned} \tag{34}$$

while the discretized mass-conservation equation for one size class of active-layer sediment (Eq. (33)) is written as:

$$\begin{aligned}
 & \rho_s(1-p)J_p \frac{(\beta E_m)_p^{n+1} - (\beta E_m)_p^n}{\Delta t} \\
 & + \theta(\text{div}q_b)_p^{n+1} + (1-\theta)(\text{div}q_b)_p^n
 \end{aligned} \tag{35}$$

$$\begin{aligned}
& +\theta\beta_p^{n+1}(S_e^t)_p^{n+1} + (1-\theta)(S_e)_p^n \\
& -\theta(S_d)_p^{n+1} - (1-\theta)(S_d)_p^n - J_p S_F = 0
\end{aligned}$$

where:

$$(\text{div}q_b)_p^{n+1} = \frac{J_e(q_{b\xi})_e^{n+1} - J_w(q_{b\xi})_w^{n+1}}{\Delta\xi} + \frac{J_n(q_{b\eta})_n^{n+1} - J_s(q_{b\eta})_s^{n+1}}{\Delta\eta} \quad (36)$$

stands for the divergence of the bedload flux vector, evaluated by using flow variables at time level (n+1) and bed i.e. active-layer sediment variables at time level n.

$$(\text{div}q_b)_p^n = \frac{J_e(q_{b\xi})_e^n - J_w(q_{b\xi})_w^n}{\Delta\xi} + \frac{J_n(q_{b\eta})_n^n - J_s(q_{b\eta})_s^n}{\Delta\eta} \quad (37)$$

stands for the divergence of the bedload flux vector, evaluated by using flow and sediment variables at time level n.

$$(S_e^t)_p^{n+1} = -\frac{E_{k_v}}{S_{c_v}} J_p \frac{D_{v_a}^{n+1}}{H_p^{n+1}} \frac{(1-c)(\rho C)_{k=2}^{n+1} + c(\rho C)_{k=1}^{n+1} - (\rho C)_{\sigma_a}^{n+1}}{\Delta\sigma_{\Delta a}} \quad (38)$$

stands for the 'theoretical' suspended-sediment 'erosion' source term ('theoretical' in the sense that it is not reduced by β , i.e. it does not account for the availability of a particular active-layer size fraction), evaluated using flow variables at time level (n+1) and previous-iteration suspended-sediment concentrations at time level (n+1).

$$(S_e)_p^n = -\frac{E_{k_v}}{S_{c_v}} J_p \beta_p^n \frac{D_{v_a}^n}{H_p^n} \frac{(1-c)(\rho C)_{k=2}^n + c(\rho C)_{k=1}^n - (\rho C)_{\sigma_a}^n}{\Delta\sigma_{\Delta a}} \quad (39)$$

stands for the suspended-sediment 'erosion' source term, evaluated by using flow and sediment variables at time level n.

$$(S_d)_p^n = J_p R_o_f w_f [(1-c)(\rho C)_{k=2}^{n+1} + c(\rho C)_{k=1}^{n+1}] \quad (40)$$

stands for the suspended-sediment 'deposition' source term, evaluated by using flow variables at time level (n+1) and previous-iteration suspended-sediment concentrations at time level (n+1).

$$(S_d)_p^n = J_p R_o_f w_f \left[(1-c)(\rho C)_{k=2}^n + c(\rho C)_{k=1}^n \right] \quad (41)$$

stands for the suspended-sediment 'deposition' source term, evaluated by using flow and sediment variables at time level n.

The discretized equations (one Eq.(34) and KS Eqs.(35), written for a particular main computational point P, form an 'explicit' system of algebraic equations at P. 'Explicit' in this context means that all unknown sediment variables (bed elevation and KS active-layer size fractions at time level n+1) are located at point P only. Sediment variables located at neighboring computational points appear explicitly, i.e. as known values.

Even though the solution of an 'explicit' system of algebraic equations at the main computational point P does not depend on neighboring points, it still requires boundary conditions at inflow boundaries in order to evaluate bedload fluxes through the appropriate inflow control-volume faces. It is enough to assign known active-layer size fractions at inflow boundaries, requiring the basic constraint (sum of all fractions equal to unity) to be satisfied. The latter requirement actually replaces a known bed-surface elevation as an inflow boundary condition, even though the bed elevation itself appears to be unnecessary for evaluation of the bedload flux through an inflow-boundary face.

Numerical Method for Mass-Conservation Equation for Suspended-Sediment

In the original CH3D temperature and salinity computations, all but the vertical diffusion terms are discretized by using a numerical method called QUICKEST (Quadratic Upstream Interpolation for Convective Kinematics with Estimated Streaming Terms), developed by Leonard (1979). In order to be compatible with the rest of CH3D code, the same strategy is used herein for the mass-conservation equation for suspended sediment (Eq. (29)). Except for the fall-velocity and vertical-diffusion terms, all other terms in the mass-conservation equation for suspended-sediment are discretized by using a generalized version of the QUICKEST method. The fall-velocity term is discretized by using an upwind finite difference scheme, while the vertical-diffusion term is discretized by using a time weighted central differencing. The basic principles of Leonard's (1979) QUICKEST method, applied to a one-dimensional advection-diffusion equation in Cartesian coordinates

The exact form of all terms in Eq. (42) can be found in Appendix B, i.e. in Eqs. (B35), (B55) and (B79). The general meaning of the terms is briefly explained herein. Terms (1) and (2) originate in the discretization of the local rate-of-change term (Eq. (29)). Terms (3), (4), (7), (8), (11) and (12) represent advection fluxes through the west, east, south, north, bottom and top faces of the control volume built around the main computational point C (Fig. 4), respectively, and originate in the discretization of the appropriate advection terms. Terms (5), (6), (9) and (10) represent diffusion fluxes through the east, west, north and south faces of the control volume, respectively, and come from the discretization of the appropriate diffusion terms. Terms (1) to (12) are discretized by using the generalized QUICKEST method (Appendix B). Terms (13) and (15) represent fall-velocity fluxes, at the current time level (n+1), through the top and bottom faces of the control volume built around C, respectively. Terms (14) and (16) represent fall-velocity fluxes through the top and bottom faces at the known, previous, time level n, respectively. Terms (13) to (16) originate in the discretization of the fall-velocity term (using an upwind differencing). Terms (17) and (19) represent diffusion fluxes, at the current time level (n+1), through the top and bottom faces of the control volume built around C, respectively. Terms (18) and (20) represent diffusion fluxes through the top and bottom faces at the known, previous, time level n, respectively. Terms (17) to (20) originate in the discretization of the vertical diffusion term (using central differencing).

Terms (2) to (12) as well as (14), (16), (18) and (20) in Eq. (42) are all expressed explicitly in terms of sediment variables. Thus, Eq. (42) can be rewritten as:

$$a(\rho C)_B^{n+1} + b(\rho C)_c^{n+1} + c(\rho C)_T^{n+1} = d \quad (43)$$

where a, b, c, d are known coefficients presented in Appendix B. The sole unknowns in Eq. (43) are the volumetric suspended-sediment concentrations (ρC).

The boundary conditions in the ξ - and η -coordinate directions (presented in detail in Appendix B) do not influence the overall solution algorithm, for all advection and diffusion fluxes in ξ and η directions are expressed explicitly in terms of sediment variables. Boundary conditions at the bed and free surface (also presented in detail in Appendix B) are briefly discussed below.

For a point C next to the free surface, advection, fall-velocity and diffusion fluxes through the free surface (top face of the control volume around C) are equal to zero. Therefore, the terms (12), (13), (14), (17) and (18) in Eq. (42) are equal to zero. Equation (42), written for a point next to the free surface, is easily rewritten in the form of Eq. (43), where a, b, c, d, are known coefficients (Appendix B).

For a point C next to the bed, the advection flux through the bed surface (bottom face of the control volume around C) is equal to zero. Thus term (11) in Eq. (42) is equal to zero. The fall-velocity flux through the bottom face of the control volume actually represents deposition of suspended-sediment particles onto the bed. Terms (15) and (16) in Eq. (42) are treated as 'deposition' source terms (Eqs. (40) and (41)) and rewritten as:

$$\theta R_o f J_c w_f \left[(1-c)(\rho C)_T^{n+1} + c(\rho C)_c^{n+1} \right] \frac{\Delta t}{\Delta \sigma}$$

and

$$(1-\theta)(S_d)_p^n \frac{\Delta t}{\Delta \sigma}$$

respectively. The diffusion flux through the bottom face of the control volume actually represents entrainment of sediment particles from the bed into suspension. Terms (19) and (20) in Eq. (42) are treated as 'erosion' source terms (Eqs. (38) and (39)) and rewritten as:

$$\theta \frac{E_{k_v}}{S_{c_v}} J_c \beta_p^{n+1} \frac{D_{v_b}^{n+1}}{H_c^{n+1}} \frac{(1-c)(\rho C)_T^{n+1} + c(\rho C)_c^{n+1} - (\rho C)_{\sigma_a}^{n+1}}{\Delta \sigma \Delta a} \frac{\Delta t}{\Delta \sigma}$$

and

$$(1-\theta)(S_e)_p^n \frac{\Delta t}{\Delta \sigma}$$

respectively. It should be noted that, due to the iterative coupling of bed (i.e. active-layer) sediment computations and suspended-sediment computations, the active-layer size fraction at time (n+1) appears as an explicit value, known from the previous iteration, in the diffusion-flux term (19) when Equation (42) is written for a point next to the bed. Therefore, Equation (42) written for points next to the bed can also be rewritten in form of the Eq. (43), where a, b, c, d, are known coefficients (Appendix B).

The discretized mass-conservation equation for a particular size class of suspended sediment (Eq. (43)) is implicit in the vertical direction. When a particular size class Eq. (43) is written for each computational point C along a single σ -direction line, the result is a system of K algebraic equations with K unknown volumetric concentrations of the particular suspended-sediment size class (where K is the number of computational points C along a σ -direction line - Fig. 4b or 4c).

There are KS Eqs. (43) at each computational point C, one for each size class of suspended sediment. Equations (43) written for the same computational point C but different size classes of suspended sediment are theoretically coupled through the 'erosion'

source term containing the active-layer size fraction. Active-layer size fractions are mutually dependent due to the basic constraint (Eq. (4)) built into the appropriate mass-conservation equations. However, due to the iterative coupling of bed (i.e. active layer) computations and suspended-sediment computations, Eqs. (43), written for the same computational point C but different size fractions, become mutually independent during one iteration.

Algorithm for Solution of Discretized Sediment Equations

The global steps of the solution algorithm for the discretized sediment equations are as follows:

(1) One discretized global mass-conservation equation for bed sediment (Eq. (34)) and KS discretized mass-conservation equations for active-layer sediment (Eq. (35)) are solved simultaneously at the bed point P (Fig. 4b i.e. 4c). Computed are the following primary sediment unknowns: one bed-surface elevation and KS active-layer size fractions. Suspended-sediment concentrations, appearing in the source terms, are considered to be known from previous iteration.

(2) The system of K discretized mass-conservation equations for a particular size class of suspended sediment, one Eq. (43) for each computational point C along the σ -direction line above the same bed point P as in step (1) (Fig. 4b i.e. 4c), is solved. Computed are the volumetric concentrations, for a particular size class of suspended sediment, at all computational points C along the σ -direction line above the same bed point P as in step (1). The appropriate size class active-layer size fraction, computed in step (1), is used to evaluate the coefficients in Eq. (43) for a computational point C next to the bed.

(3) Step (2) is repeated for each suspended-sediment size class.

(4) Steps (1) to (3) are repeated until the appropriate convergence criteria are satisfied.

(5) Steps (1) to (4) are repeated throughout the computational domain, for each bed point P and all points C along the σ -direction line above that particular bed point P.

Solution of Discretized Global Mass-Conservation Equation for Bed Sediment and Mass-Conservation Equations for Active-Layer Sediment at the Point

The discretized equations to be solved simultaneously for the same point at the bed, are: (1) one discretized global mass-conservation equation for bed sediment (Eq. (34)) and

(2) KS discretized mass-conservation equations for active-layer sediment (Eq. (35)). The primary sediment unknowns are: (1) one bed-surface elevation and (2) KS active-layer size fractions.

Unknown sediment variables at a main computational point P can be thought of as being components of a sediment-variables vector \bar{s} at point P:

$$\bar{s}^{n+1} = (z_b^{n+1}, \beta_1^{n+1}, \dots, \beta_{ks}^{n+1}, \dots, \beta_{KS}^{n+1}) \quad (44)$$

or, in more compact notation:

$$\bar{s}^{n+1} = (s_1, s_{ks+1}) \quad ks = 1, KS \quad (45)$$

where subscript ks is introduced to denote the ks-th size class of the sediment mixture under consideration.

Equation (34), the discretized global mass-conservation equation for bed sediment, can be symbolically written as:

$$F_1(\bar{s}^{n+1}) = 0 \quad (46)$$

The discretized mass conservation equations for active-layer sediment, one Eq.(35) for each of KS size classes, are written as:

$$F_{ks+1}(\bar{s}^{n+1}) = 0 \quad ks = 1, KS \quad (47)$$

Equations (46) and (47) form a system of nonlinear algebraic equations which can be linearized and solved iteratively by using a Newton-Raphson algorithm. The resulting system of linear algebraic equations can be written as:

$$\left[\frac{\partial F_1}{\partial \bar{s}} \right] \Delta \bar{s} = -F_1(\bar{s}^{n+1}) \quad (48)$$

$$\left[\frac{\partial F_{ks+1}}{\partial \bar{s}} \right] \Delta \bar{s} = -F_{ks+1}(\bar{s}^{n+1}) \quad ks = 1, KS \quad (49)$$

in which $\left[\frac{\partial F}{\partial \bar{s}} \right]$, evaluated with previous-iteration values of the sediment-variables vector ${}^m \bar{s}^{n+1}$, represents one row of the Jacobian matrix of coefficients. Superscript m denotes the Newton-Raphson iteration level.

The unknown vector of sediment-variable corrections $\Delta \bar{s}$ can be written as:

$$\Delta \bar{s} = (\Delta s_1, \Delta s_{ks+1}) \quad ks = 1, KS \quad (50)$$

or:

$$\Delta \bar{s} = (\Delta z_b, \Delta \beta_1, \dots, \Delta \beta_{ks}, \dots, \Delta \beta_{KS}) \quad (51)$$

Coefficients in the Jacobian matrix are presented in more detail in Appendix C. The inverse matrix is computed by using a maximum pivot strategy (Carnahan, Luther and Wilkes (1969) for example).

When the vector of sediment-variable corrections at point P is obtained, the current-iteration value of the sediment-variable vector at P is computed as:

$${}^{m+1} \bar{s}^{n+1} = {}^m \bar{s}^{n+1} + \Delta \bar{s} \quad (52)$$

Iterations continue until the following convergence criterion is satisfied:

$$\Delta \bar{s} \leq \bar{\epsilon} \quad (53)$$

where $\bar{\epsilon}$ is a convergence-criterion vector.

Solution of Discretized Mass-Conservation Equations for One Size Class of Suspended Sediment along σ -Direction Line

The system of K discretized mass-conservation equations for one size class of suspended sediment (one Eq. (43) for each computational point C along the σ -direction line) is to be solved in order to compute its primary sediment unknowns: K volumetric concentrations for a particular size class of suspended sediment, one concentration at each computational point C along the σ -direction line.

The system has a tridiagonal matrix of coefficients and it is easily solved by using a standard double-sweep procedure, described in e.g. Carnahan, Luther and Wilkes (1969).

Auxiliary Relations and Active-Layer Considerations

One should note that the numerical procedure for solution of the sediment equations is formulated above without reference to the specific empirical relations which ultimately must be invoked to evaluate the auxiliary relations. This allows for use of any suitable empirical relation when evaluating a particular auxiliary relation, and renders the formal numerical procedure independent of any specific empirical relation.

Auxiliary Relations

The empirical relations adopted herein to evaluate near-bed concentration C_a , components of bedload flux q_b , active-layer thickness E_m , active-layer floor 'source' S_F , fall velocity w_f , mass-diffusion coefficient D and density of mixture containing water and suspended sediment ρ , are the same ones that are used as examples in the discussion of the nature of auxiliary relations in Chapter II.

Near-Bed Concentration

The near-bed concentration C_a is evaluated using Van Rijn's (1984b) expression:

$$C_{a_{ks}} = 0.015 \frac{D_{ks}}{a} \frac{T_{ks}^{1.5}}{D_{*_{ks}}^{0.3}} \quad (54)$$

in which

$$D_{*_{ks}} = D_{ks} \left[\frac{(s-1)g}{v^2} \right]^{1/3} \quad = \text{dimensionless particle diameter;}$$

$$T_{ks} = \frac{u_*^2 - (u_{*c})_{ks}^2}{(u_{*c})_{ks}^2} \quad = \text{transport-stage parameter;}$$

$$u_* = \frac{u\sqrt{g}}{C} \quad = \text{effective bed-shear velocity;}$$

$$C = 18 \log \left(\frac{12d}{3D_{90}} \right) \quad = \text{grain Chezy coefficient;}$$

$$s = \frac{\rho_s}{\rho} \quad = \text{dimensionless sediment density;}$$

and a =height above the bed, defined as one half of the average dune height, g =gravity; ν =kinematic viscosity; d =depth; D_{90} =characteristic particle diameter for sediment mixture; u_{*c} =critical shear velocity evaluated from Shields diagram; u =depth-averaged velocity component.

Components of Bedload Flux q

The theoretical bedload capacity is computed by using the empirical relations proposed by Van Rijn (1984a). A component of the theoretical (i.e. equilibrium, or capacity) bedload flux in, for example, the ξ -direction can be expressed, for the ks -th size class, as:

$$\left(q_b^t \right)_{ks} = 0.053 \cdot \rho_s \cdot \sqrt{(s-1)gD_{ks}} D_{ks} \frac{T_{ks}^{2.1}}{D_{*ks}^{0.3}} \quad (55)$$

where all variables have the same meaning as in Eq.(54).

Van Rijn's original expression, representing volume flux, is multiplied herein by the sediment density in order to obtain mass flux, to be consistent with the other terms in the sediment equations.

Hiding Factor

Hiding effects are taken into account through the Karim, Holly and Yang (1987) empirical relation for the hiding factor:

$$\left(\zeta_h \right)_{ks} = \left(\frac{D_{ks}}{D_{50}} \right)^{0.85} \quad (56)$$

Transport-Mode Allocation Parameter

Van Rijn (1984b) presented theoretical-experimental curves relating the ratio of suspended load to total load to the ratio of bed-shear velocity to fall velocity. The ratio of suspended load to total load is adopted herein as the transport-mode allocation parameter γ for the k_s -th size-class particles. The graphical results of Van Rijn (Van Rijn (1984b), Figure 18) are approximated by:

$$\gamma_{k_s} = \left(\frac{q_s}{q_t} \right)_{k_s} = 0.25 + 0.325 \ln \left(\frac{u_*}{w_{f_{k_s}}} \right) \quad 0.4 < \frac{u_*}{w_{f_{k_s}}} < 10 \quad (57)$$

where γ =transport-mode allocation parameter, q_s =suspended load, q_t =total load, w_f =fall velocity, and u_* =bed-shear velocity.

Active-Layer Considerations

It is pointed out in Chapter II that there is a marked difference in the treatment of the active layer during erosion as distinguished from deposition. During persistent erosion, the active layer is described as a mixing layer. As the bed elevation descends, erosion proceeds through the active stratum (underlying the active layer) with the active-layer floor changing its elevation. The active-layer thickness during erosion is defined, according to the conceptualization of Bennett and Nordin (1977), as proportional to the erosion that occurs over the current computational time step:

$$E_m = -c(z_b^{n+1} - z_b^n) \quad (58)$$

where c is a parameter.

As the bed surface approaches an armored condition, then Eq. (58) leads to a zero active-layer thickness. In such situations Borah's (Borah et al, 1982) armored-layer thickness can be used as a limiting value for the active-layer thickness:

$$E_m = -c(z_b^{n+1} - z_b^n) + \frac{1}{\sum_{k_s=m}^{KS} \beta_{k_s}} \frac{D_m}{1-p} \quad (59)$$

where D_m is the smallest nonmoving size-class.

Movement of the active-layer floor ($z_b - E_m$) generates the active-layer floor 'source' S_F . A consequence of Eq. (58) is that the active-layer floor may be descending either more quickly or more slowly than the bed elevation, depending on the current erosion rate, and that in principle the active-layer floor may even happen to rise during erosion.

If the active-layer floor descends during erosion (which is the usual case) then the active-layer floor 'source' $(S_F)_{ks}$ for the ks -th size class, when discretized over the time step, has the following form:

$$S_{F_{ks}} = -\frac{\rho_s(1-p)}{\Delta t} \left[(z_b^{n+1} - E_m^{n+1}) - (z_b^n - E_m^n) \right] (\beta_s)_{ks} \quad (60)$$

where $(\beta_s)_{ks}$ is the ks -th size-class fractional representation in the active stratum. One should note that the active-stratum size distribution remains unchanged in this case.

On rare occasions, when the erosion rate undergoes an extremely sharp decrease over the computational time step, the active-layer floor may actually rise during erosion. If this happens, then the active-layer floor 'source', discretized over the time step, has the form:

$$S_{F_{ks}} = -\frac{\rho_s(1-p)}{\Delta t} \left[(z_b^{n+1} - E_m^{n+1}) - (z_b^n - E_m^n) \right] \frac{\beta_{ks}^{n+1} + \beta_{ks}^n}{2} \quad (61)$$

where β_{ks} is the ks -th size-class fractional representation in the active layer. In such a case the active-stratum size distribution changes, as active-layer material is released to it, and in principle this calls for inclusion of the active-stratum mass-conservation equation in the simultaneous solution of sediment equations. However since such situations are expected to be rare, they are handled explicitly herein, by updating the active-stratum size-distribution at the end of computational time step, when necessary.

During persistent deposition, the active layer is described as a deposition layer. Newly deposited material is added to the existing material in the active layer and assumed to be fully mixed with it. The active-layer floor elevation is assumed to remain constant during deposition and the active-layer thickness is defined as:

$$E_m^{n+1} = E_m^n + (z_b^{n+1} - z_b^n) \quad (62)$$

while the active-layer floor 'source' is equal to zero:

$$S_{F_{ks}} = 0 \quad (63)$$

The definition of the active layer, evaluation of the active-layer thickness and treatment of the active-layer floor 'source' depend on whether erosion or deposition occurs during the current computational time step. However, the tendency toward erosion or deposition is itself a part of the solution for the computational step. To resolve this ambiguity, one can make use of an iterative solution of the sediment equations. At the beginning of each iteration either erosion or deposition is assumed, based on whether erosion or deposition occurred during the previous iteration. Then one can easily compute the derivatives of the active-layer thickness E_m and active-layer floor 'source' $(S_F)_{ks}$ with respect to sediment variables, evaluated for previous-iteration values of sediment variables. These derivatives are then used to determine the coefficients in the discretized sediment equations.

Fall Velocity

In a clear still fluid the particle fall velocity w_f of a solitary sand particle smaller than about 100 μm (Stokes range) can be described by:

$$w_{f_{ks}} = \frac{1}{18} \frac{(s-1)gD_{ks}^2}{\nu} \quad (64)$$

For suspended-sand particles in the range 100-1000 μm , the following equation, as proposed by Zanke (1977), is used:

$$w_{f_{ks}} = 10 \frac{\nu}{D_{ks}} \left[\sqrt{1 + \frac{0.01(s-1)gD_{ks}^3}{\nu^2}} - 1 \right] \quad (65)$$

For particles larger than about 1000 μm the following equation, as proposed by Van Rijn (1982), is used:

$$w_{f_{ks}} = 1.1 \sqrt{(s-1)gD_{ks}^2} \quad (66)$$

Vertical Mass-Diffusion Coefficient D_v

As described by van Rijn (1984b), the vertical mass-diffusion coefficient D_v is related to the diffusion of fluid momentum by:

$$D_v = \beta_d \phi A_v \quad (67)$$

The β_d -factor describes the difference in the diffusion of a discrete sediment particle and the diffusion of a fluid 'particle' (or small coherent fluid structure) and is assumed to be constant over the depth:

$$\beta_d = 1 + 2 \left(\frac{w_{f,ks}}{u_*} \right)^2 \quad 0.1 < \frac{w_{f,ks}}{u_*} < 1 \quad (68)$$

The ϕ -factor expresses the damping of the fluid turbulence by the sediment particles and is assumed to be dependent on the local sediment concentration:

$$\phi = 1 + \left(\frac{C}{C_0} \right)^{0.8} - 2 \left(\frac{C}{C_0} \right)^{0.4} \quad (69)$$

where $C_0 = 0.65$ = maximum volumetric near-bed concentration; C = total volumetric concentration.

The horizontal diffusivities in CH3D are assigned values.

Density of Mixture Containing Water and Suspended Sediment

According to Zhou and McCorquodale (1992), local fluid density is related to the local values of suspended-sediment concentration as follows:

$$\rho = \rho_r + C \left(1 - \frac{1}{s-1} \right) \quad (70)$$

where ρ_r = the reference density of clear water, possibly influenced by temperature and/or salinity.

CHAPTER IV

DESCRIPTION OF THE SEDIMENT-OPERATIONS PROGRAM MODULE

Introduction

A separate sediment-operations program module, based on physical and numerical principles described in Chapters II and III, has been developed as an integral part of the CH3D code. Dedication of a separate program module to sediment operations is made possible by the short-term uncoupling of hydrodynamics and sediment operations. However, the sediment module fully communicates with the rest of the CH3D code. Hydrodynamics operations provide all necessary hydrodynamic input required by the sediment module (velocities, depths, etc.). The sediment module, in turn, provides changes in bed elevations (i.e. depths), distribution of active-layer size fractions (i.e. friction coefficients) and density (due to the presence of suspended sediment) back to the CH3D hydrodynamics operations.

A block diagram for the sediment-operations program module is shown in Figure 5. The sediment module comprises a main subroutine for sediment operations, SMAIN, and 51 other subroutines. Subroutine RHOCON (called from subroutine CH3DDE of the original CH3D code) is the only subroutine outside of the sediment module that is also part of the sediment operations. The basic function of SMAIN is to manage all other sediment subroutines (except for subroutine RHOCON).

The sediment module has two major blocks: preparatory operations and sediment computations. The division between the blocks, however, is not sharp for a few subroutines used in both of them.

Data defining initial and boundary conditions are read in dimensional form and made nondimensional in the same subroutine that reads the particular data. All computations are made with dimensionless variables. The only exception is the evaluation of auxiliary relations based on empirical expressions. Empirical expressions not only require dimensional variables, but may also be dimensionally inconsistent. Thus, all necessary variables (both hydrodynamic and sediment) are made dimensional upon entry to a subroutine that evaluates a particular auxiliary relation, and the computed auxiliary relation is then made dimensionless upon return from the same subroutine.

Sediment boundary conditions are associated with control-volume faces, rather than cell-centered computational points. Hydrodynamics boundary conditions are also mostly associated with control-volume faces (impermeable or river boundaries, for example),

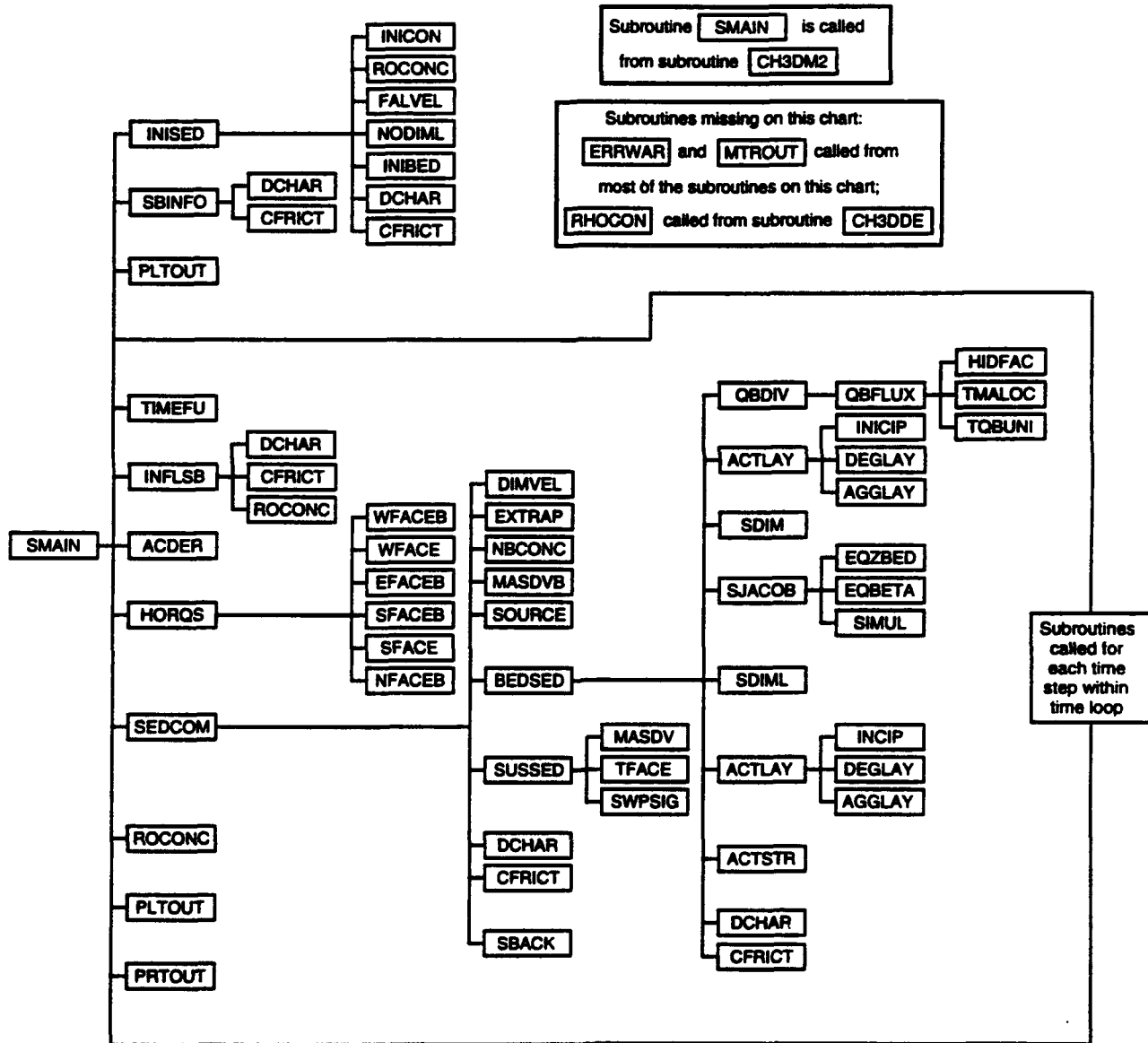


Figure 5. Summary Block Diagram of Sediment-Operations Program Module.

except for tidal boundaries, that are associated with cell-centered points. If a sediment boundary coincides with a hydrodynamics boundary assigned to a control-volume face (e.g. a river boundary with the discharge assigned at the control-volume face), the actual position of both boundaries is the same. However, if a sediment boundary coincides with a hydrodynamic tidal boundary with a tidal condition assigned at a cell-centered point, the inflow sediment boundary is then associated with an 'inner' face (pointing towards the inside of the computational domain) of the control volume built around the tidal point. Thus, the sediment computational domain coincides with the hydrodynamics computational domain except at tidal points, which are excluded from the sediment computations.

Sediment variables are associated with cell-centered computational points and stored in appropriate arrays accordingly. Thus, sediment boundary conditions, even though related to control-volume faces, are in the code stored at the 'outer' points (where 'outer' means the closest neighboring point outside the sediment computational domain).

Preparatory Operations

Preparatory operations serve to define the initial and boundary conditions for sediment computations.

Subroutine INISED reads general sediment parameters and manages the group of subroutines that define initial conditions. INICON reads initial suspended-sediment concentrations, expressed as mass of sediment particles with respect to the total mass of the mixture of water and suspended sediment. At this point subroutine ROCONC is called, within a loop on all computational points, to initialize the density of the water and suspended sediment mixture at the particular computational point. Suspended-sediment concentrations, read by INICON, are multiplied by the density of water and suspended-sediment mixture, computed in ROCONC, to yield volumetric concentrations, expressed as mass of sediment particles with respect to the volume of the water and suspended-sediment mixture. Subroutine FALVEL computes fall velocities for each sediment size class. Subroutine NODIML computes dimensionless numbers. Subroutine INIBED reads the initial number of bed material strata below the active layer. It also reads initial depths of the active layer and all the strata as well as their initial size-fraction distributions. Finally, subroutines DCHAR and CFRICT are called, within the loop on all bed computational points, to initialize the characteristic grain diameters D50 and D90, and the friction coefficient, respectively, at the particular computational point.

Subroutine SBINFO defines the sediment boundary conditions. SBINFO first reads boundary-condition information for sediment computations: position of the boundary

point and the type of boundary (inflow, impermeable, or outflow boundary). Any inflow-boundary point requires a known distribution of active-layer size fractions and suspended-sediment concentrations for each size class, all as a function of time. Therefore, for each inflow boundary point SBINFO also reads sequence numbers of specific time functions used as boundary conditions, while the time functions themselves are read at the end of all input data (subroutine TIMEFU) in order to optimize memory use. Subroutine SBINFO also calls subroutines DCHAR and CFRICT to initialize the characteristic grain diameters D50 and D90, and the friction coefficient, respectively, at the particular inflow boundary point.

At this point subroutine PLTOUT is called, as a part of preparatory operations, to store computational-point Cartesian coordinates and initial bed elevations to be used within an eventual plot output.

Sediment Computations

While the preparatory-operations block is called only once, prior to the beginning of sediment computations, the sediment-computation block is called for each time step within the CH3D time loop. Within the sediment-computations block, SMAIN calls subroutines TIMEFU and INFLSB to evaluate boundary conditions, subroutines ACDER and HORQS to evaluate auxiliary and explicit terms in the suspended-sediment equations, subroutine SEDCOM to perform sediment computations, subroutine ROCONC to evaluate the new density of the water and suspended-sediment mixture, and subroutines PLTOUT and PRTOUT to manage plot and print output.

At the beginning of each time step, subroutine TIMEFU reads and interpolates time functions used as boundary conditions for sediment computations. Subroutine INFLSB evaluates active-layer size fractions and suspended-sediment concentrations at the current time, for inflow-boundary points. INFLSB also evaluates secondary sediment unknowns, characteristic grain diameters D50 and D90, friction coefficients, and the density of the water and suspended-sediment mixture, by using DCHAR, CFRICT and ROCONC, respectively, at the current time, for inflow-boundary points. Again, concentrations evaluated at inflow boundary points are multiplied by density, computed in ROCONC, to yield volumetric concentrations.

Subroutine ACDER evaluates the so-called auxiliary concentration derivatives (to be used in further computations of concentration derivatives, as in Eqs. (B26) to (B28), for example) for all computational points at the previous time and for inflow-boundary points at the current time. Subroutine HORQS manages subroutines WFACEB, WFACE,

EFACEB, SFACEB, SFACE, and NFACEB, that compute and store (explicit) horizontal advection and diffusion fluxes (terms (3) to (10) in Eq. (42)) through the west and south faces of the control volumes built around computational points within the entire computational domain, for all size classes of suspended sediment. Flux through the west (south) face for one computational point is a flux through the east (north) face for the appropriate neighboring point. Subroutine WFACEB is called if the west face of the control volume is a boundary, while subroutine WFACE is called if it is not, and subroutine EFACEB is called if the east face of the control volume (west face for the appropriate neighboring point) is a boundary. Similarly, subroutine SFACEB is called if the south face of the control volume is a boundary, while subroutine SFACE is called if it is not, and subroutine NFACEB is called if the north face of the control volume (south face for the appropriate neighboring point) is a boundary.

Sediment computations are managed by subroutine SEDCOM. First, SEDCOM manages the loop on all locations (i,j) in a horizontal plane (except for tidal boundaries), with the group of subroutines DIMVEL, EXTRAP, NBCONC, MASDVB and SOURCE, called to compute source term; subroutine BEDSED called to manage bed-sediment computations (solution of the discretized global mass-conservation equation for bed sediment and the mass-conservation equations for active-layer sediment at the bed point); and subroutine SUSSED called to manage suspended-sediment computations (solution of the discretized mass-conservation equations for suspended sediment along a vertical-direction line above the same bed point).

After the sediment computations are completed, a zero-gradient condition is applied to tidal outflow boundary points, with subroutines DCHAR and CFRICT used to evaluate characteristic grain diameters D50, D90, and friction coefficient, respectively. Finally, subroutine SBACK is called to evaluate the sediment-computation feedback, i.e. to compute new depths and Manning friction coefficients to be used in the hydrodynamics operations of CH3D.

Source-Term Computations

Subroutine DIMVEL computes the dimensional physical components of depth-averaged velocities, to be used in empirical relations. Subroutine EXTRAP computes the extrapolation coefficient used in the 'deposition' source computations (Eq. (31)). MASDVB computes mass-diffusion coefficients at the bed, used in the 'erosion' source computations. Finally, subroutine SOURCE computes the 'deposition' and 'erosion' source terms.

Bed-Sediment Computations

Subroutine QBDIV computes the divergence of the bedload flux vector. QBFLUX computes the bedload flux for one sediment size class. TMALOC computes the transport-mode allocation parameter, HIDFAC evaluates the hiding factor and TQBUNI computes the theoretical bedload flux (or transport capacity) for uniform-size sediment.

Subroutines SJACOB, EQZBED, EQBETA, SIMUL and ACTLAY are part of the Newton-Raphson iterative solution for the system of bed-sediment equations at a bed point (one global mass-conservation equation for bed sediment, and KS mass-conservation equations for active-layer sediment). Subroutine SJACOB loads the Jacobian matrix of the system of discretized and linearized sediment equations. EQZBED computes coefficients in the global mass-conservation equation for bed sediment (z_b -equation). EQBETA computes coefficients in the mass-conservation equation for the ks-th size class of active-layer sediment (β -equation). All coefficients are presented in Appendix C. Subroutine SIMUL solves the system of linear equations.

Subroutine ACTLAY manages the active-layer operations. If degradation (i.e. erosion) is anticipated during iterations, then INCIP defines the incipient motion, i.e. identifies the smallest non-moving grain size. DEGLAY then computes the active-layer thickness, active-layer floor source and their derivatives with respect to sediment variables. If aggradation (deposition) is assumed during iterations, the active layer thickness, active-layer floor source and their derivatives are computed by AGGLAY. Subroutine ACTLAY (together with AGGLAY or INCIP and DEGLAY) is also called prior to the Newton-Raphson iterations to evaluate the active layer thickness, active-layer floor source and their derivatives at the zero-iteration level.

Subroutines SDIM and SDIML are used to test the bed-sediment computations; they do not influence the computations in any way. Subroutine SDIM makes all necessary sediment variables dimensional, so that bed-sediment computations could also be performed in a dimensional environment. After the bed computations are completed, subroutine SDIML makes all sediment variables dimensionless again.

After the Newton-Raphson iterative solution is obtained at a point, subroutine ACTSTR is used to update the active-stratum thickness and size-fraction distribution if appropriate. DCHAR computes the characteristic grain size D50. It also computes the sediment size D90 used by CFRICT to evaluate the friction coefficient related to grain roughness.

An important feature of the sediment-module structure is that whenever an empirical expression is used (e.g. to compute bedload flux, hiding factor etc.) its evaluation is restricted to a single subroutine independent of the rest of the code. This makes it possible to incorporate the best available empirical information, even site-specific, without changing the rest of the code.

Suspended-Sediment Computations

Subroutine MASDV computes and stores the vertical mass-diffusion coefficients at the top faces of control volumes built around computational points along a vertical-direction line, for all size classes of suspended sediment.

Subroutine TFACE computes and stores the (explicit) vertical advection fluxes (terms (11) and (12) in Eq. (42)) through the top faces of control volumes built around computational points along a vertical-direction line, for all size classes of suspended sediment. Flux through the top face for one computational point is a flux through the bottom face for the appropriate neighboring point.

Subroutine SWPSIG is called from SUSSED for each size class of suspended sediment. SWPSIG evaluates coefficients a, b, c, and d, in the discretized mass-conservation equations for one size class of suspended sediment (Eq. (43)) and performs the double-sweep solution procedure along a vertical-direction line.

The last two subroutines, used repeatedly in the sediment module, are ERRWAR, which prints error and warning messages, and MTROUT, which prints matrix-form output.

Subroutine RHOCON (called from subroutine CH3DDE of the original CH3D code) computes the density of the water and suspended-sediment mixture to be used in the hydrodynamic computations of CH3D. Subroutine CH3DDE evaluates the 'initial' density of water (with or without temperature and/or salinity effects). At this point subroutine RHOCON is called to compute the density of the water and suspended-sediment mixture. The mixture density is nondimensionalized differently in the hydrodynamics and sediment equations. Thus, the dimensionless densities of the water and suspended-sediment mixture are evaluated by two slightly different subroutines, RHOCON and ROCONC, and stored in two different arrays.

Memory and Time Requirements

The required memory size for the sediment module is obtained by adding the following array sizes, multiplied by the appropriate number of arrays:

Array size (bytes)	Number of arrays
$(IM+1)*(JM+1)*(KM+1)*(KSMAX)*8$	2
$(IM+1)*(JM+1)*(K)*(KSMAX)*8$	8
$(IM+1)*(JM+1)*(LMAX)*(KSMAX)*8$	1
$(IM+1)*(JM+1)*(KM+1)*8$	3
$(IM+1)*(JM+1)*(KM+1)*4$	1
$(IM+1)*(JM+1)*(KSMAX)*8$	4
$(MAXBP)*(KM+1)*(KSMAX)*8$	3
$(IM+1)*(JM+1)*(LMAX)*8$	1
$(IM+1)*(JM+1)*8$	8
$(IM+1)*(JM+1)*4$	3
$(KM+1)*(KSMAX)*8$	3
$(KM)*(KSMAX)*8$	2
$(MAXBP)*(KSMAX)*8$	3
$(KSMAX)*(NSVAR)*8$	1
$(NSVAR)*(NSVAR1)*8$	1
$(KSMAX)*8$	23
$(LMAX)*8$	1
$(LMAX)*4$	1
$(NSBINF)*4$	1
$(NSVAR)*8$	2
$(NSVAR)*4$	3

where:

$IM = ICELLES+2$ $ICELLES$ = Exact number of computational cells in the longest KSI-direction computational row

$JM = JCELLS+2$ $JCELLS$ = Exact number of computational cells in the longest ETA-direction computational column

KM = Exact number of computational points in the vertical direction

$KSMAX$ = Exact number of sediment size classes

$LMAX$ = Maximum number of bed strata

$MAXBP = 2*(IM+JM)$ Maximum number of boundary points

$NSBINF = 2*MAXBP$ Maximum number of sediment boundary data indentifiers (sequence numbers of sediment boundary data in the list of time-dependent data) stored in the INFOSB array

$NSVAR = 1+KSMAX$ Number of bed-sediment unknowns at a point

$NSVAR1 = NSVAR+1$ Dimension of the bed-sediment Jacobian matrix

The sediment-module memory size for the Old River model ($ICELLES=51$, $JCELLS=24$), with 3 sediment size classes and a maximum of 10 bed strata, is about 4.5 Mb. More than 80% of that memory is used by the four-dimensional arrays.

The CPU time required is highly dependent on the structure of the model data and the type of computer and compiler being used. The CPU time required for the runs of the Old River model on the University of Iowa's HP 750 computer is reported along with the sediment-module tests in Chapter V of this report.

Sediment Module Input Data Guide (May 1993)

This sediment module input-data guide is limited essentially to the formal structure and requirements of the input data; the user may need to refer to the rest of this report for further guidance on recommended parameter values, etc.

In the data guide, "rec" refers to the logical record number in the input data stream, and "var" refers to the variable name as it is used in the code itself. The name of the subroutine in which particular records are read is given as a banner entry preceding the usual record description.

An input-data guide for the remainder of the CH3D code is presented in Appendix D. The only data related to sediment operations read outside the sediment module are two parameters: ISCOM and NTSED0. These parameters are read in the "timestep info" record (record 2 in subroutine CH3DIR), shown in Appendix D. The "Timestep info" record is repeated here for convenient reference.

Input Data Guide

rec	var	Format (columns)	Variable description and remarks
*SUBROUTINE CH3DIR			
Note: "Timestep info" record data are read from the main input file (file 4 : main.inp)			
Timestep info:			
	DUMMY		
	IT1	I8 (1-8)	
	IT2	I8 (9-16)	
	DT	F8.0 (17-24)	
	ISTART	I8 (25-32)	
	ITEST	I8 (33-40)	
	ITSALT	I8 (41-48)	
	ISCOM	I8 (49-56)	=0 No sediment computations =1 Sediment computations are performed
	NTSED0	I8 (57-64)	Number of time steps before sediment computations are initiated
Note: All following data are read from sediment-computation input file (file 80: sed.inp)			
*SUBROUTINE SMAIN			
1	NBUGS		

	NBUGE	5(2I8) (1-80)	Pairs of debug-output flags 5 pairs per record 100 pairs total
	<p>Debug output for subroutine M is written if(NT.ge.NBUGS(M).and.NT.le.NBUGE(M))</p> <p>Subroutine debug identifications M :</p>		
	M=1-SMAIN	13-TIMEFU	36-ERRWAR
	2-SEDCOM	14-INFLSB	37-MTROUT
	3-INISED	15-EXTRAP	38-PRTOUT
	4-INICON	16-NBCONC	39-PLTOUT
	5-ROCONC	17-MASDVB	40-ACDER
	6-FALVEL	18-SOURCE	41-HORQS
	7-NODIML	19-BEDSED	42-WFACEB
	8-INIBED	20-QBDIV	43-WFACE
	9-DIMVEL	21-QBFLUX	44-EFACEB
	10-DCHAR	22-HIDFAC	45-SFACEB
	11-CFRICT	23-TMALOC	46-SFACE
	12-SBINFO	24-TQBUNI	47-NFACEB
	25-ACTLAY	48-SUSSED	
	26-INCIP	49-MASDV	
	27-DEGLAY	50-TFACE	
	28-AGGLAY	51-SWPSIG	
	29-SDIML	52-SBACK	
	30-SJACOB	53-RHOCON	
	31-EQZBED		
	32-EQBETA		
	33-SIMUL		
	34-SDIM		
	35-ACTSTR		
2	NPRSED	I8 (1-8)	Time-step frequency for printing sediment-computation results (file 81: prtseed.out)
	NDIAGS	I8 (9-16)	Time-step frequency for printing sediment-computation diagnostics (max. errors, number of iterations etc.)
	NPLOT	I8 (17-24)	Plot output file (FORT ref num) (filename: pltsed.out) NPLOT=0 : no plot output NPLOT>0 : short output (bed-surface elevation and active-layer size fractions) NPLOT<0 : long output (all of the above plus: cell-centered depths, all three cell-centered Cartesian velocity components, suspended-sediment concentrations and suspended-sediment source terms)
3	NPLT	I8 (25-32)	Time-step frequency for NPLOT output
	IDENS	I2 (1-2)	Option for printing: density of water & suspended mixt! (1 = print ; 0 = no print)
	ICONC	I2 (3-4)	suspended-sedim. concentrations
	IZBED	I2 (5-6)	bed elevation
	IDZBED	I2 (7-8))	bed-elev change over time step
	IDZB0	I2 (9-10)	cumulative bed-elev change
	IEM	I2 (11-12)	active-layer depth
	IBETA	I2 (13-14)	active-layer size fractions

4	ILSTR	I2 (15-16)	number of strata
	ISTRDP	I2 (17-18)	depths of strata
	IBSTR	I2 (19-20)	strata size fractions
	ID50	I2 (21-22)	characteristic grain diameter
	ICFRIC	I2 (23-24)	friction coefficient
	ISORCD	I2 (25-26)	susp-sed 'deposition' source
	ISORCE	I2 (27-28)	susp-sed 'erosion' source
	ISBTYP	I2 (29-30)	sediment-comput boundary types
	IBED	I2 (1-2)	Option for including/excluding: complete bed-sed computations (1 = include ; 0 = exclude)
	ISUS	I2 (3-4)	complete sus-sed computations
	IADV	I2 (5-6)	i-direction sus-sed advection
	IDIF	I2 (7-8))	i-direction sus-sed diffusion
	JADV	I2 (9-10)	j-direction sus-sed advection
	JDIF	I2 (11-12)	j-direction sus-sed diffusion
KADV	I2 (13-14)	k-direction sus-sed advection	
*SUBROUTINE INISED			
1	ISDBG	I8 (1-8)	1 : sediment debug output at chosen points 0 : no sediment debug
	IBSDIM	I8 (9-16)	1 : dimensional bed-sed comp 0 : dimensionless bed-sed comp
2	IB,JB,KB	3I8 (1-16)	Position of the points chosen for sediment debug output Last record must have IB<0 Records 2 omitted if ISDBG=0
3	SDIAM	5F16.0 (1-80)	Standard sediment sizes (m) defining size intervals 5 values per record KSMAX values altogether (KSMAX=number of size classes)
4	VISCOS	F16.0 (1-16)	Kinematic viscosity of water (m ² /s)
5	SDENS	F8.0 (1-8)	Sediment particle density (t/m ³)
6	POROS	F8.0 (9-16)	Porosity of sediment mixture in the bed
	THETAS	F8.0 (1-8)	Implication factor used in sediment computations
7	STRMAX	F8.0 (9-16)	Maximum depth of active stratum (m)
	ALMIN	F8.0 (17-24)	Minimum depth of active layer (m), criterion for closing a deposition layer
	ABED	F8.0 (25-32)	Near-bed position 'a' (m)
	DABED	F8.0 (33-40)	Near-bed position increment (m)
	EPSZB	F16.0 (1-16)	Threshold value (m) of bed-elevation changes for terminating iterations during sediment comput at a point
	EPSBET	F16.0 (16-32)	Threshold value (-) of active-layer size-fraction changes for terminating iterations during sediment comput at a point
8	MAXITS	I8 (1-8)	Maximum number of iterations during bed-sed computations at a bed point
9	DH	F8.0 (1-8)	Horizontal mass diffusivity (m ² /s)
*SUBROUTINE INICON			

Note: suspended-sediment concentrations are initially assigned a negative value (= -0.001) at all computational points, in order to distinguish points inside the flow domain (where concentration is computed) from points outside the flow domain (conc remains equal to -0.001)

1	IPAR	I8 (1-8)	<p>Parameter indicating chosen option for furnishing initial data</p> <p>IPAR=0 : only record 2 is furnished, records 3-5 are omitted</p> <p>IPAR=1 : records 2-4 are furnished, records 5 are omitted</p> <p>IPAR=-1 : records 5 are furnished, records 2-4 are omitted</p>
<p>Record 2 is repeated KMAX times (where KMAX is the number of computational points along the vertical direction) starting with the point k=KMAX next to the free surface, until the entire set of vertical concentration profiles is defined for all size classes</p>			
2	CREAD	10F8.0 (1-80)	<p>Default suspended-sediment concentrations (-), for all size classes at a point, KSMAX values (KSMAX=number of size classes)</p>
<p>Record 3 is repeated KMAX times (where KMAX is the number of computational points along the vertical direction) starting with the point k=KMAX next to the free surface, until the entire set of vertical concentration profiles is defined for all size classes</p> <p>Each set of vertical concentration profiles, for all size classes, defined by KMAX records 3, is followed by one or more records 4</p> <p>Record(s) 4 specify points to which set of vertical concentration profiles, for all size classes, defined by KMAX records 3, applies</p> <p>IAXES<0 : end of records 4 related to one particular set of records 3</p> <p>IJ<0 : end of records 3 and 4 related to initial suspended-sediment concentrations</p>			
3	CREAD	10F8.0 (1-80)	<p>Other-than-default suspended-sediment concentrations (-) for all size classes at a point KSMAX values (KSMAX=number of size classes)</p>
4	IAXES	I8 (1-8)	<p> AXES =1 : XI coordinate line</p>
	IJ	I8 (9-16)	<p> AXES =2 : ETA coordinate line</p>
	IJS	I8 (17-24)	<p> J specifies particular XI or ETA coordinate line</p>
	IJE	I8 (25-32)	<p>Record 3 applies to points IJS to IJE along the particular</p>

5	PCONC	10F8.0 (1-80)	coordinate line Initial suspended-sediment concentrations (-), for all size classes at a point KSMAX values (KSMAX=number of size classes)
<p>Record 5 is repeated KMAX times (where KMAX is number of computational points along the vertical direction) starting with the point k=KMAX next to the free surface, until the entire set of vertical concentration profiles is defined for all size classes</p> <p>Set of KMAX records 5 is repeated for each vertical direction line within the flow domain, row-by-row starting from the first row inside the domain</p>			
*SUBROUTINE INIBED			
<p>Note: bed elevations, active-layer depth and size fractions, number of strata, and each stratum depth and size fractions, are all initially set to zero at all points</p>			
1	RELO	F8.0 (1-8)	Relative elevation used to evaluate initial bed-surface elevations (m)
2	IPAR	I8 (1-8)	Parameter indicating chosen option for furnishing initial data IPAR=0 : records 3 and 4 are furnished, records 5-9 are omitted IPAR=1 : records 3-7 are furnished, records 8-9 are omitted IPAR=-1 : records 8-9 are furnished, records 3-7 are omitted
3	ITYPBA	I8 (1-8)	Type of size-fraction distribution for active layer (default value)
	LSTRAT	I8 (9-16)	Number of strata below the active layer at the point (default value)
	ITYPBS	8I8 (17-80)	Types of size-fraction distributions for strata LSTRAT values (default)
4	EMINIT	I8 (1-8)	starting from active stratum Initial active-layer depth (m) (default)
	STRDEP	I8 (9-16) 8F8.0 (17-80)	Not used Initial strata depths (m) LSTRAT values (default) starting from active stratum

<p>Records 5,6 are followed by one or more records 7 Record(s) 7 specify points to which records 5,6 apply IAXES<0 : end of records 7 related to particular records 5,6 IJ<0 : end of records 5,6 and 7 related to initial bed-material data</p>			
5	ITYPBA	I8 (1-8)	Other-than-default type of size-fraction distribution for active layer
	LSTRAT	I8 (9-16)	Other-than-default number of strata below the active layer at the point
	ITYPBS	8I8 (17-80)	Other-than-default types of size-fraction distributions for strata LSTRAT values starting from active stratum
6	EMINIT	I8 (1-8)	Other-than-default initial active-layer depth (m)
	STRDEP	I8 (9-16) 8F8.0 (17-80)	Not used Other-than-default initial strata depths (m) LSTRAT values starting from active stratum
7	IAXES	I8 (1-8)	IIAXES =1 : XI coordinate line IIAXES =2 : ETA coordinate line
	IJ	I8 (9-16)	IIJ specifies particular XI or ETA coordinate line
	IJS	I8 (17-24)	Records 5,6 apply to points IJS
	IJE	I8 (25-32)	to IJE along the particular coordinate line
8	ITYPBA	I8 (1-8)	Type of size-fraction distribution for active layer
	LSTRAT	I8 (9-16)	Number of strata below the active layer at the point
	ITYPBS	8I8 (17-80)	Types of size-fraction distributions for strata LSTRAT values starting from active stratum
9	EMINIT	I8 (1-8) I8 (9-16)	Initial active-layer depth (m)
	STRDEP	8F8.0 (17-80)	Not used Initial strata depths (m) LSTRAT values starting from active stratum
<p>Records 8 and 9 are repeated for each point at the bed, within the flow domain, row-by-row, starting from the first row inside the domain</p>			
10	ITYPB	I8 (1-8)	IIITYPB : size-fraction distribution type, must agree with one of types associated with active layer or strata at computational points
	BREAD	9F8.0 (9-80)	Size-fraction distribution (-) KSMAX values

(KS MAX=number of size classes)

Last record 10 must have ITYPB<0

***SUBROUTINE SBINFO**

The following record is read:
FIRST for all points along ETA-direction boundary line(s)
THEN for all points along XI-direction boundary line(s)

1	I	I8 (1-8)	III : XI-direction index of the sediment-computation boundary point Last record 1 must have I<0
1	J	I8 (9-16)	J : ETA-direction index of the sediment-computation boundary point
	ITYP	I8 (17-24)	Boundary-condition type associated with the sediment-computation boundary point
	NSEQB	I8 (25-32)	Sequence number of the active-layer size-fraction distribution in list of time-dependent data
	NSEQC	I8 (33-40)	Sequence number of the set of suspended-sediment vertical concentration profiles in list of time-dependent data

ITYP=1 : inflow boundary
ITYP=-1 : outflow boundary, NSEQB, NSEQC not used
ITYP=0 : assigned automatically to impermeable boundary

***SUBROUTINE TIMEFU**

The following records load time-dependent boundary data

1	IDAYR	I8 (1-8)	Day and hour defining time of reading time-dependent data
	IHOURL	I8 (9-16)	
2	NOBT	I16 (1-16)	Sequence number (1,2,.....)
	BTR	8F8.0 (17-80)	Active-layer size-fraction distribution (-), its sequence number NOBT consistent with the NSEQB sequence numbers assigned to sediment-computation boundary points with ITYP=1 (subroutine SBINFO, record 1)

The total number of records 2 must be equal to total number of different active-layer size-fraction distributions assigned in SBINFO

3	NOCT	I16 (1-16)	Sequence number (1,2,.....)
	CTR	8F8.0 (17-80)	Set of suspended-sediment

4	CTR	I16 (1-16) 8F8.0 (17-80)	concentrations (-), at point k=KMAX next to the free surface, for all size classes, its sequence number NOCT consistent with the NSEQC sequence numbers assigned to sediment-computation boundary points with ITYP=1 (SBINFO, record 1) Not used Set of suspended-sediment concentrations (-), at point k-1, for all size classes
<p>Record 4 is repeated KMAX-1 times, until the entire set of vertical concentration profiles, for all size classes, and sequence number NOCT, is defined Total number of concentration-profile sets, defined by records 3 and 4, must be equal to the total number of different sets of suspended-sediment concentrations assigned in SBINFO</p>			

Structure of Sediment Plot Output
(pltsed.out loaded in subroutine P)

Record Contents

Heading Records:

- 1 NPLOT, IM, JM, KM, KS MAX
- 2 XCT(IC1,JC1)
- 3 YCT(IC1,JC1)
- 4 PZBED(0:IM,0:JM)

Time-Dependent Records:

- 5 IT
- 6 ZBED(0:IM,0:JM)
- 7 BETAA(0:IM,0:JM,KS MAX)
- 8 AHSS(0:IM,0:JM)
- 9 U(0:IM,0:JM,KM)
- 10 V(0:IM,0:JM,KM)
- 11 W(0:IM,0:JM,KM)
- 12 CONC(0:IM,0:JM,0:KM,KS MAX)
- 13 PSORCD(0:IM,0:JM,KS MAX)
- 14 PSORCE(0:IM,0:JM,KS MAX)

Short output: records 5-7

Long output : records 5-14

CHAPTER V

TESTS

In contrast to man-made watercourses, such as channels, natural watercourses are characterized by continuous irregularity. Irregular contours of the flow domain, irregular shape of the bed surface, etc. are rather the rule than the exception in natural water bodies. Such a variety of shapes is impossible to find in man-made watercourses. Therefore, the application of the CH3D code with its new sediment-operations program module to a natural prototype case is imperative in order to validate all the procedures and to demonstrate the capabilities of the sediment module, which was developed to simulate mobile-bed phenomena in natural water-bodies.

The Mississippi River at the Old River Control Structure complex was used as a prototype case in order to test and validate the new mobile-bed numerical procedures in the CH3D code.

Model of the Mississippi River at the Old River

An approximately 12-mile long stretch of the Mississippi River (between River Mile 307 and River Mile 319) in the vicinity of the Old River Control Structure complex is modelled (Fig. 6). The entrance channel of the Sidney A. Murray Hydropower facility is located at River Mile 316.5. The Low Sill Structure is located at River Mile 315 and the Auxiliary Structure is located at River Mile 312. The Sidney A. Murray Hydropower facility is operated by the City of Vidalia, Louisiana. The Low Sill and Auxiliary Structures are operated by the U.S. Army Engineer District, New Orleans.

The model domain and computational grid (Fig. 7), as well as all data required for the CH3D hydrodynamics computations have been provided by Waterways Experiment Station personnel. Boundary (1) (Fig. 7) is an upstream inflow boundary. Boundary (2) is a downstream boundary. The entrance channel of the Sidney A. Murray Hydropower facility (boundary (3)) and the Low Sill and Auxiliary Structures (boundary (4)) are treated as closed during hydrodynamic computations. Thus, boundaries (3) and (4) could be treated as impermeable boundaries, just as for the other closed domain boundaries. The hydrodynamics simulations, performed by WES personnel before the sediment-operations program module had been built into the CH3D code, are briefly described in the following paragraph.

The hydrodynamic simulations used a computational time step of 30 seconds, and the simulated time period was 30 days. The imposed condition along the upstream inflow boundary (1) (Fig. 7) was a so-called 'river' condition (imposed unit discharges across the river), while the condition along the downstream boundary (2) was a so-called 'tidal' condition (imposed free-surface elevations across the river). The remaining domain boundaries were treated as impermeable. So called 'zero-flow' initial conditions (i.e. horizontal free-surface elevation and zero velocity field) were used. The chosen combination of initial and boundary conditions (downstream free-surface elevation and non-zero upstream discharge imposed on initially still water) is known to produce a disturbance (wave) that propagates back and forth throughout the flow domain. A so-called 'stabilization period' is required to allow the disturbance to eventually die out.

The sediment module was tested by repeating the simulation described in the previous paragraph, but with all or some of the sediment operations switched on.

The sediment-computation tests were made with a computational time step of 30 seconds, and the simulated period was 5 days and 10 hours. Initial and boundary conditions for the hydrodynamics computations were as previously described. Sediment computations were initiated 10 hours after the beginning of the hydrodynamics computations. A stabilization period of 10 hours proved to be sufficient for the dissipation of the most severe wave propagation in the domain.

The main source of sediment data was the Hall and Fagerburg (1990) paper. The paper describes the sampling techniques and provides some results of two field surveys of the hydrodynamics and suspended-sediment transport of the Mississippi River at the Old River Control Structure complex, completed in February and June 1990.

Six ranges were established across the Mississippi River in the vicinity of the Old River Control Structure complex, from River Mile 310 to River Mile 320. One range was also established parallel to the bank of the Mississippi River across the entrance channels of the Low Sill and Auxiliary Structures. An additional range was established parallel to the bank of the Mississippi River across the entrance channel of the Sidney A. Murray Hydropower facility. The location of the ranges is shown in Figure 6.

According to Hall and Fagerburg (1990), bed material was very uniform throughout the study reach, with predominant bed-material grain diameters varying between 0.125 mm and 0.5 mm. Hall and Fagerburg (1990) classified the suspended sediment as suspended silt and clay (with grain diameter less than 0.0625 mm), and suspended sand (with grain diameter greater than or equal to 0.0625 mm). The suspended silt and clay concentration was described as nearly uniform in the vertical direction and across the range, at each range, and the measured concentration of silt and clay was approximately 250 mg/l.

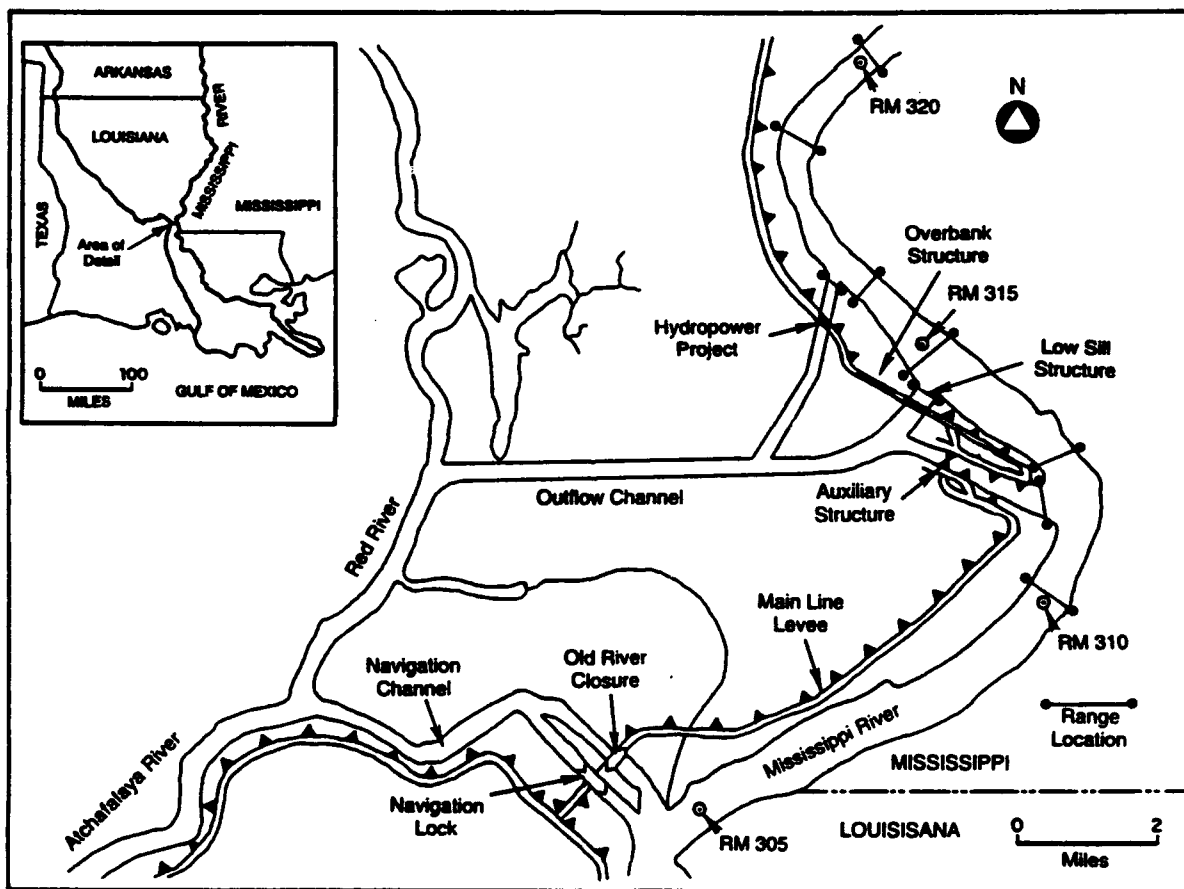


Figure 6. Mississippi River at the Old River Control Structure Complex: Location Map.

The suspended sand concentration was described as varying significantly in the vertical direction, as well as varying in maximum concentration along the channel bed laterally across the range. The only measured vertical suspended-sand concentration profiles are shown in Figure 3 of the Hall and Fagerburg (1990) paper. The Figure shows suspended-sand concentration at the right bank line, channel center line, and left bank line measured during the June 1990 survey at range 2, located at the upstream end of the study reach.

The data presented by Hall and Fagerburg (1990) are not sufficiently detailed for a definitive numerical study of the Mississippi River near the Old River Control Structure complex. A definitive numerical study would require more detailed measured sediment data in order to better define initial and boundary conditions for the sediment computations, and to permit comparison of computed results and measured data. Detailed measured hydrodynamic data would also be necessary, in order to detect any significant discrepancies between measured and computed velocities and depths that may influence the sediment computations.

However, the goal of the tests reported herein is not to do a detailed numerical study, but to test and verify the new numerical procedures, and to demonstrate the capabilities of the newly developed sediment-operations program module. The data presented by Hall and Fagerburg (1990) are sufficient to permit construction of an appropriate sediment data set that describes the Mississippi River near the Old River closely enough for verification and demonstration purposes. Indeed, a data set used for a detailed numerical study may not always be suitable for test purposes. For example, even though the initial size-fraction distribution is in reality different at each bed point, demonstration of the sediment module's capability to compute changes in size-fraction distribution at different bed points over time is much easier followed if the same size-fraction distribution is initially assigned to all bed points.

Three size classes were chosen to simulate the natural sediment mixture in the Mississippi River near the Old River complex. Size class 1, with an equivalent diameter of 0.01 mm, represents the fine sediment mainly moving in suspension without having much contact with the bed, and corresponds to suspended clay and silt as defined by Hall and Fagerburg (1990). Size class 2, with an equivalent diameter of 0.1 mm, represents sand that may move in suspension, but also has extensive contact with the bed and is an important component of the sediment mixture on the bed. Size class 3, with an equivalent diameter of 0.5 mm, remains mainly on or near the bed.

Boundaries (1) and (2) (Fig. 7) are defined as sediment inflow and outflow boundaries, respectively, while the remaining domain boundaries are treated as impermeable.

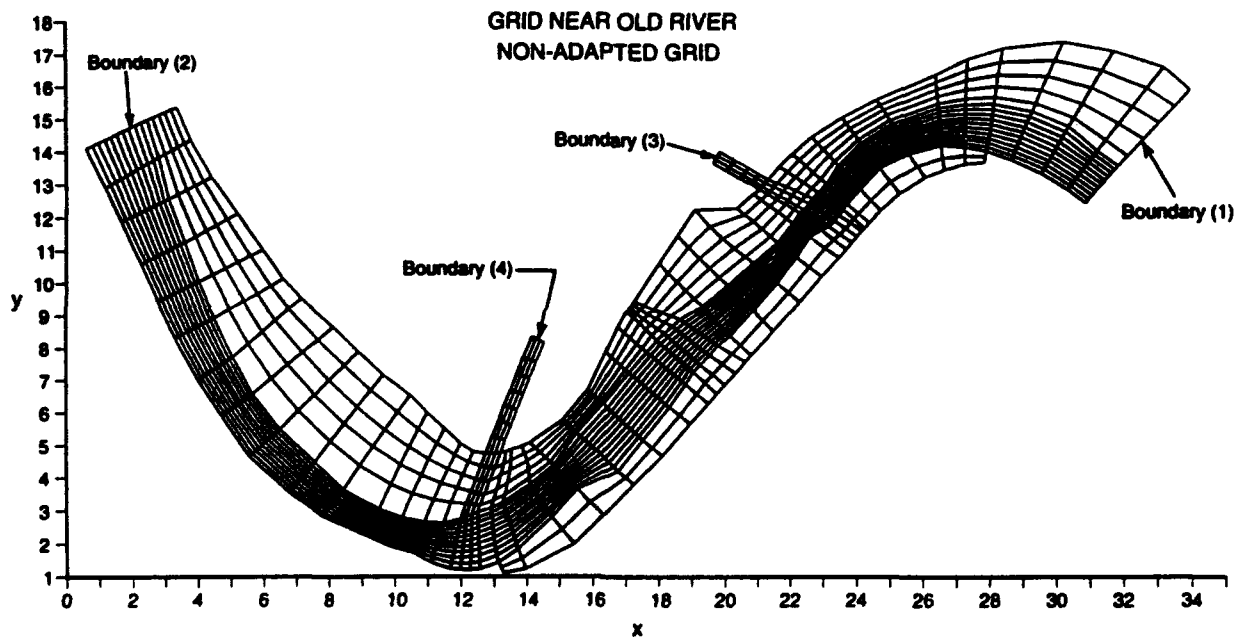


Figure 7. The Model Domain and Computational Grid.

Boundary conditions for sediment computations are required along inflow boundary (1) only.

An active-layer size-fraction distribution with 0% of size class 1, 50% of size class 2, and 50% of size class 3, was assigned at all points along inflow boundary (1).

Also, at the inflow boundary (1) vertical suspended-sediment concentration profiles were assigned for all three size classes. For size class 1, a constant vertical concentration profile of 250 ppm was assigned to all inflow boundary points. The initial suspended-sand concentration at the right bank line, channel center line, and left bank line measured during the June 1990 survey at range 2 (located at the upstream end of the study reach) (Hall and Fagerburg (1990), Fig.3) inspired the construction of the three different vertical concentration profiles for size class 2 (Figure 8). Concentration profile 1 (Fig. 8) is assigned to inflow boundary points close to the right bank. Concentration profile 2 (Fig. 8) is assigned to the inflow boundary points around the centerline, while concentration profile 3 (Fig. 8) is assigned to points next to the left bank. Finally, for size class 3, a constant vertical concentration profile, with concentration equal to zero, is assigned to all inflow boundary points.

The described inflow sediment boundary conditions are kept constant for the duration of the simulation.

Initial conditions for sediment computations are required for all points inside the flow domain. An initial active-layer size-fraction distribution, with 0% of size class 1, 50% of size class 2, and 50% of size class 3, was assigned to all points. Also, initial vertical suspended-sediment concentration profiles were assigned for the three size classes, at all points. For size class 1, a constant vertical concentration profile of 250 ppm was assigned to all points. For size class 2, an initial vertical concentration profile identical to the centerline profile 2 (Fig. 8) is assigned to all points. Finally, for size class 3, a constant vertical concentration profile, with concentration equal to zero, is assigned to all points.

A sample input-data set used for the tests herein is presented in Appendix E.

Printed Output and Test Results

The sediment-computation program module has a built-in system for checking sediment input data and issuing error-warning messages. Error-warning messages contain several parameters identifying the location of error (such as time-step index and (i,j,k) indexes defining the location of the point), and a few parameters suggesting the nature of the error. In cases for which more information about the error/warning is needed, the messages also contain an error/warning message number identifying the subroutine where the

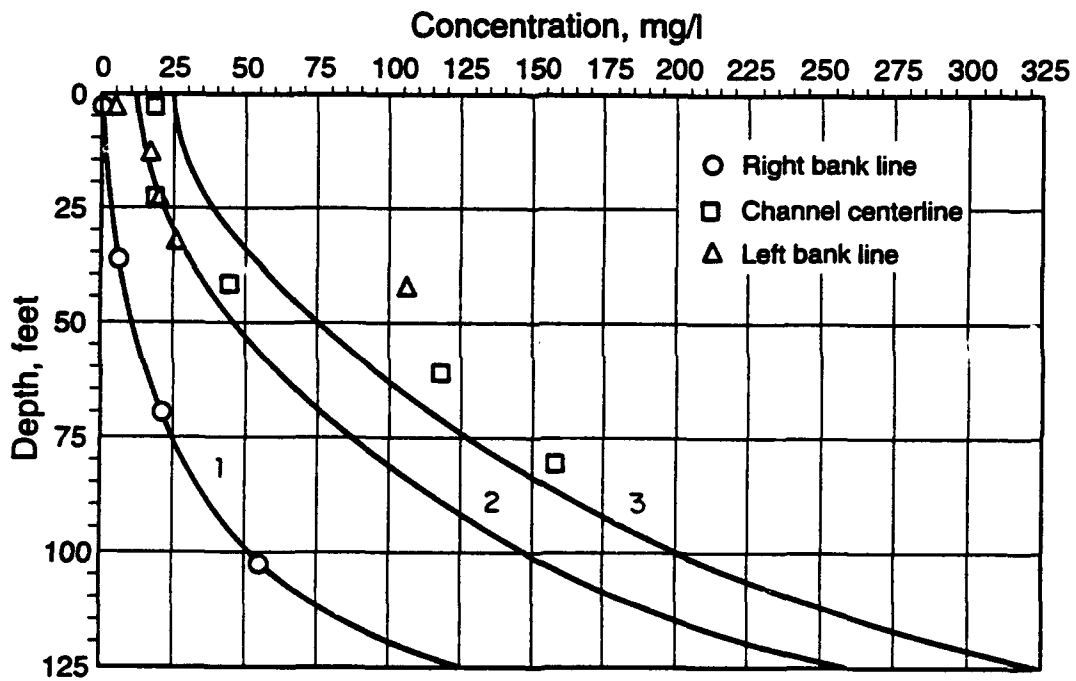


Figure 8. Vertical Concentration Profiles for Size Class 2 at the Model Upstream Boundary.

message originates. The last two digits to the right of the error/warning message number denote the error/warning sequential number in a specific subroutine (there is room for a maximum of 99 messages per subroutine). The remaining digits to the left of the error/warning message number denote the subroutine number (corresponding to the subroutine debug identification M listed in the Input Data Guide, Chapter IV).

The sediment-computation program module has the capability of including/excluding different computation steps, in order to permit separate testing of different procedures, using parameters IBED, ISUS, IADV, IDIF, JADV, JDIF, KADV (Input Data Guide, Chapter IV). First, the complete suspended-sediment computations were excluded in order to test only the bed-sediment computations (bedload transport and bed-evolution processes). Then the complete bed-sediment computations were excluded in order to test only the suspended-sediment transport. Furthermore, during testing of the suspended-sediment transport procedures, first some, and then all, of the advection and diffusion fluxes computed using the QUICKEST method were excluded, in order to separately test the implicit vertical-diffusion and fall-velocity procedures. Finally, the complete sediment-computation program module was tested. Only the test results for the complete sediment-computation module are reported herein.

The sediment-computations program module has number of built-in computation tests. Results of these tests for the particular run are designated 'sediment-computation diagnostics' in the printed output (file PRTSED.OUT). These diagnostics are printed with the chosen time-step frequency NDIAGS (see Input Data Guide, Chapter IV). The sediment-computation diagnostics are printed in the dimensionless form. The general structure of the sediment-computation diagnostics, as well as the specific diagnostics for the Old-River Complex model test runs, are briefly described below.

Sediment-computation diagnostics start with information concerning the number of Newton-Raphson iterations performed during bed-sediment computations. Reported are: maximum number of Newton-Raphson iterations (MITERS), for all bed points in the domain, during the current time step; indexes (IMITS, JMITS) defining the position (i,j) of the bed computational point with the maximum number of Newton-Raphson iterations; the average number of Newton-Raphson iterations (AVITS), for the entire domain during one time step; and the total number of Newton-Raphson iterations (ITSUM) for all bed points during one time step. The maximum number of Newton-Raphson iterations for the test runs was generally 5-6, while the average number of iterations was about 3.

Information concerning bed-sediment computation errors at the end of the Newton-Raphson iterations is reported next: the maximum change in bed elevation between two iterations (MAXDZB), for all bed points in the domain, during the current time step;

indexes (IMDZB,JMDZB) defining the position (i,j) of the bed computational point with the maximum change in bed elevation; the maximum change in active-layer size fraction between two iterations (MAXDB), for all bed points and all size fractions, during the current time step; and indexes (IMDB,JMDB,KSMDB) defining the position (i,j) of the bed computational point and the size class (ks) of the active-layer size fraction with the maximum change. For the test runs, the number of Newton-Raphson iterations was always less than the maximum allowed number, meaning that the maximum changes in bed elevation and active-layer size fractions between the two last iterations were always less than the specified threshold values.

Negative values of active-layer size-class fractions have no physical meaning, and if they occur in the computations, they indicate possible computational anomalies. Therefore, the sediment-computation diagnostics also report: the total number of negative computed active-layer size fractions (NEGBET), within the entire domain and for all size classes; the minimum computed active-layer size fraction (MINBET), within the entire domain and for all size classes; and indexes (IMINB,JMINB,KSMINB) defining the position (i,j) of the bed computational point and the size class (ks) of the minimum computed active-layer size fraction. There were no negative computed active-layer size fractions during the test runs.

The basic constraint of the sum of all active-layer size fractions being equal to unity is also checked. The sediment-computation diagnostics report: the maximum error in the basic constraint (ERSUMB, departure from unity), for all bed computational points in the domain, during the current time step; and indexes (IERSB,JERSB) defining the position (i,j) of the point with the maximum departure from unity. The maximum departure from unity during the test runs was of the order of 1.E-10.

Mass-conservation errors during bed-sediment computations are computed and compared (where appropriate) to the corresponding total mass. The sediment-computation diagnostics report: the maximum mass-conservation error in the global mass-conservation equation for bed sediment (MZBED), for all bed computational points in the domain, during the current time step; indexes (IMZBED,JMZBED) defining the position (i,j) of the bed computational point with the maximum mass-conservation error in the global mass-conservation equation for bed sediment; the sum of all mass-conservation errors in the global mass-conservation equation for bed sediment (SZBED); the maximum mass-conservation error in the mass-conservation equation for one size class of active-layer sediment (MBETA), for all bed computational points in the domain and all size classes, during the current time step; indexes (IMBETA,JMBETA) defining the position (i,j) of the bed computational point with the maximum mass-conservation error in the mass-conservation equation for one size class of active-layer sediment; index (KMBETA) defining the size class

(ks) of the active-layer equation with the maximum mass-conservation error; the total mass (MASB) of sediment in active-layer control volume built around the bed computational point with the maximum mass-conservation error in the mass-conservation equation for one size class of active-layer sediment; the sum (SBETA) of all mass-conservation errors in mass-conservation equations for one size class of active-layer sediment, in the entire domain, during the current time step; and the total mass (SMASB) of active-layer sediment, in the entire domain, during the current time step.

During the test runs, the maximum mass-conservation error in the global mass-conservation equation for bed sediment (MZBED) was of the order of 1.E-13; the sum of all mass-conservation errors in the global mass-conservation equations for bed sediment (SZBED) was of the order of 1.E-12; the maximum mass-conservation error in the mass-conservation equation for one size class of active-layer sediment (MBETA) was of the order of 1.E-13; the total mass of sediment in the corresponding active-layer control volume (MASB) was of the order of 1.E-2; the sum of all mass-conservation errors in mass-conservation equations for one size class of active-layer sediment (SBETA) was of the order of 1.E-13 to 1.E-15, depending on the size class; and the total mass of active-layer sediment (SMASB) was of the order of 1.E-0.

Mass-conservation errors during the suspended-sediment computations are also computed and compared (where appropriate) to the corresponding total mass. The sediment-computation diagnostics report: the maximum mass-conservation error in the mass-conservation equation for one size class of suspended sediment (MCONC), for all computational points in the domain and for all size classes, during the current time step; indexes (IMCON, JMCON, KMCON) defining the position (i,j,k) of the computational point with the maximum mass-conservation error in the mass-conservation equation for one size class of suspended sediment; the index (KMSCON) defining the size class (ks) of suspended-sediment equation with the maximum mass-conservation error; the total mass (MASC) of suspended sediment in a control volume, computed for the computational point and size class that define the maximum mass-conservation error in the conservation equation; the sum (SCONC) of all mass-conservation errors in the mass-conservation equations for one size class of suspended sediment, in the entire domain, during the current time step; the total mass (SMASC) of suspended sediment, in the entire domain, during the current time step; the maximum relative (with respect to the appropriate total mass) mass-conservation error in the mass-conservation equation for one size class of suspended sediment (MCONR), for all computational points in the domain and for all size classes, during the current time step; the indexes (IMCR, JMCR, KMCR) defining the position (i,j,k) of the computational point with the maximum relative mass-conservation error in the mass-con-

ervation equation for one size class of suspended sediment; the index (KMSCR) defining the size class (ks) of the suspended-sediment equation with the maximum relative mass-conservation error; and the total mass (MASC) of suspended sediment in the control volume, computed for the computational point and size class that define the maximum relative mass-conservation error in the conservation equation. During the test runs, the maximum mass-conservation error in the mass-conservation equation for one size class of suspended sediment (MCONC) was of the order of 1.E-18; the total mass of sediment in the corresponding suspended-sediment control volume (MASC) was of the order of 1.E-5; the sum of all mass-conservation errors in the mass-conservation equations for one size class of suspended sediment (SCONC) was of the order of 1.E-17 to 1.E-18, depending on the size class; the sum of total mass of suspended sediment (SMASC) was of the order of 1.E-1; the maximum relative mass-conservation error in the mass-conservation equation for one size class of suspended sediment (MCONR) was of the order of 1.E-11; and the total mass (MASC) of suspended sediment in the corresponding control volume varied depending on the control-volume size.

It is known that the quadratic interpolations used in the QUICKEST method sometimes yield negative suspended-sediment concentrations. The sediment-computation diagnostics report: the total number of computed negative suspended-sediment concentrations (NEGCON), for all computational points in the domain, and for all size classes, during the current time step; the minimum computed negative suspended-sediment concentration (MINCON), for all computational points in the domain, and for all size classes, during the current time step; the indexes (IMINC, JMINC, KMINC) defining the position (i,j,k) of the computational point with the minimum computed concentration of suspended sediment; and the index (KSMINC) defining the size class (ks) of the minimum computed suspended-sediment concentration. During the test runs, the total number of computed negative suspended-sediment concentrations was as high as 2000, but the minimum computed concentration was of the order of -1.E-6.

The sediment-computation program module prints selected results (in the dimensional form) on the output file PRTSED.OUT with a selected time-step frequency NPRSED (Input Data Guide, Chapter IV). The available output matrices include: densities of water-sediment mixture, suspended-sediment concentrations, bed elevations, bed-elevation changes over a time step, cumulative bed-elevation changes, active-layer depths, active-layer size fractions, numbers of strata, depths of strata, strata size fractions, characteristic grain diameters, friction coefficients, suspended-sediment 'deposition' sources, suspended-sediment 'erosion' sources, and sediment-computation boundary types. These output matrices are selected by setting parameters IDENS, ICONC, IZBED, IDZBED,

IDZB0, IEM, IBETA, ILSTR, ISTRDP, IBSTR, ID50, ICFRIC, ISORCD, ISORCE, ISBTYP, (see Input Data Guide, Chapter IV) to unity, respectively.

Several basic sediment variables (suspended-sediment concentrations, cumulative bed-elevation changes (instead of bed elevations), and active-layer size fractions), at the end of a five-day simulation period for the Old-River complex test run are briefly described below.

The suspended-sediment concentration for the finest size class, with an equivalent diameter of 0.01 mm, (roughly corresponding to suspended clay and silt as defined by Hall and Fagerburg (1990)) varies both across the flow and along the Mississippi River reach, between 60-70 ppm and 300 ppm; but the vertical concentration profile remains roughly uniform. The suspended-sediment concentration for the medium size class, with an equivalent diameter of 0.1 mm, (roughly corresponding to suspended sand as defined by Hall and Fagerburg (1990)) varies not only across and along the flow, but also over the depth. Vertical concentration profiles are relatively steep, with mid-depth concentration being between 1 and 5 ppm. The coarsest size class, with an equivalent diameter of 0.5 mm, (roughly corresponding to the bed material of Hall and Fagerburg (1990)) is also entrained into suspension from place to place. However, where they exist, vertical concentration profiles are rather steep, with the third-depth concentration being close to 1 ppm. It is obvious that the suspended-sediment concentration for the coarsest size class must vary significantly across and along the flow.

Cumulative bed-elevation changes show the total erosion or deposition at the end of a simulated period. The maximum erosion occurs immediately upstream of the Auxiliary Structure. Erosion in that area varies between 30 and 90 cm. The highest computed erosion (90 cm) is probably unrealistic, occurring due to the schematic representation of initial (and boundary) data. For example, initial active-layer size-fraction distribution was simply assumed, due to the lack of data. The time history of the highest computed erosion (40 cm of erosion during the first simulated day and another 30 cm of erosion during the second simulated day, with the erosion rate of 6-7 cm for remaining three simulated days) also suggests an initial imbalance in input data. Maximum erosion in other parts of the domain does not exceed 20-30 cm. Maximum deposition is around 30 cm and occurs immediately downstream of the Auxiliary Structure, as well as immediately downstream of the inflow boundary of the domain. The deposition downstream of the Auxiliary Structure occurs next to the right bank, away from the main flow, due to the low velocities in that region. The deposition downstream of the inflow boundary occurs due to the constant inflow of suspended sediment, assigned as a boundary condition.

The finest size class generally plays a minor role in the sediment mixture at the bed. The only significant amount of the finest size class is computed in the low velocity region downstream of the Auxiliary Structure, next to the right bank. Significant amounts of medium size-class particles are found at the bed where deposition occurs. In regions where deposition occurs, the medium size class usually comprises between 30 and 60% of the sediment mixture at the bed, while the coarsest size class comprises the remainder. In regions where erosion occurs, the coarsest size class usually comprises over 90% of the sediment mixture at the bed.

The total simulated period, after 10 hours of stabilization, was 5 days. The CPU time required for that simulation was about 25 hours on an HP 750. The corresponding unit CPU time was about 6 seconds per time step, or 7 milliseconds per time step and per bed computational point and per each suspended-sediment computational point above a bed point.

CHAPTER VI

CONCLUSIONS AND SUGGESTIONS FOR FURTHER DEVELOPMENT

During the course of this research the innovative two-dimensional mobile-bed modelling techniques recently developed for depth-averaged, two-dimensional modelling at the Iowa Institute of Hydraulic Research, were generalized and merged with the CH3D three-dimensional hydrodynamic simulation code, thus generalizing CH3D to include mobile-bed processes (such as aggradation and scour, bed-material sorting, and movement of both bedload and suspended load of nonuniform sediment mixtures).

The original IIHR conceptualization of sediment transport and bed evolution is fully preserved:

1. - Sediment movement is identified as either suspended-sediment transport, bedload transport, or a combination of both. To describe suspended-sediment transport, the advection/diffusion (mass-conservation) equation is used. To describe bedload transport and bed evolution, a mass-conservation equation for active-layer sediment and a global mass-conservation equation for bed sediment are used. As defined herein, the active layer comprises sediment particles at (or immediately below) the bed surface and sediment particles moving as bedload close to the bed surface. The suspended-sediment 'erosion' and 'deposition' sources are defined as the exchange between bedload and suspended-sediment transport. Criteria for distinguishing between bedload and suspended-sediment transport are incorporated into expressions for the bedload flux.

2. - There is no need to seek any *a priori* recognition of washload and its possible interaction with the bed. This recognition occurs naturally and implicitly in the algorithm's distinctly different treatment of bedload and suspended-sediment transport.

3. - The sediment mixture in a natural watercourse is described by a number of discrete size classes. Mass-conservation equations for active-layer sediment and suspended sediment are written for each size class separately. The procedure assumes no restriction on the number of discrete size classes.

4. - The friction coefficient is determined by the distribution of active-layer size fractions (i.e. by the sediment size distribution at the bed surface).

The IIHR two-dimensional mobile-bed techniques were generalized to ensure their compatibility with the overall CH3D environment. First, the governing sediment equations (initially written in vector form and standard Cartesian coordinates) were redefined by (1) taking into account the non-constant density of the water-sediment mixture; (2) introducing

a 'fall-velocity' term into the three-dimensional suspended-sediment equation; (3) defining the suspended-sediment 'erosion' source as an upward near-bed diffusion flux; (4) defining the suspended-sediment 'deposition' source as a downward near-bed fall-velocity flux; (5) and introducing several new auxiliary relations (e.g. mass-diffusion coefficient, density of a mixture containing water and suspended sediment etc.). Then the governing sediment equations were rederived in σ -stretched coordinates, then nondimensionalized and rederived in general (nonorthogonal) horizontal curvilinear coordinates.

The described generalization improves the original IHR mobile-bed techniques in several ways:

1. - Three-dimensional computations allow actual computation of vertical concentration profiles, rather than computing depth-averaged concentrations and assuming theoretical self-similar concentration profiles, as is done in two-dimensional computations.

2. - Accommodation of the non-constant density of the water-sediment mixture allows the numerical procedures to become more general, even offering the possibility to analyze density currents.

3. - In the three-dimensional environment, both 'erosion' and 'deposition' suspended-sediment sources are defined more physically than is possible in the two-dimensional depth-averaged environment.

4. - General curvilinear coordinates allow for better representation of natural-water-course complex geometry than do orthogonal curvilinear coordinates.

5. - The non-constant density of the water-sediment mixture makes it possible to simulate how sediment-transport and bed-evolution processes influence the flow field through changes in the density of water-sediment mixture, in addition to the influences arising from changes in the friction coefficient and bed elevation.

The newly-developed procedure opens a number of possibilities for further research. The general computational framework makes it possible to isolate, study and possibly improve a number of specific aspects of sediment-flow interaction that rely on empirical relations. Specific experiments may even be designed to isolate particular details of sediment-flow interaction, and experimental results then might be compared to the appropriate computational results. Specific aspects of sediment-flow interaction to be studied in this way may include: the diffusion of suspended sediment, particularly the diffusion coefficient; the density of the water-sediment mixture; bedload transport etc.

REFERENCES

- Aris, R., (1962), *Vectors, Tensors and the Basic Equations of Fluid Mechanics*, Prentice-Hall, Englewood Cliffs, N.J.
- Bennett, J.P. and Nordin, C.F., (1977), "Simulation of Sediment Transport and Armoring", *Hydrological Sciences Bulletin*, XXII, Vol.4, No.12, pp. 555-569.
- Borah, D.K., Alonso, C.V., and Prasad, S.H., (1982), "Routing Graded Sediments in Streams: Formulations." *Journal of the Hydraulics Division, ASCE*, Vol. 108, No. HY12, pp. 1486-1505.
- Carnahan, B., Luther, H.A., and Wilkes, J.O., (1969), *Applied Numerical Methods*, J. Wiley and Sons.
- Gosman, A.D. Pun, W.M., Runchal, A.K., Spalding D.B. and Wolfhstain, M. (1969), *Heat and Mass Transfer in Recirculating Flows*, Academic Press, New York.
- Hall, B.R., and Fagerburg, T.L., (1990), "Field Measurements of Hydrodynamics and Sediment Transport of the Mississippi River at Old River", U.S. Army Engineer Waterways Experimental Station, Vicksburg, Mississippi.
- Holly, F.M. Jr., and Rahuel, J.L., (1989), "New Numerical/Physical Framework for Mobile-Bed Modelling Part I - Numerical and Physical Principles", *Journal of Hydraulic Research, IAHR*, November 1989.
- Karim, F., and Kennedy, J.F., (1982), "IALLUVIAL: A Computer-Based Flow and Sediment-Routing Model for Alluvial Streams and its Application to the Missouri River." Report No. 250, Iowa Institute of Hydraulic Research, University of Iowa, Iowa City, Iowa.
- Karim, F., Holly, F.M., Jr., and Yang, J.C., (1987), "IALLUVIAL: Numerical Simulation of Mobile-Bed Rivers; Part I, Theoretical and Numerical Principles", Iowa Institute of Hydraulic Research Report No. 309, April 1987, The University of Iowa, Iowa City, Iowa.
- Leonard, B.P., (1979), "A Stable and Accurate Convective Modelling Procedure Based on Quadratic Upstream Interpolation", *Computer Methods in Applied Mechanics and Engineering*, Vol. 19, pp. 59-98.
- Richmond, M.C., Chen, H.C. and Patel, V.C., (1986), "Equations of Laminar and Tubulent Flows in General Curvilinear Coordinates", IIHR Report No.300, Iowa Institute of Hydraulic Research, The University of Iowa, Iowa City, Iowa, U.S.A.
- Shen, H.W., and Lu, J.Y., (1983), "Development and Prediction of Bed Armoring", *Journal of Hydraulic Engineering, ASCE*, Vol. 109, No. 4, April, pp. 611-629.

- Sheng, Y.P., and Lick, W., (1980), "A Two-Mode Free-Surface Numerical Model for the Three-Dimensional Time-Dependent Currents in Large Lakes", U.S. Environmental Protection Agency Report EPA - 600/3-80-047.
- Sheng, Y.P., (1983), "Mathematical Modeling of Three-Dimensional Coastal Currents and Sediment Dispersion: Model Development and Application", A.R.A.P. Report No. 485; also as Technical Report CERC-83-2, Waterways Experimental Station, Vicksburg.
- Sheng, Y.P., (1986), "Numerical Solution of Shallow Water Equations in Boundary Fitted Grid", Tech. Memo 84-15, Aeronautical Research Associates of Princeton, Inc., Princeton, N.J.
- Sheng, Y.P., (1986), "A Three-Dimensional Mathematical Model of Coastal, Estuarine and Lake Currents Using Boundary Fitted Grid", A.R.A.P. Report No. 585.
- Sokolnikoff, I.S., (1951), Tensor Analysis - Theory and Applications, Applied Mathematics Series, John Wiley and Sons, New York.
- Spasojevic, M., (1988), "Numerical Simulation of Two-Dimensional (plan-view) Unsteady Water and Sediment Movement in Natural Watercourses", Theses presented to the University of Iowa, at Iowa City, Iowa, in partial fulfillment of the requirements for the degree of Doctor of Philosophy.
- Spasojevic, M., and Holly, F.M., Jr, (1990), "2-D Bed Evolution in Natural Watercourses - New Simulation Approach", Journal of Waterway, Port, Coastal, and Ocean Engineering, Vol 116, No. 4, July/August.
- Spasojevic, M., and Holly, F.M., Jr, (1990), "MOBED2 - Numerical Simulation of Two-Dimensional Mobile-Bed Processes", Iowa Institute of Hydraulic Research Report No. 344, October 1990, The University of Iowa, Iowa City, Iowa.
- van Rijn, L.C., (1984a), "Sediment Transport, Part I: Bed Load Transport", Journal of Hydraulic Engineering, ASCE, Vol. 110, No. 10, pp. 1431-1456.
- van Rijn, L.C., (1984b), "Sediment Transport, Part II: Suspended Load Transport", Journal of Hydraulic Engineering, ASCE, Vol. 110, No. 11, pp. 1613-1641.
- van Rijn, L.C., (1982), "Computation of Bedload and Suspended Load", Report S487-I, Delft Hydraulics Laboratory, Delft, The Netherlands.
- Zanke, U., (1977), "Berechnung der Sinkgeschwindigkeiten von Sedimenten", Mitt. des Franzius-Instituts fur Wasserbau, Heft 46, Seite 243, Technical University, hannover, West Deutschland.
- Zhou, S., and McCorquodale, J.A., (1992), "Modeling of Rectangular Settling Tanks", Journal of Hydraulic Engineering, Vol. 118, No. 10, October 1992.

APPENDIX A

QUICKEST METHOD

The basic concepts of Leonard's (1979) QUICKEST method are summarized herein. First, a simple one-dimensional transport (advection) equation is considered:

$$\frac{\partial \phi}{\partial t} = -\frac{\partial(u\phi)}{\partial \xi} \quad (\text{A1})$$

Equation (A1) is integrated over a time step and a control volume built around main computational point C:

$$\int_{\frac{-\Delta \xi}{2}}^{\frac{\Delta \xi}{2}} \phi^{n+1} dp - \int_{\frac{-\Delta \xi}{2}}^{\frac{\Delta \xi}{2}} \phi^n dp = \int_0^{\Delta t} u_w \phi_w d\tau - \int_0^{\Delta t} u_e \phi_e d\tau \quad (\text{A2})$$

(1) (2) (3) (4)

where: (1) and (2) are local rate-of-change terms; (3) and (4) are advection terms; τ, p are local coordinates (Fig. A1); subscripts e, w denote east and west faces of the control volume built around the main computational point C (Fig. A1); subscripts E and W denote main computational points neighboring C (to the east and the west, respectively) (Fig. A1).

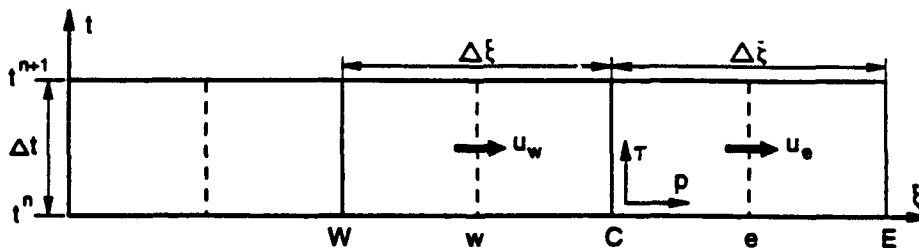


Figure A1.

Local rate-of-change terms are evaluated by representing $\phi(p)$ as a quadratic function between W and E computational points (using main-point values at W, C, and E computational points), and then by integrating that function from 'w' to 'e':

$$\int_{-\frac{\Delta\xi}{2}}^{\frac{\Delta\xi}{2}} \phi(p) dp = \Delta\xi \left[\phi_c + \frac{\Delta\xi^2}{24} \left(\frac{\partial^2 \phi}{\partial \xi^2} \right)_c \right] \quad (\text{A3})$$

where the following notation is invoked:

$$\left(\frac{\partial^2 \phi}{\partial \xi^2} \right)_c = \frac{\phi_E - 2\phi_c + \phi_W}{\Delta\xi^2}$$

Advection terms are treated by using a so-called 'upstream quadratic interpolation'. Consider, for example, the term (3) in Eq. (A2).

When the continuity equation (mass-conservation for fluid flow) is invoked, Eq. (A1) becomes:

$$\frac{\partial \phi}{\partial t} + u \frac{\partial \phi}{\partial \xi} = 0 \quad (\text{A4})$$

When the Lagrangian approach is used, Equation (A4) reduces to:

$$\frac{D\phi}{Dt} = 0 \quad \text{i.e.} \quad \phi = \text{const.} \quad (\text{A5})$$

valid along the trajectory of a fluid particle defined by:

$$u = \frac{d\xi}{dt} \quad (\text{A6})$$

Figure A2 shows particle trajectories, with their 'departure' points (d) at time $\tau = 0$, and their 'arrival' points (a) on the control volume w-face at different times between 0 and $\tau = \Delta t$.

If the trajectories are straight and parallel ($u = \text{const.}$), as in Fig. A2, then it is fully justified to write:

$$\int_0^{\Delta t} u_w \phi_w d\tau = \int_0^{p_D} \phi^n dp \quad (A7)$$

where:

$$p_D = u_w \Delta t = \frac{u_w \Delta t}{\Delta \xi} \Delta \xi = \tilde{C}_{r_w} \Delta \xi$$

and τ, p are local coordinates as in Fig. (A2).

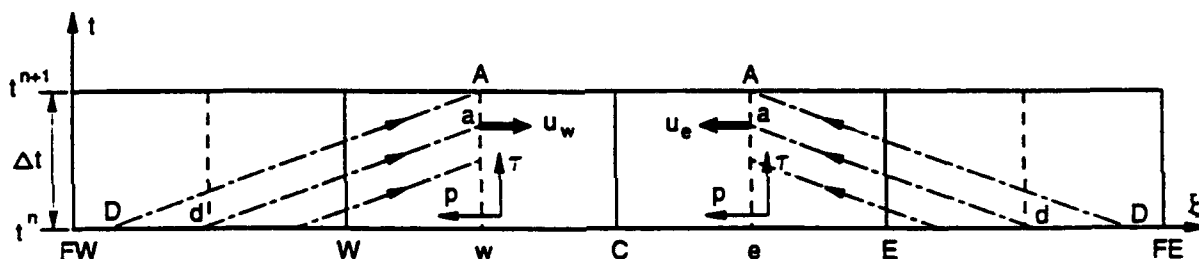


Figure A2.

The advection term is now evaluated by upstream quadratic interpolation: if the velocity direction is as in Fig. A2, $\phi(p)$ is represented as a quadratic function between FW and C (using main-point values at FW, W, and C computational points), and then the function is integrated from 0 to p_D :

$$\begin{aligned} \int_0^{\Delta t} u_w \phi_w d\tau &= \tilde{C}_{r_w} \Delta \xi \int_0^{p_D} \phi^n dp \\ &= \tilde{C}_{r_w} \Delta \xi \left[\frac{\phi_c^n + \phi_w^n}{2} - \frac{\Delta \xi}{2} \tilde{C}_{r_w} \left(\frac{\partial \phi}{\partial \xi} \right)_w^n + \frac{\Delta \xi^2}{6} \tilde{C}_{r_w}^2 \left(\frac{\partial^2 \phi}{\partial \xi^2} \right)_w^n - \frac{\Delta \xi^2}{8} \left(\frac{\partial^2 \phi}{\partial \xi^2} \right)_w^n \right] \end{aligned} \quad (A8)$$

where the following notation is invoked:

$$\left(\frac{\partial\phi}{\partial\xi}\right)_w^n = \frac{\phi_c^n - \phi_w^n}{\Delta\xi}$$

$$\left(\frac{\partial^2\phi}{\partial\xi^2}\right)_w^n = \frac{\phi_c^n - 2\phi_w^n + \phi_{FW}^n}{\Delta\xi^2} \quad \text{for } \bar{C}_{r_w} \geq 0$$

$$\bar{C}_{r_w} = \frac{\bar{u}_w \Delta t}{\Delta\xi}$$

$$\bar{u}_w = \frac{u_w^{n+1} + u_w^n}{2}$$

If the velocity direction is the opposite to what is shown in Fig. A2, Eq. (A8) remains the same, except that:

$$\left(\frac{\partial^2\phi}{\partial\xi^2}\right)_w^n = \frac{\phi_E^n - 2\phi_c^n + \phi_W^n}{\Delta\xi^2} \quad \text{for } \bar{C}_{r_w} < 0$$

A similar expression is easily obtained for the advection flux through the e-face of control volume (Fig. A2):

$$\begin{aligned} \int_0^{\Delta t} u_e \phi_e d\tau &= \int_0^{\bar{C}_{r_e} \Delta\xi} \phi^n dp \\ &= \bar{C}_{r_e} \Delta\xi \left[\frac{\phi_E^n + \phi_C^n}{2} - \frac{\Delta\xi}{2} \bar{C}_{r_e} \left(\frac{\partial\phi}{\partial\xi}\right)_e^n + \frac{\Delta\xi^2}{6} \bar{C}_{r_e}^2 \left(\frac{\partial^2\phi}{\partial\xi^2}\right)_e^n - \frac{\Delta\xi^2}{8} \left(\frac{\partial^2\phi}{\partial\xi^2}\right)_e^n \right] \end{aligned} \quad (\text{A9})$$

where:

$$\left(\frac{\partial\phi}{\partial\xi}\right)_e^n = \frac{\phi_E^n - \phi_C^n}{\Delta\xi}$$

$$\left(\frac{\partial^2\phi}{\partial\xi^2}\right)_e^n = \frac{\phi_E^n - 2\phi_C^n + \phi_W^n}{\Delta\xi^2} \quad \text{for } \bar{C}_{r_e} \geq 0$$

$$\left(\frac{\partial^2 \phi}{\partial \xi^2}\right)_e^n = \frac{\phi_{FE}^n - 2\phi_E^n + \phi_C^n}{\Delta \xi^2} \quad \text{for } \bar{C}_{r_e} \geq 0$$

$$\bar{C}_{r_e} = \frac{\bar{u}_e \Delta t}{\Delta \xi}$$

$$\bar{u}_e = \frac{u_e^{n+1} + u_e^n}{2}$$

The local rate-of-change term:

$$\frac{\frac{\Delta \xi}{2} \int \phi^{n+1} dp - \frac{\Delta \xi}{2} \int \phi^n dp}{\frac{\Delta \xi}{2}} = \Delta \xi (\phi_c^{n+1} - \phi_c^n) + \Delta \xi \frac{\Delta \xi^2}{24} \left[\left(\frac{\partial^2 \phi}{\partial \xi^2}\right)_c^{n+1} - \left(\frac{\partial^2 \phi}{\partial \xi^2}\right)_c^n \right] \quad (\text{A10})$$

where p is a local coordinate as in Fig. A1, is further manipulated by using the governing Eq. (A1). Equation (A1) can be written as:

$$\frac{\partial}{\partial t} \left(\frac{\partial^2 \phi}{\partial \xi^2} \right) = - \frac{\partial}{\partial \xi} \left[\frac{\partial^2 (u\phi)}{\partial \xi^2} \right] \quad (\text{A11})$$

The left-hand-side of Eq. (A11) can be written as:

$$\frac{\partial}{\partial t} \left(\frac{\partial^2 \phi}{\partial \xi^2} \right) = \frac{1}{\Delta t} \left[\left(\frac{\partial^2 \phi}{\partial \xi^2}\right)_c^{n+1} - \left(\frac{\partial^2 \phi}{\partial \xi^2}\right)_c^n \right] \quad (\text{A12})$$

while the right-hand-side of Eq. (A11) is approximated, assuming a constant velocity, by:

$$\frac{\partial}{\partial \xi} \left(\frac{\partial^2 (u\phi)}{\partial \xi^2} \right) = \frac{\partial}{\partial \xi} \left[u \frac{\partial^2 \phi}{\partial \xi^2} \right] = \frac{1}{\Delta \xi} \left[\bar{u}_e \left(\frac{\partial^2 \phi}{\partial \xi^2}\right)_e^n - \bar{u}_w \left(\frac{\partial^2 \phi}{\partial \xi^2}\right)_w^n \right] \quad (\text{A13})$$

The final outcome is:

$$\left(\frac{\partial^2 \phi}{\partial \xi^2}\right)_c^{n+1} - \left(\frac{\partial^2 \phi}{\partial \xi^2}\right)_c^n = \bar{C}_{r_w} \left(\frac{\partial^2 \phi}{\partial \xi^2}\right)_w^n - \bar{C}_{r_e} \left(\frac{\partial^2 \phi}{\partial \xi^2}\right)_e^n \quad (\text{A14})$$

When Eq. (A14) is introduced into Eq. (A10), the local rate-of-change terms become:

$$\frac{\frac{\Delta \xi}{2}}{\frac{\Delta \xi}{2}} \int \phi^{n+1} dp - \frac{\frac{\Delta \xi}{2}}{\frac{\Delta \xi}{2}} \int \phi^n dp = \Delta \xi (\phi_c^{n+1} - \phi_c^n) + \Delta \xi \frac{\Delta \xi^2}{24} \left[\bar{C}_{r_w} \left(\frac{\partial^2 \phi}{\partial \xi^2}\right)_w^n - \bar{C}_{r_e} \left(\frac{\partial^2 \phi}{\partial \xi^2}\right)_e^n \right] \quad (\text{A15})$$

By using Eqs. (A8), (A9) and (A15), the discretized Eq. (A2) reads:

$$\begin{aligned} \phi^{n+1} - \phi^n = & \bar{C}_{r_w} \left[\frac{\phi_c^n + \phi_w^n}{2} - \frac{\Delta \xi}{2} \bar{C}_{r_w} \left(\frac{\partial \phi}{\partial \xi}\right)_w^n - \frac{\Delta \xi^2}{6} (1 - \bar{C}_{r_w}^2) \left(\frac{\partial^2 \phi}{\partial \xi^2}\right)_w^n \right] \\ & - \bar{C}_{r_e} \left[\frac{\phi_e^n + \phi_c^n}{2} - \frac{\Delta \xi}{2} \bar{C}_{r_e} \left(\frac{\partial \phi}{\partial \xi}\right)_e^n - \frac{\Delta \xi^2}{6} (1 - \bar{C}_{r_e}^2) \left(\frac{\partial^2 \phi}{\partial \xi^2}\right)_e^n \right] \end{aligned} \quad (\text{A16})$$

A simple advection-diffusion equation is considered next:

$$\frac{\partial \phi}{\partial t} = - \frac{\partial(u\phi)}{\partial \xi} + \frac{\partial}{\partial \xi} \left(D \frac{\partial \phi}{\partial \xi} \right) \quad (\text{A17})$$

Equation (A17) is integrated over a time step and a control volume built around a main computational point C (Fig. A1):

$$\begin{aligned} \frac{\frac{\Delta \xi}{2}}{\frac{\Delta \xi}{2}} \int \phi^{n+1} dp - \frac{\frac{\Delta \xi}{2}}{\frac{\Delta \xi}{2}} \int \phi^n dp = & \int_0^{\Delta t} u_w \phi_w d\tau - \int_0^{\Delta t} u_e \phi_e d\tau + \int_0^{\Delta t} D_e \left(\frac{\partial \phi}{\partial \xi}\right)_e d\tau - \int_0^{\Delta t} D_w \left(\frac{\partial \phi}{\partial \xi}\right)_w d\tau \end{aligned} \quad (\text{A18})$$

(1) (2) (3) (4) (5) (6)

The local rate-of-change terms (1) and (2), as well as the advection terms (3) and (4) are treated as previously described. The diffusion terms (5) and (6) are also treated

according to the same idea of 'upstream quadratic interpolation'. Consider, for example, the term (6):

$$\int_0^{\Delta t} D_w \left(\frac{\partial \phi}{\partial \xi} \right)_w d\tau = \bar{D}_w \left(\frac{\partial \phi}{\partial \xi} \right)_w \Delta t \quad (\text{A19})$$

where

$$\bar{D}_w = \frac{D_w^{n+1} + D_w^n}{2}$$

and

$$\left(\frac{\partial \phi}{\partial \xi} \right)_w = \left(\frac{\partial \phi}{\partial \xi} \right)_w^{n+\frac{1}{2}}$$

is the w-wall gradient of ϕ evaluated at $\frac{\Delta t}{2}$.

It is further assumed that the gradient of ϕ is convected downstream essentially unchanged, along the constant-slope trajectory (Fig. A3). It remains to find the departure point D of the trajectory that arrives at the w-face of the control volume at $\frac{\Delta t}{2}$ and to evaluate the gradient at D by the upstream quadratic interpolation. If the w-wall velocity direction is as in Fig. A3 ϕ is represented as a quadratic function between FW and C (using main-point values at FW, W, and C computational points), with the gradient of ϕ readily derived from the function. The departure point of the trajectory is defined as:

$$p_D = -\bar{u}_w \frac{\Delta t}{2} = -\frac{\bar{u}_w \Delta t}{\Delta \xi} \frac{\Delta \xi}{2} = -\frac{\Delta \xi}{2} \bar{C}_{rw} \quad (\text{A20})$$

where p_D is the position of the departure point in local coordinates (Fig. A3), and the gradient of ϕ is evaluated at D, leading to:

$$\int_0^{\Delta t} D_w \left(\frac{\partial \phi}{\partial \xi} \right)_w d\tau = \bar{D}_w \left(\frac{\partial \phi}{\partial \xi} \right)_w \Delta t = \bar{\alpha}_w \Delta \xi \left[\Delta \xi \left(\frac{\partial \phi}{\partial \xi} \right)_w^n - \frac{\Delta \xi^2}{2} \bar{C}_{rw} \left(\frac{\partial^2 \phi}{\partial \xi^2} \right)_w^n \right] \quad (\text{A21})$$

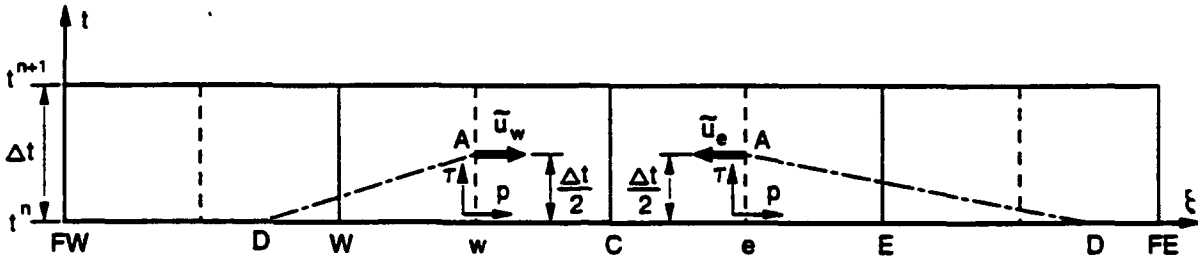


Figure A3.

where:

$$\bar{\alpha}_w = \frac{\bar{D}_w \Delta t}{\Delta \xi^2}$$

and the right-hand-side derivatives have the same meaning as in Eq. (A8).

A similar expression is easily obtained for the diffusion flux across the e-face of control volume:

$$\int_0^{\Delta t} D_e \left(\frac{\partial \phi}{\partial \xi} \right)_e d\tau = \bar{D}_e \left(\frac{\partial \phi}{\partial \xi} \right)_e \Delta t = \bar{\alpha}_e \Delta \xi \left[\Delta \xi \left(\frac{\partial \phi}{\partial \xi} \right)_e^n - \frac{\Delta \xi^2}{2} \bar{C}_{re} \left(\frac{\partial^2 \phi}{\partial \xi^2} \right)_e^n \right] \quad (\text{A22})$$

where

$$\bar{\alpha}_e = \frac{\bar{D}_e \Delta t}{\Delta \xi^2}$$

and the right-hand-side derivatives have the same meaning as in Eq. (A9).

By using Eqs. (A8), (A9), (A15), (A21) and (A22), the discretized advection-diffusion equation (Eq. (A17) i.e. (A18)) reads:

$$\begin{aligned}
\phi_c^{n+1} - \phi_c^n = & \bar{C}_{r_w} \left[\frac{\phi_c^n + \phi_w^n}{2} - \frac{\Delta\xi}{2} \bar{C}_{r_w} \left(\frac{\partial\phi}{\partial\xi} \right)_w^n - \frac{\Delta\xi^2}{6} (1 - \bar{C}_{r_w}^2) \left(\frac{\partial^2\phi}{\partial\xi^2} \right)_w^n \right] \\
& - \bar{C}_{r_e} \left[\frac{\phi_E^n + \phi_C^n}{2} - \frac{\Delta\xi}{2} \bar{C}_{r_e} \left(\frac{\partial\phi}{\partial\xi} \right)_e^n - \frac{\Delta\xi^2}{6} (1 - \bar{C}_{r_e}^2) \left(\frac{\partial^2\phi}{\partial\xi^2} \right)_e^n \right] \\
& + \bar{\alpha}_e \left[\Delta\xi \left(\frac{\partial\phi}{\partial\xi} \right)_e^n - \frac{\Delta\xi^2}{2} \bar{C}_{r_e} \left(\frac{\partial^2\phi}{\partial\xi^2} \right)_e^n \right] \\
& - \bar{\alpha}_w \left[\Delta\xi \left(\frac{\partial\phi}{\partial\xi} \right)_w^n - \frac{\Delta\xi^2}{2} \bar{C}_{r_w} \left(\frac{\partial^2\phi}{\partial\xi^2} \right)_w^n \right]
\end{aligned} \tag{A23}$$

The discretized Eq. (A23) is explicit, meaning that the unknown scalar ϕ is related to the main computational point C only. Scalars ϕ related to the neighboring computational points appear in Eq. (A23) explicitly, i.e. as known values.

Boundary conditions differ depending on the type of the boundary (impermeable, outflow or inflow). Following the recommendation of Leonard (1979), boundary conditions are specified to be control-volume wall values, rather than node values. Also, special interpolations are required at boundary points, or at points next to the boundary. Boundary conditions are summarized below.

First, in order to make further discussion of boundary conditions more clear, Eq. (A23) is rewritten as:

$$\begin{aligned}
\phi_c^{n+1} - \phi_c^n = & (\text{adv})_w - (\text{adv})_e + (\text{dif})_e - (\text{dif})_w \tag{A24} \\
(\text{adv})_w = & \bar{C}_{r_w} \left[\frac{\phi_c^n + \phi_w^n}{2} - \frac{\Delta\xi}{2} \bar{C}_{r_w} \left(\frac{\partial\phi}{\partial\xi} \right)_w^n - \frac{\Delta\xi^2}{6} (1 - \bar{C}_{r_w}^2) \left(\frac{\partial^2\phi}{\partial\xi^2} \right)_w^n \right] \\
(\text{adv})_e = & \bar{C}_{r_e} \left[\frac{\phi_E^n + \phi_C^n}{2} - \frac{\Delta\xi}{2} \bar{C}_{r_e} \left(\frac{\partial\phi}{\partial\xi} \right)_e^n - \frac{\Delta\xi^2}{6} (1 - \bar{C}_{r_e}^2) \left(\frac{\partial^2\phi}{\partial\xi^2} \right)_e^n \right]
\end{aligned}$$

$$(\text{dif})_w = \bar{\alpha}_w \left[\Delta\xi \left(\frac{\partial\phi}{\partial\xi} \right)_w - \frac{\Delta\xi^2}{2} \bar{C}_{r_w} \left(\frac{\partial^2\phi}{\partial\xi^2} \right)_w \right]$$

$$(\text{dif})_e = \bar{\alpha}_e \left[\Delta\xi \left(\frac{\partial\phi}{\partial\xi} \right)_e - \frac{\Delta\xi^2}{2} \bar{C}_{r_e} \left(\frac{\partial^2\phi}{\partial\xi^2} \right)_e \right]$$

where $(\text{adv})_w$ and $(\text{adv})_e$ stand for advection fluxes across the w-face and the e-face of the control volume, respectively, while $(\text{dif})_w$ and $(\text{dif})_e$ stand for diffusion fluxes across the w-face and the e-face of control volume, respectively:

Outflow Boundary at w-Face of Control Volume

The same procedure, as described by Eqs. (A1) to (A24), is applied to the computational point that has an outflow boundary at the w-face of control volume. The only difference is that the appropriate upstream quadratic interpolation, next to the w-face of control volume, uses known values at points E, C and the known outflow boundary value at B_w , i.e. at the w-face of the control volume built around the computational point C.

As a result, advection and diffusion fluxes across the e-face of the the control volume, $(\text{adv})_e$ and $(\text{dif})_e$, have the same form as in Eq. (A24).

Advection and diffusion fluxes across the w-face of the control volume, $(\text{adv})_w$ and $(\text{dif})_w$, have the following form:

$$(\text{adv})_w = \bar{C}_{r_w} \left[\phi_{B_w}^n - \frac{\Delta\xi}{2} \bar{C}_{r_w} \left(\frac{\partial\phi}{\partial\xi} \right)_{B_w}^n - \frac{\Delta\xi^2}{6} \left(\frac{1}{4} - \bar{C}_{r_w}^2 \right) \left(\frac{\partial^2\phi}{\partial\xi^2} \right)_{B_w}^n \right] \quad (\text{A25})$$

$$(\text{dif})_w = \bar{\alpha}_w \left[\Delta\xi \left(\frac{\partial\phi}{\partial\xi} \right)_{B_w}^n - \frac{\Delta\xi^2}{2} \bar{C}_{r_w} \left(\frac{\partial^2\phi}{\partial\xi^2} \right)_{B_w}^n \right] \quad (\text{A26})$$

where

$$\left(\frac{\partial\phi}{\partial\xi}\right)_{B_w}^n = \frac{-8\phi_{B_w}^n + 9\phi_c - \phi_E^n}{3\Delta\xi}$$

$$\left(\frac{\partial^2\phi}{\partial\xi^2}\right)_{B_w}^n = \frac{4\phi_E^n - 12\phi_c^n + 8\phi_{B_w}^n}{3\Delta\xi^2}$$

are derivatives evaluated at the boundary, i.e. at the w-face of the control volume.

Inflow Boundary at w-Face of Control Volume

The same procedure as described by Eqs. (A1) to (A24) is applied to a computational point that has an inflow boundary at the w-face of the control volume. The difference is that the appropriate upstream quadratic interpolation, next to the w-face of the control volume, uses known values at points E, C and a known outflow boundary value at B_w , i.e. at the w-face of the control volume built around computational point C. Also, the term (3) of Eq. (A2) (or Eq. (A18)) is evaluated by using straightforward integration, with the known inflow boundary value at B_w , i.e. at the w-face of the control volume:

$$\int_0^{\Delta t} u_w \phi_w d\tau = \bar{u}_w \bar{\phi}_{B_w} \Delta t = \bar{C}_{rw} \bar{\phi}_{B_w} \Delta\xi \quad (A27)$$

where

$$\bar{\phi}_{B_w} = \frac{\phi_{B_w}^{n+1} + \phi_{B_w}^n}{2}$$

As a result, advection and diffusion fluxes across the e-face of the control volume, $(adv)_e$ and $(dif)_e$, have the same form as in Eq. (A24).

Advection and diffusion fluxes across the w-face of the control volume, $(adv)_w$ and $(dif)_w$, have the following form:

$$(adv)_w = \bar{C}_{rw} \left[\bar{\phi}_{B_w} - \frac{\Delta\xi^2}{24} \left(\frac{\partial^2\phi}{\partial\xi^2} \right)_{B_w}^n \right] \quad (A28)$$

$$(\text{dif})_w = \bar{\alpha}_w \Delta \xi_s \left(\frac{\partial \phi}{\partial \xi} \right)_{B_w}^n \quad (\text{A29})$$

where

$$\left(\frac{\partial^2 \phi}{\partial \xi^2} \right)_{B_w}^n = \frac{4\phi_E^n - 12\phi_C^n + \phi_{B_w}^n}{3\Delta \xi^2}$$

$$\left(\frac{\partial \phi}{\partial \xi} \right)_{B_w}^n = \frac{-8\phi_{B_w}^n + 9\phi_C^n - \phi_E^n}{3\Delta \xi^2}$$

are derivatives evaluated at the boundary B_w , i.e. at the w-face of the control volume. The second right-hand-side term of Eq. (A28) originates from the appropriate rate-of-change term, as in Eq. (A15).

Impermeable Boundary at w-Face of Control Volume

The same procedure as described by Eqs. (A1) to (A24) is applied to a computational point that has an impermeable boundary at the w-face of the control volume. The advection term (3) and the diffusion term (6) in Eq. (A18) are equal to zero. The velocity \bar{u}_w i.e. the Courant number \bar{C}_{r_w} are also equal to zero, which eliminates the appropriate term in Eq. (A15).

As a result, both advection and diffusion fluxes across the w-face of the control volume are equal to zero:

$$(\text{adv})_w = 0 \quad (\text{A30})$$

$$(\text{dif})_w = 0 \quad (\text{A31})$$

while the advection and diffusion fluxes across the e-face of the control volume $(\text{adv})_e$ and $(\text{dif})_e$, have the same form as in Eq. (A24).

Outflow Boundary at e-Face of Control Volume

The same approach as for the outflow boundary at the w-face of the control volume is used. The appropriate upstream quadratic interpolation, next to the e-face of the control

volume, uses known values at points W, C and the known outflow boundary value at B_e , i.e. at the e-face of the control volume built around C.

As a result, advection and diffusion fluxes across the w-face of the control volume, $(adv)_w$ and $(dif)_w$, have the same form as in Eq. (A24).

Advection and diffusion fluxes across the e-face of the control volume, $(adv)_e$ and $(dif)_e$, have the following form:

$$(adv)_e = \bar{C}_{r_e} \left[\phi_{B_e}^n - \frac{\Delta\xi}{2} \bar{C}_{r_e} \left(\frac{\partial\phi}{\partial\xi} \right)_{B_e}^n - \frac{\Delta\phi^2}{6} \left(\frac{1}{4} - \bar{C}_{r_e}^2 \right) \left(\frac{\partial^2\phi}{\partial\xi^2} \right)_{B_e}^n \right] \quad (A32)$$

$$(dif)_e = \bar{\alpha}_e \left[\Delta\xi \left(\frac{\partial\phi}{\partial\xi} \right)_{B_e}^n - \frac{\Delta\xi^2}{2} \bar{C}_{r_e} \left(\frac{\partial^2\phi}{\partial\xi^2} \right)_{B_e}^n \right] \quad (A33)$$

where

$$\left(\frac{\partial\phi}{\partial\xi} \right)_{B_e}^n = \frac{8\phi_{B_e}^n - 9\phi_C^n + \phi_W^n}{3\Delta\xi}$$

$$\left(\frac{\partial^2\phi}{\partial\xi^2} \right)_{B_e}^n = \frac{8\phi_{B_e}^n - 12\phi_C^n + \phi_W^n}{3\Delta\xi^2}$$

are derivatives evaluated at the boundary, i.e. at the e-face of the control volume.

Inflow Boundary at e-Face of Control Volume

The same approach as for the outflow boundary at the w-face of the control volume is used. The appropriate upstream quadratic interpolation, next to the e-face of the control volume, uses known values at points W, C and the known outflow boundary value at B_e , i.e. at the e-face of the control volume built around C. Term (4) of Eq. (A2) (or Eq. (A18)) is evaluated by using straightforward integration, with the known inflow boundary value at B_e , i.e. at the e-face of the control volume built around C.

As a result, advection and diffusion fluxes across the w-face of the control volume, $(adv)_w$ and $(dif)_w$, have the same form as in Eq. (A24).

Advection and diffusion fluxes across the e-face of the control volume, $(adv)_e$ and $(dif)_e$, have the following form:

$$(adv)_e = \bar{C}_{r_e} \left[\bar{\phi}_{B_e} - \frac{\Delta\xi^2}{24} \left(\frac{\partial^2 \phi}{\partial \xi^2} \right)_{B_e}^n \right] \quad (A34)$$

$$(dif)_e = \bar{\alpha}_e \Delta\xi \left(\frac{\partial \phi}{\partial \xi} \right)_{B_e}^n \quad (A35)$$

where

$$\bar{\phi}_{B_e} = \frac{\phi_{B_e}^{n+1} + \phi_{B_e}^n}{2}$$

$$\left(\frac{\partial \phi}{\partial \xi} \right)_{B_e}^n = \frac{8\phi_{B_e}^n - 9\phi_c^n + \phi_w^n}{3\Delta\xi}$$

$$\left(\frac{\partial^2 \phi}{\partial \xi^2} \right)_{B_e}^n = \frac{8\phi_{B_e}^n - 12\phi_c^n + 4\phi_w^n}{3\Delta\xi^2}$$

are evaluated at the boundary, i.e. at the e-face of the control volume.

Impermeable Boundary at e-Face of Control Volume

Following the same arguments as for impermeable boundary at w-face of control volume, it is easy to conclude that both advection and diffusion fluxes across an impermeable e-face of the control volume are equal to zero:

$$(adv)_e = 0 \quad (A36)$$

$$(dif)_e = 0 \quad (A37)$$

while advection and diffusion fluxes across the w-face of the control volume, $(adv)_w$ and $(dif)_w$, have the same form as in Eq.(A24).

Interpolations for Points Next to the Boundary

Consider the w-face of the control volume built around the computational point C.

First assume that the direction of the velocity is as in Fig. A4 and that the w-face of the control volume built around the computational point W is a boundary B_{fw} .

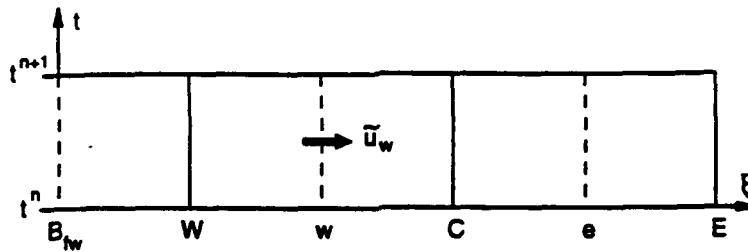


Figure A4.

The same procedure, as described by Eqs. (A1) to (A24), is applied to the computational point C. Advection and diffusion fluxes across the w-face, $(adv)_w$ and $(dif)_w$, of the control volume built around the computational point C have the same form as in Eq. (A24), the only difference being that the appropriate upstream quadratic interpolation uses known values at points C, W, and boundary B_{fw} , so that:

$$\left(\frac{\partial^2 \phi}{\partial \xi^2}\right)_w^n = \frac{4\phi_C^n - 12\phi_W^n + 8\phi_{B_{fw}}^n}{3\Delta\xi^2} \quad (A38)$$

Now, assume that the direction of the velocity is as in Fig. A5 and that the e-face of the control volume built around the computational point C is a boundary B_e .

The same procedure as described by Eqs. (A1) to (A24) is applied to the computational point C. Advection and diffusion fluxes across the w-face, $(adv)_w$ and $(dif)_w$, of the control volume built around the computational point C have the same form as in Eq. (A24), with one difference, namely that the appropriate upstream quadratic interpolation uses known values at points W, C, and boundary B_e , so that:

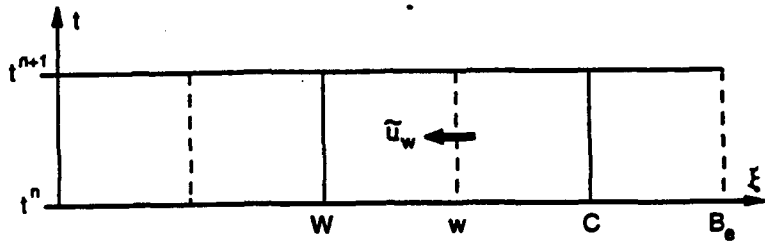


Figure A5.

APPENDIX B

DISCRETIZED MASS-CONSERVATION EQUATION FOR SUSPENDED SEDIMENT

First, the mass-conservation equation for suspended sediment (Eq. 29)) is rewritten as follows:

$$\begin{aligned}
 & \frac{\partial}{\partial t}(\text{JH}\rho\text{C}) + \text{R}_o \left[\frac{\partial}{\partial \xi}(\text{JH}\rho\text{Cu}) + \frac{\partial}{\partial \eta}(\text{JH}\rho\text{Cv}) + \frac{\partial}{\partial \sigma}(\text{JH}\rho\text{C}\omega) \right] - \text{R}_{of} \frac{\partial}{\partial \sigma}(\text{J}\rho\text{C}\omega_f) = \\
 & = \frac{\text{E}_{kH}}{\text{S}_{cH}} \text{H} \left[\frac{\partial}{\partial \xi} \left(\frac{\text{D}_H}{\text{J}} g_{22} \frac{\partial(\rho\text{C})}{\partial \xi} \right) - \frac{\partial}{\partial \xi} \left(\frac{\text{D}_H}{\text{J}} g_{12} \frac{\partial(\rho\text{C})}{\partial \eta} \right) \right. \\
 & \quad \left. - \frac{\partial}{\partial \eta} \left(\frac{\text{D}_H}{\text{J}} g_{12} \frac{\partial(\rho\text{C})}{\partial \xi} \right) + \frac{\partial}{\partial \eta} \left(\frac{\text{D}_H}{\text{J}} g_{11} \frac{\partial(\rho\text{C})}{\partial \eta} \right) \right] \quad (\text{B1}) \\
 & + \frac{\text{E}_{kV}}{\text{S}_{cV}} \frac{\text{J}}{\text{H}} \frac{\partial}{\partial \sigma} \left(\text{D}_V \frac{\partial(\rho\text{C})}{\partial \sigma} \right)
 \end{aligned}$$

Then, a sort of split-operator approach is used to split Eq.(B1) into three parts. The local rate of change due to the action of advection and diffusion terms in the ξ -coordinate

direction, denoted as $\left[\frac{\partial}{\partial t}(\text{JH}\rho\text{C}) \right]^\xi$, can be expressed as:

$$\left[\frac{\partial}{\partial t}(\text{JH}\rho\text{C}) \right]^\xi = -\text{R}_o \frac{\partial}{\partial \xi}(\text{JH}\rho\text{Cu}) + \frac{\text{E}_{kH}}{\text{S}_{cH}} \text{H} \frac{\partial}{\partial \xi} \left(\frac{\text{D}_H}{\text{J}} g_{22} \frac{\partial(\rho\text{C})}{\partial \xi} - \frac{\text{D}_H}{\text{J}} g_{12} \frac{\partial(\rho\text{C})}{\partial \eta} \right) \quad (\text{B2})$$

In a similar notation, the local rate of change due to the action of advection and diffusion terms in the η -coordinate direction, added to the action of advection and diffusion terms in the ξ -coordinate direction, is expressed as:

$$\begin{aligned}
 & \left[\frac{\partial}{\partial t}(\text{JH}\rho\text{C}) \right]^\eta = \left[\frac{\partial}{\partial t}(\text{JH}\rho\text{C}) \right]^\xi \\
 & - \text{R}_o \frac{\partial}{\partial \eta}(\text{JH}\rho\text{Cv}) + \frac{\text{E}_{kH}}{\text{S}_{cH}} \text{H} \frac{\partial}{\partial \eta} \left(\frac{\text{D}_H}{\text{J}} g_{11} \frac{\partial(\rho\text{C})}{\partial \eta} - \frac{\text{D}_H}{\text{J}} g_{12} \frac{\partial(\rho\text{C})}{\partial \xi} \right) \quad (\text{B3})
 \end{aligned}$$

Finally, the local rate of change due to the action of advection, fall-velocity and diffusion terms in the σ -coordinate direction, added to the combined action of advection and diffusion terms in the ξ - and η -coordinate directions, is expressed as:

$$\left[\frac{\partial}{\partial t} (JH\rho C) \right]^\sigma = \left[\frac{\partial}{\partial t} (JH\rho C) \right]^\eta \quad (B4)$$

$$-R_o \frac{\partial}{\partial \sigma} (JH\rho C\omega) + R_{of} \frac{\partial}{\partial \sigma} (J\rho Cw_f) + \frac{E_{kv}}{S_{cv}} \frac{J}{H} \frac{\partial}{\partial \sigma} \left(D_v \frac{\partial (\rho C)}{\partial \sigma} \right)$$

The mass-conservation equation for suspended sediment (Eq.(34)) is discretized in three successive steps: (1) ξ -direction step i.e discretization of Eq. (B2) by using a generalized version of the QUICKEST method; (2) η -direction step i.e. discretization of Eq. (B3), also by using a generalized QUICKEST method; (3) σ -direction step i.e. discretization of Eq. (B4) by using the QUICKEST method for local rate-of-change and advection terms, an upwind finite-difference scheme for the fall-velocity term, and a time weighted central differencing for the diffusion term. A complete discretized mass-conservation equation for suspended sediment is obtained by adding the results of the three successive steps.

ξ -direction step

The original Leonard's (1979) QUICKEST method, briefly outlined in Appendix A for the one-dimensional advection-diffusion equation in Cartesian coordinates, is generalized herein in order to accomodate the appropriate suspended-sediment equation terms in a three-dimensional curvilinear context.

First, a simplified equation is considered:

$$\frac{\partial}{\partial t} (JH\rho C) = -R_o \frac{\partial}{\partial \xi} (JH\rho C u) \quad (B5)$$

Equation (B5) is integrated over a time step and a control volume built around a main computational point C:

$$\begin{aligned}
& \frac{\Delta \xi}{2} \int J H^{n+1} (\rho C)^{n+1} dp - \frac{\Delta \xi}{2} \int J H^n (\rho C)^n dp \\
& \quad (1) \qquad \qquad \qquad (2) \\
& = R_o \int_0^{\Delta t} J_w H_w (\rho C)_w u_w d\tau - R_o \int_0^{\Delta t} J_e H_e (\rho C)_e u_e dt \\
& \quad (3) \qquad \qquad \qquad (4)
\end{aligned}
\tag{B6}$$

where: (1) and (2) are local rate-of-change terms; (3) and (4) are advection terms; τ, p are local coordinates (Fig. B1); subscripts e,w denote east and west faces of the control volume built around the main computational point C (Fig. B1).

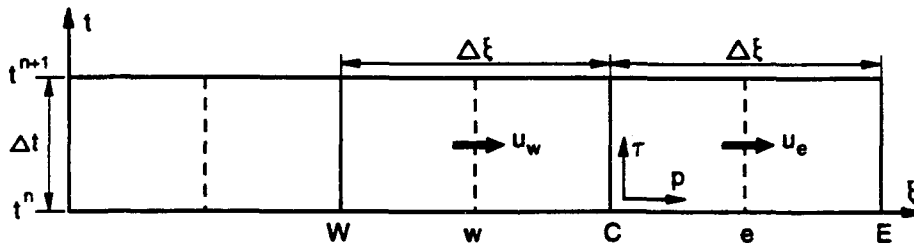


Fig. B1.

The integral Equation (B6) is further simplified, to facilitate the application of the QUICKEST method:

$$\begin{aligned}
& J_c H_c^{n+1} \int_{\frac{\Delta\xi}{2}}^{\frac{\Delta\xi}{2}} (\rho C)^{n+1} dp - J_c H_c^n \int_{\frac{\Delta\xi}{2}}^{\frac{\Delta\xi}{2}} (\rho C)^n dp \\
& \quad (1) \qquad \qquad \qquad (2) \\
& = R_o J_w \bar{H}_w \int_0^{\Delta t} (\rho C)_w u_w d\tau - R_o J_e \bar{H}_e \int_0^{\Delta t} (\rho C)_e u_e dt \\
& \quad \quad \quad (3) \qquad \qquad \quad (4)
\end{aligned} \tag{B7}$$

where

$$\bar{H} = \frac{H^{n+1} + H^n}{2}$$

Local rate-of-change terms are evaluated by representing (ρC) as a quadratic function between W and E (using known values at W, C and E), and then by integrating that function from 'w' to 'e':

$$J_c H_c \int_{\frac{\Delta\xi}{2}}^{\frac{\Delta\xi}{2}} (\rho C) dp = J_c H_c \Delta\xi \left[(\rho C)_c + \frac{\Delta\xi^2}{24} \left(\frac{\partial^2(\rho C)}{\partial \xi^2} \right)_c \right] \tag{B8}$$

where

$$\left(\frac{\partial^2(\rho C)}{\partial \xi^2} \right)_c = \frac{(\rho C)_E - 2(\rho C)_c + (\rho C)_W}{\Delta\xi^2}$$

Advection terms are treated by using a so-called 'upstream quadratic interpolation'. Consider, for example, term (3) in Eq. (B7).

When the continuity equation (mass conservation for fluid flow) is invoked, Eq. (B5) becomes:

$$\frac{\partial(\rho C)}{\partial t} + R_o u \frac{\partial(\rho C)}{\partial \xi} = 0 \tag{B9}$$

When the Lagrangian approach is used, Eq. (B9) reduces to:

$$\frac{D(\rho C)}{Dt} = 0 \quad \text{i.e.} \quad \rho C = \text{const.} \quad (\text{B10})$$

valid along the trajectory of a fluid particle defined by:

$$R_0 u = \frac{d\xi}{dt} \quad (\text{B11})$$

Figure B2 shows particle trajectories, with their 'departure' points (d) at time t^n and their 'arrival' points (a) on the w-face of the control volume at different times between 0 and Δt .

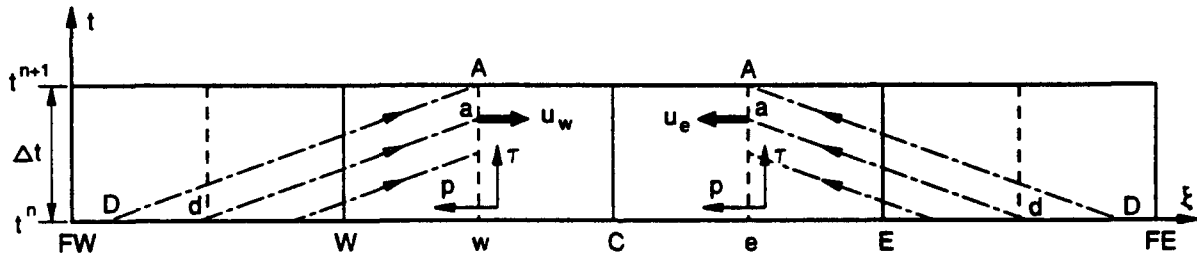


Fig. B2.

If the trajectories are straight and parallel ($u = \text{const}$), as in Fig. B2, then it is fully justified to write:

$$R_0 J_w \bar{H}_w \int_0^{\Delta t} (\rho C)_w u_w dt = J_w \bar{H}_w \int_0^{p_D} (\rho C)^n dp \quad (\text{B12})$$

where:

$$p_D = R_0 u_w \Delta t = R_0 \frac{u_w \Delta t}{\Delta \xi} \Delta \xi = \bar{C}_{r_w} \Delta \xi$$

$$\bar{C}_{r_w} = R_0 \frac{\bar{u}_w \Delta t}{\Delta \xi}$$

and τ, p are local coordinates as in Fig. B2.

The advection term is now evaluated by upstream quadratic interpolation: if the velocity direction is as in Fig. B2, (ρC) is represented as a quadratic function between FW and C (using main-point values at FW, W, and C), and then the function is integrated from 0 to p_D :

$$J_w \bar{H}_w \int_0^{\bar{C}_{r_w} \Delta \xi} (\rho C)^n dp = J_w \bar{H}_w \bar{C}_{r_w} \Delta \xi \left[\frac{(\rho C)_C + (\rho C)_W}{2} - \frac{\Delta \xi}{2} \left(\frac{\partial(\rho C)}{\partial \xi} \right)_W + \frac{\Delta \xi^2}{6} \bar{C}_{r_w} \left(\frac{\partial^2(\rho C)}{\partial \xi^2} \right)_W - \frac{\Delta \xi^2}{8} \left(\frac{\partial^2(\rho C)}{\partial \xi^2} \right)_W \right] \quad (B13)$$

where the following notation is invoked:

$$\left(\frac{\partial(\rho C)}{\partial \xi} \right)_W = \frac{(\rho C)_C - (\rho C)_W}{\Delta \xi}$$

$$\left(\frac{\partial^2(\rho C)}{\partial \xi^2} \right)_W = \frac{(\rho C)_C - 2(\rho C)_W + (\rho C)_{FW}}{\Delta \xi^2} \quad \text{for } \bar{C}_{r_w} \geq 0$$

$$\bar{C}_{r_w} = R_0 \frac{\bar{u}_w \Delta t}{\Delta \xi}$$

$$\bar{u}_w = \frac{\bar{u}_w^{n+1} + u_w^n}{2}$$

If the velocity direction is the opposite to what is shown in Fig. B2, Eq. (B13) remains the same, except that:

$$\left(\frac{\partial^2(\rho C)}{\partial \xi^2}\right)_w^n = \frac{(\rho C)_E^n - 2(\rho C)_c^n + (\rho C)_W^n}{\Delta \xi^2} \quad \text{for } \bar{C}_{r_w} < 0$$

A similar expression is easily obtained for the advection flux through the e-face of the control volume (Fig. B2):

$$\begin{aligned} J_e \bar{H}_e \int_0^{\bar{C}_{r_e} \Delta \xi} (\rho C)^n dp &= J_e \bar{H}_e \Delta \xi \left[\frac{(\rho C)_E^n + (\rho C)_c^n}{2} - \frac{\Delta \xi}{2} \left(\frac{\partial(\rho C)}{\partial \xi}\right)_e^n \right. \\ &\left. + \frac{\Delta \xi^2}{6} \bar{C}_{r_e}^2 \left(\frac{\partial^2(\rho C)}{\partial \xi^2}\right)_e^n - \frac{\Delta \xi^2}{8} \left(\frac{\partial^2(\rho C)}{\partial \xi^2}\right)_e^n \right] \end{aligned} \quad (\text{B14})$$

where:

$$\left(\frac{\partial(\rho C)}{\partial \xi}\right)_e^n = \frac{(\rho C)_E^n - (\rho C)_c^n}{\Delta \xi}$$

$$\left(\frac{\partial^2(\rho C)}{\partial \xi^2}\right)_e^n = \frac{(\rho C)_E^n - 2(\rho C)_c^n + (\rho C)_W^n}{\Delta \xi^2} \quad \text{for } \bar{C}_{r_e} \geq 0$$

$$\left(\frac{\partial^2(\rho C)}{\partial \xi^2}\right)_e^n = \frac{(\rho C)_{FE}^n - 2(\rho C)_E^n + (\rho C)_c^n}{\Delta \xi^2} \quad \text{for } \bar{C}_{r_e} < 0$$

$$\bar{C}_{r_e} = R_0 \frac{\bar{u}_e \Delta t}{\Delta \xi}$$

$$\bar{u}_e = \frac{u_e^{n+1} + u_e^n}{2}$$

The local rate-of-change term:

$$J_c H_c^{n+1} \int_{-\frac{\Delta \xi}{2}}^{\frac{\Delta \xi}{2}} (\rho C)^{n+1} dp - J_c H_c^n \int_{-\frac{\Delta \xi}{2}}^{\frac{\Delta \xi}{2}} (\rho C)^n dp$$

$$\begin{aligned}
&= \Delta\xi \left[J_c H_c^{n+1} (\rho C)_c^{n+1} - J_c H_c^n (\rho C)_c^n \right] \\
&+ \Delta\xi \frac{\Delta\xi^2}{24} \left[J_c H_c^{n+1} \left(\frac{\partial^2 (\rho C)}{\partial \xi^2} \right)_c^{n+1} - J_c H_c^n \left(\frac{\partial^2 (\rho C)}{\partial \xi^2} \right)_c^n \right] \quad (B15)
\end{aligned}$$

where p is a local coordinate as in Fig. B1, is further manipulated by using the governing Eq. (B5). Equation (B5) can be written as:

$$\frac{\partial}{\partial t} \left[\frac{\partial^2}{\partial \xi^2} (JH\rho C) \right] = -R_o \frac{\partial}{\partial \xi} \left[\frac{\partial^2}{\partial \xi^2} (JH\rho Cu) \right] \quad (B16)$$

The left-hand-side of Eq. (B16) is approximated by:

$$\frac{\partial}{\partial t} \left[\frac{\partial^2}{\partial \xi^2} (JH\rho C) \right] \cong \frac{\partial}{\partial t} \left[JH \frac{\partial^2 (\rho C)}{\partial \xi^2} \right] = \frac{1}{\Delta t} \left[J_c H_c^{n+1} \frac{\partial^2 (\rho C)}{\partial \xi^2}_c^{n+1} - J_c H_c^n \left(\frac{\partial^2 (\rho C)}{\partial \xi^2} \right)_c^n \right] \quad (B17)$$

while the right-hand-side of Eq. (B16) is approximated by:

$$\begin{aligned}
-R_o \frac{\partial}{\partial \xi} \left[\frac{\partial^2}{\partial \xi^2} (JH\rho Cu) \right] &\cong R_o \frac{\partial}{\partial \xi} \left[JHu \frac{\partial^2 (\rho C)}{\partial \xi^2} \right] \\
&= \frac{R_o}{\Delta \xi} \left[J_e \bar{H}_e \bar{u}_e \left(\frac{\partial^2 (\rho C)}{\partial \xi^2} \right)_e^n - J_w \bar{H}_w \bar{u}_w \left(\frac{\partial^2 (\rho C)}{\partial \xi^2} \right)_w^n \right] \quad (B18)
\end{aligned}$$

The final outcome is:

$$\begin{aligned}
&J_c H_c^{n+1} \left(\frac{\partial^2 (\rho C)}{\partial \xi^2} \right)_c^{n+1} - J_c H_c^n \left(\frac{\partial^2 (\rho C)}{\partial \xi^2} \right)_c^n \\
&= J_w \bar{H}_w \bar{C}_{r_w} \left(\frac{\partial^2 (\rho C)}{\partial \xi^2} \right)_w^n - J_e \bar{H}_e \bar{C}_{r_e} \left(\frac{\partial^2 (\rho C)}{\partial \xi^2} \right)_e^n \quad (B19)
\end{aligned}$$

When Eq. (B19) is introduced into Eq. (B15), the local rate-of-change terms become:

$$\begin{aligned}
& J_c H_c^{n+1} \int_{-\frac{\Delta\xi}{2}}^{\frac{\Delta\xi}{2}} (\rho C)^{n+1} dp - J_c H_c^n \int_{-\frac{\Delta\xi}{2}}^{\frac{\Delta\xi}{2}} (\rho C)^n dp \\
&= \Delta\xi \left[J_c H_c^{n+1} (\rho C)_c^{n+1} - J_c H_c^n (\rho C)_c^n \right] \\
&+ \Delta\xi \frac{\Delta\xi^2}{24} \left[J_w \bar{H}_w \bar{C}_{r_w} \left(\frac{\partial^2(\rho C)}{\partial \xi^2} \right)_w^n - J_e \bar{H}_e \bar{C}_{r_e} \left(\frac{\partial^2(\rho C)}{\partial \xi^2} \right)_e^n \right]
\end{aligned} \tag{B20}$$

By using Eqs. (B13), (B14) and (B20), the discretized Eq. (B7) reads:

$$\begin{aligned}
& J_c H_c^{n+1} (\rho C)_c^{n+1} - J_c H_c^n (\rho C)_c^n \\
&= J_w \bar{H}_w \bar{C}_{r_w} \left[\frac{(\rho C)_c^n + (\rho C)_w^n}{2} - \frac{\Delta\xi}{2} \left(\frac{\partial(\rho C)}{\partial \xi} \right)_w^n - \frac{\Delta\xi^2}{6} (1 - \bar{C}_{r_w}^2) \left(\frac{\partial^2(\rho C)}{\partial \xi^2} \right)_w^n \right] \\
&J_e \bar{H}_e \bar{C}_{r_e} \left[\frac{(\rho C)_e^n + (\rho C)_c^n}{2} - \frac{\Delta\xi}{2} \left(\frac{\partial(\rho C)}{\partial \xi} \right)_e^n - \frac{\Delta\xi^2}{6} (1 - \bar{C}_{r_e}^2) \left(\frac{\partial^2(\rho C)}{\partial \xi^2} \right)_e^n \right]
\end{aligned} \tag{B21}$$

A complete Eq. (B2) is considered next. Equation (B2) is integrated over a time step and the control volume built around a main computational point C (Fig. B1):

$$\begin{aligned}
& \frac{\Delta\xi}{2} \int_{-\frac{\Delta\xi}{2}}^{\frac{\Delta\xi}{2}} J H^{n+1} (\rho C)^{n+1} dp - \frac{\Delta\xi}{2} \int_{-\frac{\Delta\xi}{2}}^{\frac{\Delta\xi}{2}} J H^n (\rho C)^n dp
\end{aligned}$$

(1)

(2)

$$= R_o \int_0^{\Delta t} J_w H_w (\rho C)_w u_w dt - R_o \int_0^{\Delta t} J_e H_e (\rho C)_e u_e dt$$

(3)

(4)

$$+ \frac{E_{kH}}{S_{cH}} \tilde{H}_c \int_0^{\Delta t} \frac{D_{H_e}}{J_e} \left[g_{22_e} \left(\frac{\partial(\rho C)}{\partial \xi} \right)_e - g_{12_e} \left(\frac{\partial(\rho C)}{\partial \eta} \right)_e \right] d\tau$$

(5)

(B22)

$$\frac{E_{kH}}{S_{cH}} \tilde{H}_c \int_0^{\Delta t} \frac{D_{H_w}}{J_w} \left[g_{22_w} \left(\frac{\partial(\rho C)}{\partial \xi} \right)_w - g_{12_w} \left(\frac{\partial(\rho C)}{\partial \eta} \right)_w \right] d\tau$$

(6)

The local rate-of-change terms (1) and (2), as well as the advection terms (3) and (4) are treated as previously described. The diffusion terms (5) and (6) are also treated according to the same idea of 'upstream quadratic interpolation'. Consider, for example, term (6):

$$\frac{E_{kH}}{S_{cH}} \tilde{H}_c \int_0^{\Delta t} \frac{D_{H_w}}{J_w} \left[g_{22_w} \left(\frac{\partial(\rho C)}{\partial \xi} \right)_w - g_{12_w} \left(\frac{\partial(\rho C)}{\partial \eta} \right)_w \right] d\tau =$$

(B23)

$$= \frac{E_{kH}}{S_{cH}} \tilde{H}_c \frac{\tilde{D}_{H_w}}{J_w} \left[g_{22_w} \left(\frac{\partial(\tilde{\rho C})}{\partial \xi} \right)_w - g_{12_w} \left(\frac{\partial(\tilde{\rho C})}{\partial \eta} \right)_w \right] \Delta \tau =$$

where

$$\tilde{D}_{H_w} = \frac{D_{H_w}^{n+1} + D_{H_w}^n}{2}$$

and

$$\left(\frac{\partial(\tilde{\rho C})}{\partial \xi} \right)_w = \left(\frac{\partial(\rho C)}{\partial \xi} \right)_w^{n+1/2}$$

$$\left(\frac{\partial(\tilde{\rho C})}{\partial \eta} \right)_w = \left(\frac{\partial(\rho C)}{\partial \eta} \right)_w^{n+1/2}$$

are w-wall gradients of (ρC) evaluated at $\frac{\Delta t}{2}$.

It is further assumed that the gradients of (ρC) are advected downstream essentially unchanged, along the constant-slope trajectory (Fig. B3). It remains to find the departure point D of the trajectory that arrives at the w-face of the control volume at $\frac{\Delta t}{2}$ and to evaluate gradients at D by upstream quadratic interpolation. The departure point of the trajectory is defined as:

$$p_D = -R_0 \bar{u}_w \frac{\Delta t}{2} = -R_0 \frac{\bar{u}_w \Delta t}{\Delta \xi} \frac{\Delta \xi}{2} = -\bar{C}_{r_w} \frac{\Delta \xi}{2} \quad (\text{B24})$$

where p_D is the position of the departure point in local coordinates (Fig. B3).

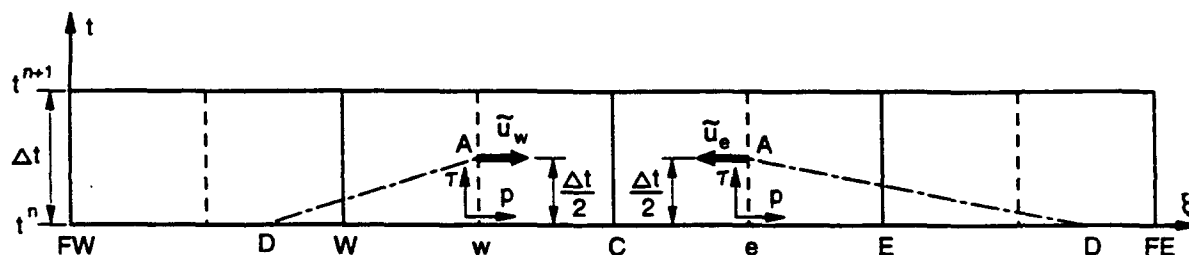


Figure B3.

Further treatment of gradients $\left(\frac{\partial(\tilde{\rho C})}{\partial \xi}\right)$ and $\left(\frac{\partial(\tilde{\rho C})}{\partial \eta}\right)$ slightly differs. If the w-wall velocity direction is as in Fig. B3, (ρC) is represented as a quadratic function between FW and C (using main-point values at FW, W, and C), with the gradient $\left(\frac{\partial(\rho C)}{\partial \xi}\right)$ readily derived from the function. The gradient $\left(\frac{\partial(\rho C)}{\partial \xi}\right)^n$ evaluated at D, reads:

$$\left(\frac{\partial(\tilde{\rho C})}{\partial \xi}\right)_w = \left(\frac{\partial(\rho C)}{\partial \xi}\right)_D^n = \Delta \xi \frac{1}{\Delta \xi^2} \left[\Delta \xi \left(\frac{\partial(\rho C)}{\partial \xi}\right)_w^n - \frac{\Delta \xi^2}{2} \bar{C}_{r_w} \left(\frac{\partial^2(\rho C)}{\partial \xi^2}\right)_w^n \right] \quad (\text{B25})$$

and the right-hand-side derivatives have the same meaning as in Eq. (B13). If the w-wall velocity has the opposite direction from what is shown in Fig. B3, the right-hand-side derivatives again have the same meaning as in Eq. (B13).

Since it is not possible to derive the gradient $\left(\frac{\partial(\rho C)}{\partial \eta}\right)$ from a function defined along the ξ direction, the solution is found in defining previous-time-level auxiliary derivatives $\left(\frac{\partial(\rho C)}{\partial \eta}\right)^n$ at main computational points (by simple central differencing) and evaluating the gradients $\left(\frac{\partial(\rho C)}{\partial \eta}\right)_D^n$ by upstream linear interpolation. Linear interpolation is justified for gradients of a quadratic function. The gradient $\left(\frac{\partial(\rho C)}{\partial \eta}\right)^n$ evaluated at D reads:

$$\left(\frac{\partial(\tilde{\rho C})}{\partial \eta}\right)_w = \left(\frac{\partial(\rho C)}{\partial \eta}\right)_D^n = \frac{1 - \bar{C}_{r_w}}{2} \left(\frac{\partial(\rho C)}{\partial \eta}\right)_c^n + \frac{1 + \bar{C}_{r_w}}{2} \left(\frac{\partial(\rho C)}{\partial \eta}\right)_w^n \quad \text{for } |\bar{C}_{r_w}| < 1 \quad (\text{B26})$$

i.e.

$$\left(\frac{\partial(\tilde{\rho C})}{\partial \eta}\right)_w = \left(\frac{\partial(\rho C)}{\partial \eta}\right)_D^n = \frac{3 - \bar{C}_{r_w}}{2} \left(\frac{\partial(\rho C)}{\partial \eta}\right)_w^n + \frac{\bar{C}_{r_w} - 1}{2} \left(\frac{\partial(\rho C)}{\partial \eta}\right)_{FW}^n \quad \text{for } \bar{C}_{r_w} > 1 \quad (\text{B27})$$

i.e.

$$\left(\frac{\partial(\tilde{\rho C})}{\partial \eta}\right)_w = \left(\frac{\partial(\rho C)}{\partial \eta}\right)_D^n = \frac{3 + \bar{C}_{r_w}}{2} \left(\frac{\partial(\rho C)}{\partial \eta}\right)_c^n - \frac{1 - \bar{C}_{r_w}}{2} \left(\frac{\partial(\rho C)}{\partial \eta}\right)_E^n \quad \text{for } \bar{C}_{r_w} < -1 \quad (\text{B28})$$

where the Courant-type number \bar{C}_{r_w} shows not only the w-wall velocity direction, but also the interpolation interval.

Similar expressions are easily obtained for the diffusion flux across the e-face of the control volume:

$$\begin{aligned} \frac{E_{kH} \bar{H}_c}{S_{cH}} \int_0^{\Delta t} \frac{D_{H_e}}{J_e} \left[g_{22_e} \left(\frac{\partial(\rho C)}{\partial \xi} \right)_e - g_{12_e} \left(\frac{\partial(\rho C)}{\partial \eta} \right)_e \right] d\tau = \\ = \frac{L_{kH} \bar{H}_c}{S_{cH}} \frac{\bar{D}_{H_e}}{J_e} \left[g_{22_e} \left(\frac{\partial(\tilde{\rho C})}{\partial \xi} \right)_e - g_{12_e} \left(\frac{\partial(\tilde{\rho C})}{\partial \eta} \right)_e \right] \Delta \tau \end{aligned} \quad (B29)$$

where

$$\bar{D}_{H_e} = \frac{D_{H_e}^{n+1} + D_{H_e}^n}{2}$$

The gradient $\left(\frac{\partial(\tilde{\rho C})}{\partial \xi} \right)_e$ reads:

$$\left(\frac{\partial(\tilde{\rho C})}{\partial \xi} \right)_e = \left(\frac{\partial(\rho C)}{\partial \xi} \right)_D^n = \Delta \xi \frac{1}{\Delta \xi^2} \left[\Delta \xi \left(\frac{\partial(\rho C)}{\partial \xi} \right)_e^n - \frac{\Delta \xi^2}{2} \bar{C}_{r_e} \left(\frac{\partial^2(\rho C)}{\partial \xi^2} \right)_e^n \right] \quad (B30)$$

where the right-hand-side derivatives have the same meaning as in Eq. (B14).

The gradient $\left(\frac{\partial(\tilde{\rho C})}{\partial \eta} \right)_e$ reads:

$$\left(\frac{\partial(\tilde{\rho C})}{\partial \eta} \right)_e = \left(\frac{\partial(\rho C)}{\partial \eta} \right)_D^n = \frac{1 - \bar{C}_{r_e}}{2} \left(\frac{\partial(\rho C)}{\partial \eta} \right)_E^n + \frac{1 + \bar{C}_{r_e}}{2} \left(\frac{\partial(\rho C)}{\partial \eta} \right)_C^n \quad \text{for } |\bar{C}_{r_e}| < 1 \quad (B31)$$

i.e.

$$\left(\frac{\partial(\tilde{\rho C})}{\partial \eta} \right)_e = \left(\frac{\partial(\rho C)}{\partial \eta} \right)_D^n = \frac{3 - \bar{C}_{r_e}}{2} \left(\frac{\partial(\rho C)}{\partial \eta} \right)_C^n + \frac{\bar{C}_{r_e} - 1}{2} \left(\frac{\partial(\rho C)}{\partial \eta} \right)_W^n \quad \text{for } \bar{C}_{r_e} > 1 \quad (B32)$$

i.e.

$$\left(\frac{\partial \tilde{\rho C}}{\partial \eta}\right)_e = \left(\frac{\partial(\rho C)}{\partial \eta}\right)_D = -\frac{1 + \bar{C}_{r_e}}{2} \left(\frac{\partial(\rho C)}{\partial \eta}\right)_{FE} + \frac{3 + \bar{C}_{r_e}}{2} \left(\frac{\partial(\rho C)}{\partial \eta}\right)_E \quad \text{for } \bar{C}_{r_e} < -1 \quad (\text{B33})$$

where the Courant-type number \bar{C}_{r_e} shows not only the e-wall velocity direction, but also the interpolation interval.

Finally, the discretized Equation (B2), i.e. (B22), reads:

$$\begin{aligned} & J_c H_c^{n+1} (\rho C)_c^{n+1} - J_c H_c^n (\rho C)_c^n \\ &= J_w \bar{H}_w \bar{C}_{r_w} \left[\frac{(\rho C)_c^n + (\rho C)_w^n}{2} - \frac{\Delta \xi}{2} \left(\frac{\partial(\rho C)}{\partial \xi}\right)_w - \frac{\Delta \xi^2}{6} (1 - \bar{C}_{r_w}^2) \left(\frac{\partial^2(\rho C)}{\partial \xi^2}\right)_w \right] \\ & - J_e \bar{H}_e \bar{C}_{r_e} \left[\frac{(\rho C)_e^n + (\rho C)_c^n}{2} - \frac{\Delta \xi}{2} \left(\frac{\partial(\rho C)}{\partial \xi}\right)_e - \frac{\Delta \xi^2}{6} (1 - \bar{C}_{r_e}^2) \left(\frac{\partial^2(\rho C)}{\partial \xi^2}\right)_e \right] \\ & + \bar{\alpha}_{H_e} \frac{\bar{H}_c}{J_e} \left\{ g_{22_e} \left[\Delta \xi \left(\frac{\partial(\rho C)}{\partial \xi}\right)_e - \frac{\Delta \xi^2}{2} \bar{C}_{r_e} \left(\frac{\partial^2(\rho C)}{\partial \xi^2}\right)_e \right] - g_{12_e} \Delta \xi \left(\frac{\partial \tilde{\rho C}}{\partial \eta}\right)_e \right\} \\ & - \bar{\alpha}_w \frac{\bar{H}_c}{J_w} \left\{ g_{22_w} \left[\Delta \xi \left(\frac{\partial(\rho C)}{\partial \xi}\right)_w - \frac{\Delta \xi^2}{2} \bar{C}_{r_w} \left(\frac{\partial^2(\rho C)}{\partial \xi^2}\right)_w \right] - g_{12_w} \Delta \xi \left(\frac{\partial \tilde{\rho C}}{\partial \eta}\right)_w \right\} \end{aligned} \quad (\text{B34})$$

where:

$$\bar{\alpha}_{H_w} = \frac{E_{kH}}{S_{cH}} \frac{\bar{\Gamma}_{H_w} \Delta t}{\Delta \xi^2} \quad \bar{\alpha}_{H_e} = \frac{E_{kH}}{S_{cH}} \frac{\bar{D}_{H_e} \Delta t}{\Delta \xi^2}$$

The discretized Eq. (B34) is explicit, meaning that the unknown suspended-sediment concentration is related to the computational point C only. Suspended-sediment concentrations related to neighboring computational points appear in Eq. (B34) explicitly, i.e. as known values. It is useful to point out those elements of the discretized equation that are expressed explicitly in terms of sediment variables by introducing a special notation for them. Therefore, Equation (B34) is rewritten as:

$$J_c H_c^E (\rho C)_c^E - J_c H_c^n (\rho C)_c^n = (\text{adv})_w - (\text{adv})_e + (\text{dif})_e - (\text{dif})_w \quad (\text{B35})$$

$$\begin{aligned}
(\text{adv})_e &= J_w \tilde{H}_w \tilde{C}_{r_w} \left[\frac{(\rho C)_c^n + (\rho C)_w^n}{2} - \frac{\Delta \xi}{2} \left(\frac{\partial(\rho C)}{\partial \xi} \right)_w^n - \frac{\Delta \xi^2}{6} (1 - \tilde{C}_{r_w}^2) \left(\frac{\partial^2(\rho C)}{\partial \xi^2} \right)_w^n \right] \\
(\text{adv})_w &= J_w \tilde{H}_w \tilde{C}_{r_w} \left[\frac{(\rho C)_e^n + (\rho C)_c^n}{2} - \frac{\Delta \xi}{2} \left(\frac{\partial(\rho C)}{\partial \xi} \right)_e^n - \frac{\Delta \xi^2}{6} (1 - \tilde{C}_{r_e}^2) \left(\frac{\partial^2(\rho C)}{\partial \xi^2} \right)_e^n \right] \\
(\text{dif})_w &= \tilde{\alpha}_{H_w} \frac{\tilde{H}_c}{J_w} \left\{ g_{22_w} \left[\Delta \xi \left(\frac{\partial(\rho C)}{\partial \xi} \right)_w^n - \frac{\Delta \xi^2}{2} \tilde{C}_{r_w} \left(\frac{\partial^2(\rho C)}{\partial \xi^2} \right)_w^n \right] - g_{12_w} \Delta \xi \left(\frac{\partial(\tilde{\rho C})}{\partial \eta} \right)_w \right\} \\
(\text{dif})_e &= \tilde{\alpha}_{H_e} \frac{\tilde{H}_c}{J_e} \left\{ g_{22_e} \left[\Delta \xi \left(\frac{\partial(\rho C)}{\partial \xi} \right)_e^n - \frac{\Delta \xi^2}{2} \tilde{C}_{r_e} \left(\frac{\partial^2(\rho C)}{\partial \xi^2} \right)_e^n \right] - g_{12_e} \Delta \xi \left(\frac{\partial(\tilde{\rho C})}{\partial \eta} \right)_e \right\}
\end{aligned}$$

where $(\text{adv})_w$ and $(\text{adv})_e$ stand for advection fluxes across the w-face and the e-face of the control volume, respectively, while $(\text{dif})_e$ and $(\text{dif})_w$ stand for diffusion fluxes across the w-face and the e-face of the control volume, respectively:

Boundary Conditions

Boundary conditions for Eq. (B34) (i.e. Eq. (B35)) differ depending on the type of the boundary (impermeable, outflow or inflow). Following the recommendation of Leonard (1979), boundary conditions are specified to be control-volume wall values, rather than node values. Also, special interpolations are required at boundary points, or at points next to the boundary. Boundary conditions are summarized below.

Outflow Boundary at w-Face of Control Volume

The same procedure as described by Eqs. (B5) to (B35) is applied to a computational point that has an outflow boundary at the w-face of the control volume. The only difference is that the appropriate upstream quadratic interpolation, next to the w-face of the control volume, uses known values at points E, C and known outflow boundary value at B_w , i.e. at the w-face of the control volume built around point C.

As a result, advection and diffusion fluxes across the e-face of the control volume, $(\text{adv})_e$ and $(\text{dif})_e$, have the same form as in Eq. (B35).

Advection and diffusion fluxes across the w-face of the control volume, $(adv)_w$ and $(dif)_w$, have the following form:

$$(adv)_w = J_w \tilde{H}_w \tilde{C}_{r_w} \left[(\rho C)_{B_w}^n - \frac{\Delta \xi}{2} \tilde{C}_{r_w} \left(\frac{\partial(\rho C)}{\partial \xi} \right)_{B_w}^n - \frac{\Delta \xi^2}{6} \left(\frac{1}{4} - \tilde{C}_{r_w}^2 \right) \left(\frac{\partial^2(\rho C)}{\partial \xi^2} \right)_{B_w}^n \right] \quad (B36)$$

$$(dif)_w = \bar{\alpha}_{H_w} \frac{\tilde{H}_c}{J_w} \left\{ g_{22_w} \left[\Delta \xi \left(\frac{\partial(\rho C)}{\partial \xi} \right)_{B_w}^n - \frac{\Delta \xi^2}{2} \tilde{C}_{r_w} \left(\frac{\partial^2(\rho C)}{\partial \xi^2} \right)_{B_w}^n \right] - g_{12_w} \Delta \xi \left(\frac{\partial \tilde{(\rho C)}}{\partial \eta} \right)_{B_w} \right\} \quad (B37)$$

where

$$\left(\frac{\partial(\rho C)}{\partial \xi} \right)_{B_w}^n = \frac{-8(\rho C)_{B_w}^n + g(\rho C)_c^n - (\rho C)_E^n}{3\Delta \xi}$$

$$\left(\frac{\partial^2(\rho C)}{\partial \xi^2} \right)_{B_w}^n = \frac{4(\rho C)_E^n - 12(\rho C)_c^n + 8(\rho C)_{B_w}^n}{3\Delta \xi^2}$$

$$\left(\frac{\partial \tilde{(\rho C)}}{\partial \eta} \right)_{B_w} = (1 + \tilde{C}_{r_w}) \left(\frac{\partial(\rho C)}{\partial \eta} \right)_{B_w}^n - \tilde{C}_{r_w} \left(\frac{\partial(\rho C)}{\partial \eta} \right)_C^n \quad \text{for } -1 < C_{r_w} < 0$$

i.e.

$$\left(\frac{\partial \tilde{(\rho C)}}{\partial \eta} \right)_{B_w} = \frac{3 + \tilde{C}_{r_w}}{2} \left(\frac{\partial(\rho C)}{\partial \eta} \right)_C^n - \frac{1 + \tilde{C}_{r_w}}{2} \left(\frac{\partial(\rho C)}{\partial \eta} \right)_E^n \quad \text{for } \tilde{C}_{r_w} < -1$$

are derivatives evaluated at the boundary B_w , i.e. at the w-face of the control volume built around point C.

Inflow Boundary at w-Face of Control Volume

The same procedure as described by Eqs. (B5) to (B35) is applied to a computational point that has an inflow boundary at the w-face of the control volume. The difference is that the appropriate upstream quadratic interpolation, next to the the w-face of the control volume, uses known values at points E, C and the known outflow boundary value at B_w , i.e. at the w-face of the control volume built around C. Also, the term (3) of Eq. (B6) (or Eq. (B22)) is evaluated by using straightforward integration, with the known inflow boundary value at B_w , i.e. at the w-face of the control volume built around C:

$$R_0 J_w \bar{H}_w \int_0^{\Delta t} (\rho C)_w u_w d\tau = R_0 J_w \bar{H}_w \bar{u}_w (\tilde{\rho C})_{B_w} \Delta t = J_w \bar{H}_w \bar{C}_{r_w} (\tilde{\rho C})_{B_w} \Delta \xi \quad (B38)$$

where

$$(\tilde{\rho C})_{B_w} = \frac{(\rho C)_{B_w}^{n+1} + (\rho C)_{B_w}^n}{2}$$

As a result, advection and diffusion fluxes across the e-face of the control volume, $(adv)_e$ and $(dif)_e$, have the same form as in Eq. (B35).

Advection and diffusion fluxes across the w-face of control volume, $(adv)_w$ and $(dif)_w$, have the following form:

$$(adv)_w = J_w \bar{H}_w \bar{C}_{r_w} = \left[(\tilde{\rho C})_{B_w} - \frac{\Delta \xi^2}{24} \left(\frac{\partial^2 (\rho C)}{\partial \xi^2} \right)_{B_w}^n \right] \quad (B39)$$

$$(dif)_w = \bar{\alpha}_{H_w} \frac{\bar{H}_c}{J_w} \left[g_{22_w} \Delta \xi \left(\frac{\partial (\rho C)}{\partial \xi} \right)_{B_w}^n - g_{12_w} \Delta \xi \left(\frac{\partial (\rho C)}{\partial \eta} \right)_{B_w} \right] \quad (B40)$$

where

$$\left(\frac{\partial^2 (\rho C)}{\partial \xi^2} \right)_{B_w}^n = \frac{4(\rho C)_E^n - 12(\rho C)_C^n + (\rho C)_{B_w}^n}{3\Delta \xi^2}$$

$$\left(\frac{\partial(\rho C)}{\partial \xi}\right)_{B_w}^n = \frac{-8(\rho C)_{B_w}^n + 9(\rho C)_c^n - (\rho C)_E^n}{\Delta \xi}$$

$$\left(\frac{\partial \tilde{(\rho C)}}{\partial \eta}\right)_{B_w} = \frac{1}{2} \left[\left(\frac{\partial(\rho C)}{\partial \eta}\right)_{B_w}^{n+1} + \left(\frac{\partial(\rho C)}{\partial \eta}\right)_{B_w}^n \right]$$

are derivatives evaluated at the boundary, i.e. at the w-face of the control volume. The second right-hand-side term of Eq. (B39) originates from the appropriate rate-of-change term, as in Eq. (B20).

Impermeable Boundary at w-Face of Control Volume

The same procedure as described by Eqs. (B5) to (B35) is applied to a computational point that has an impermeable boundary at the w-face of the control volume. The advection term (3) in Eq. (B22) is equal to zero. The velocity \bar{u}_w , i.e. the Courant number \bar{C}_{r_w} , are also equal to zero, which eliminates the appropriate term in Eq. (B20). The first derivative across the impermeable boundary is also set to zero.

As a result, advection and diffusion fluxes across the w-face of the control volume read:

$$(\text{adv})_w = 0 \quad (\text{B41})$$

$$(\text{dif})_w = \bar{\alpha}_{H_w} \frac{\bar{H}_c}{J_w} \left\{ \xi_{22_w} \Delta \xi \left(\frac{\partial \tilde{(\rho C)}}{\partial \xi}\right)_{B_w} - \xi_{12_w} \Delta \xi \left(\frac{\partial \tilde{(\rho C)}}{\partial \eta}\right)_{B_w} \right\} \quad (\text{B42})$$

where:

$$\left(\frac{\partial \tilde{(\rho C)}}{\partial \xi}\right)_{B_w} = 0$$

$$\left(\frac{\partial \tilde{(\rho C)}}{\partial \eta}\right)_{B_w} = \left(\frac{\partial(\rho C)}{\partial \eta}\right)_{B_w}^n$$

are derivatives evaluated at the boundary, i.e. at the w-face of the control volume built around point C.

Advection and diffusion fluxes across the e-face of the control volume, $(adv)_e$ and $(dif)_e$, have the same form as in Eq. (B35).

Outflow Boundary at e-Face of Control Volume

The same approach as for an outflow boundary at the w-face of the control volume is used. The appropriate upstream quadratic interpolation, next to the e-face of the control volume, uses known values at points W, C and a known outflow boundary value at B_e , i.e. at the e-face of the control volume built around point C.

As a result, advection and diffusion fluxes across the w-face of the control volume, $(adv)_w$ and $(dif)_w$, have the same form as in Eq. (B35).

Advection and diffusion fluxes across the e-face of control volume, $(adv)_e$ and $(dif)_e$, have the following form:

$$(adv)_e = J_e \bar{H}_e \bar{C}_{r_e} \left[(\rho C)_{B_e}^n - \frac{\Delta \xi}{2} \bar{C}_{r_e} \left(\frac{\partial(\rho C)}{\partial \xi} \right)_{B_e}^n - \frac{\Delta \xi^2}{6} \left(\frac{1}{4} - \bar{C}_{r_e}^2 \right) \left(\frac{\partial^2(\rho C)}{\partial \xi^2} \right)_{B_e}^n \right] \quad (B43)$$

$$(dif)_e = \bar{\alpha}_{H_e} \frac{\bar{H}_c}{J_e} \left\{ g_{22_e} \left[\Delta \xi \left(\frac{\partial(\rho C)}{\partial \xi} \right)_{B_e}^n - \frac{\Delta \xi^2}{2} \bar{C}_{r_e} \left(\frac{\partial^2(\rho C)}{\partial \xi^2} \right)_{B_e}^n \right] - g_{12_e} \Delta \xi \left(\frac{\partial(\rho C)}{\partial \eta} \right)_{B_e}^n \right\} \quad (B44)$$

where

$$\left(\frac{\partial(\rho C)}{\partial \xi} \right)_{B_e}^n = \frac{-8(\rho C)_{B_e}^n - 9(\rho C)_c^n + (\rho C)_w^n}{3\Delta \xi}$$

$$\left(\frac{\partial^2(\rho C)}{\partial \xi^2} \right)_{B_e}^n = \frac{8(\rho C)_{B_e}^n - 12(\rho C)_c^n + 4(\rho C)_w^n}{3\Delta \xi^2}$$

$$\left(\frac{\partial(\tilde{\rho C})}{\partial \eta}\right)_{B_e} = (1 - \bar{C}_{r_e}) \left(\frac{\partial(\rho C)}{\partial \eta}\right)_{B_e}^n + \bar{C}_{r_e} \left(\frac{\partial(\rho C)}{\partial \eta}\right)_C^n \quad \text{for } 0 < C_{r_e} < 1$$

i.e.

$$\left(\frac{\partial(\tilde{\rho C})}{\partial \eta}\right)_{B_e} = \frac{3 - \bar{C}_{r_e}}{2} \left(\frac{\partial(\rho C)}{\partial \eta}\right)_C^n + \frac{\bar{C}_{r_e} - 1}{2} \left(\frac{\partial(\rho C)}{\partial \eta}\right)_W^n \quad \text{for } C_{r_e} > 1$$

are derivatives evaluated at the boundary, i.e. at e-face of control volume built around C.

Inflow Boundary at e-Face of Control Volume

The same approach as for an inflow boundary at the w-face of the control volume is used. The appropriate upstream quadratic interpolation, next to the e-face of the control volume, uses known values at points W, C and a known outflow boundary value at B_e , i.e. at the e-face of the control volume built around point C. Term (4) of Eq. (B6) (or Eq. (B22)) is evaluated by using straightforward integration, with a known inflow boundary value at B_e , i.e. at the e-face of the control volume.

As a result, advection and diffusion fluxes across the w-face of the control volume, $(adv)_w$ and $(dif)_w$, have the same form as in Eq. (B35).

Advection and diffusion fluxes across the e-face of the control volume, $(adv)_e$ and $(dif)_e$, have the following form:

$$(adv)_e = J_e \bar{H}_e \bar{C}_{r_e} \left[(\tilde{\rho C})_{B_e} - \frac{\Delta \xi^2}{24} \left(\frac{\partial^2(\rho C)}{\partial \xi^2}\right)_{B_e}^n \right] \quad (B45)$$

$$(dif)_e = \bar{\alpha}_{H_e} \frac{\bar{H}_e}{J_e} \left\{ g_{22_e} \Delta \xi \left(\frac{\partial(\rho C)}{\partial \xi}\right)_{B_e}^n - g_{12_e} \Delta \xi \left(\frac{\partial(\rho C)}{\partial \eta}\right)_{B_e} \right\} \quad (B46)$$

where

$$\left(\frac{\partial^2(\rho C)}{\partial \xi^2}\right)_{B_e}^n = \frac{8(\rho C)_{B_e}^n - 12(\rho C)_C^n + 4(\rho C)_W^n}{3\Delta \xi^2}$$

$$\left(\frac{\partial(\rho C)}{\partial \xi}\right)_{B_e}^n = \frac{8(\rho C)_{B_e}^n - 9(\rho C)_c^n + (\rho C)_w^n}{3\Delta \xi}$$

$$\left(\frac{\partial(\tilde{\rho C})}{\partial \eta}\right)_{B_e} = \frac{1}{2} \left[\left(\frac{\partial(\rho C)}{\partial \eta}\right)_{B_e}^{n+1} + \left(\frac{\partial(\rho C)}{\partial \eta}\right)_{B_e}^n \right]$$

$$(\tilde{\rho C})_{B_e} = \frac{1}{2} [(\rho C)_{B_e}^{n+1} + (\rho C)_{B_e}^n]$$

are evaluated at the boundary, i.e. at the e-face of the control volume built around C.

Impermeable Boundary at e-Face of Control Volume

Following the same arguments as for an impermeable boundary at the w-face of the control volume, it is easy to derive expressions for advection and diffusion fluxes across an impermeable e-face of the control volume:

$$(\text{adv})_e = 0 \quad (\text{B47})$$

$$(\text{dif})_e = \tilde{\alpha}_{H_e} \frac{\tilde{H}_c}{J_e} \left\{ g_{22_e} \Delta \xi \left(\frac{\partial(\tilde{\rho C})}{\partial \xi}\right)_{B_e} - g_{12_e} \Delta \xi \left(\frac{\partial(\tilde{\rho C})}{\partial \eta}\right)_{B_e} \right\} \quad (\text{B48})$$

where

$$\left(\frac{\partial(\tilde{\rho C})}{\partial \xi}\right)_{B_e} = 0$$

$$\left(\frac{\partial(\tilde{\rho C})}{\partial \eta}\right)_{B_e} = \left(\frac{\partial(\rho C)}{\partial \eta}\right)_{B_e}^n$$

while advection and diffusion fluxes across the w-face of the control volume, $(\text{adv})_w$ and $(\text{dif})_w$, have the same form as in Eq. (B35).

Interpolations for Points Next to the Boundary

Consider the w-face of a control volume built around a computational point C.

First assume that the direction of the velocity is as in Fig. B4 and that the w-face of the control volume built around the computational point W is a boundary B_{fw} .

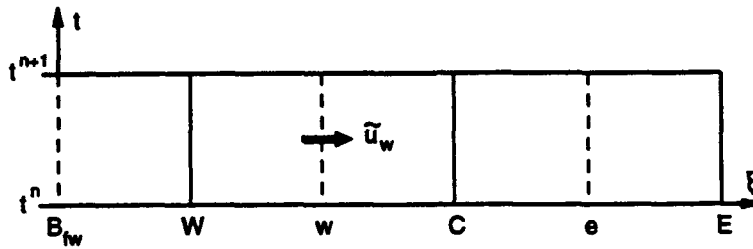


Figure B4.

The same procedure as described by Eqs. (B5) to (B35) is applied to the computational point C. Advection and diffusion fluxes across the w-face of the control volume built around the computational point C, $(adv)_w$ and $(dif)_w$, have the same form as in Eq. (B35), the only difference being that the appropriate upstream quadratic interpolations use known values at points C, W and boundary B_{fw} , so that:

$$\left(\frac{\partial^2(\rho C)}{\partial \xi^2}\right)_w^n = \frac{4(\rho C)_C^n - 12(\rho C)_W^n + 8(\rho C)_{B_{fw}}^n}{3\Delta \xi^2} \quad (B49)$$

$$\left(\frac{\partial \tilde{(\rho C)}}{\partial \eta}\right)_w = (2 - \tilde{C}_{r_w}) \left(\frac{\partial(\rho C)}{\partial \eta}\right)_W^n + (\tilde{C}_{r_w} - 1) \left(\frac{\partial(\rho C)}{\partial \eta}\right)_{B_{fw}}^n \quad \text{for } \tilde{C}_{r_w} > 1 \quad (B50)$$

Now, assume that the direction of the velocity is as in Fig. B5 and that the e-face of the control volume built around the computational point C is a boundary B_e .

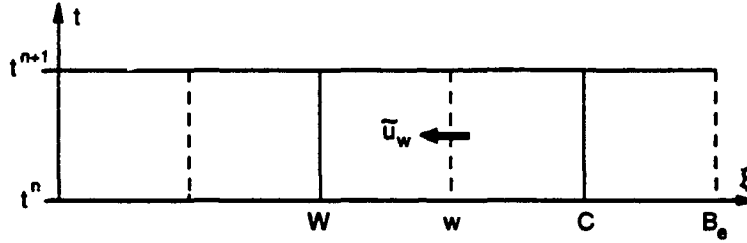


Figure B5.

The same procedure as described by Eqs. (B5) to (B35) is applied to the computational point C. Advection and diffusion fluxes across the w-face of the control volume built around the computational point C, $(adv)_w$ and $(dif)_w$, have the same form as in Eq. (B35), with one difference, namely that the appropriate different upstream interpolations use known values at points W, C and boundary B_e , so that:

$$\left(\frac{\partial^2(\rho C)}{\partial \xi^2}\right)_w^n = \frac{8(\rho C)_{B_e}^n - 12(\rho C)_C^n + 4(\rho C)_W^n}{3\Delta\xi^2} \quad (B51)$$

$$\left(\frac{\partial \tilde{(\rho C)}}{\partial \eta}\right)_w = (2 + \tilde{C}_{r_w}) \left(\frac{\partial(\rho C)}{\partial \eta}\right)_C^n - (1 - \tilde{C}_{r_w}) \left(\frac{\partial(\rho C)}{\partial \eta}\right)_{B_e}^n \quad \text{for } \tilde{C}_{r_w} < -1 \quad (B52)$$

η -direction step

Equation (B3) is discretized by using the same adapted version of the QUICKEST method as in the ξ -direction step. The only difference is that the local rate-of-change due to the action of the ξ -direction terms $\left[\frac{\partial}{\partial t}(JH\rho C)\right]^\xi$ is integrated from the south to the north face of the control volume, assuming that cell-centered variables are representative of the entire integration interval:

$$\frac{\Delta \xi}{2} \int J H^{\xi}(\rho C)^{\xi} dp - \int J H^n(\rho C)^n dp = \Delta \eta J_c H_c^{\xi}(\rho C)_c^{\xi} - \Delta \eta J_c H_c^n(\rho C)_c^n \quad (B53)$$

The discretized Equation (B3) reads:

$$\begin{aligned} J_c H_c^n(\rho C)_c^n - J_c H_c^{\xi}(\rho C)_c^{\xi} &= J_c H_c^{\xi}(\rho C)_c^{\xi} - J_c H_c^n(\rho C)_c^n \\ &+ J_s \bar{H}_s \bar{C}_{r_s} \left[\frac{(\rho C)_c^n + (\rho C)_s^n}{2} - \frac{\Delta \eta}{2} \bar{C}_{r_s} \left(\frac{\partial(\rho C)}{\partial \eta} \right)_s^n - \frac{\Delta \eta^2}{6} (1 - \bar{C}_{r_s}^2) \left(\frac{\partial^2(\rho C)}{\partial \eta^2} \right)_s^n \right] \\ &- J_n \bar{H}_n \bar{C}_{r_n} \left[\frac{(\rho C)_c^n + (\rho C)_n^n}{2} - \frac{\Delta \eta}{2} \bar{C}_{r_n} \left(\frac{\partial(\rho C)}{\partial \eta} \right)_s^n - \frac{\Delta \eta^2}{6} (1 - \bar{C}_{r_n}^2) \left(\frac{\partial^2(\rho C)}{\partial \eta^2} \right)_n^n \right] \\ &+ \bar{\alpha}_{H_n} \frac{\bar{H}_c}{J_n} \left\{ g_{11_n} \left[\Delta \eta \left(\frac{\partial(\rho C)}{\partial \eta} \right)_n^n - \frac{\Delta \eta^2}{2} \bar{C}_{r_n} \left(\frac{\partial^2(\rho C)}{\partial \eta^2} \right)_n^n \right] - g_{12_n} \Delta \eta \left(\frac{\partial(\rho C)}{\partial \xi} \right)_n^n \right\} \\ &- \bar{\alpha}_{H_s} \frac{\bar{H}_c}{J_s} \left\{ g_{11_s} \left[\Delta \eta \left(\frac{\partial(\rho C)}{\partial \eta} \right)_s^n - \frac{\Delta \eta^2}{2} \bar{C}_{r_s} \left(\frac{\partial^2(\rho C)}{\partial \eta^2} \right)_s^n \right] - g_{12_s} \Delta \eta \left(\frac{\partial(\rho C)}{\partial \xi} \right)_s^n \right\} \end{aligned} \quad (B54)$$

where superscripts ξ and η define variables at time $(n+1)$ after the ξ - and η -direction steps, respectively; subscripts n,s define the north and south faces of the control volume built around a main computational point C , respectively, (Fig. B6); subscripts N and S define main computational points north and south from C , respectively; subscripts FN and FS define main computational points far north and far south from C (Fig. B6); and where:

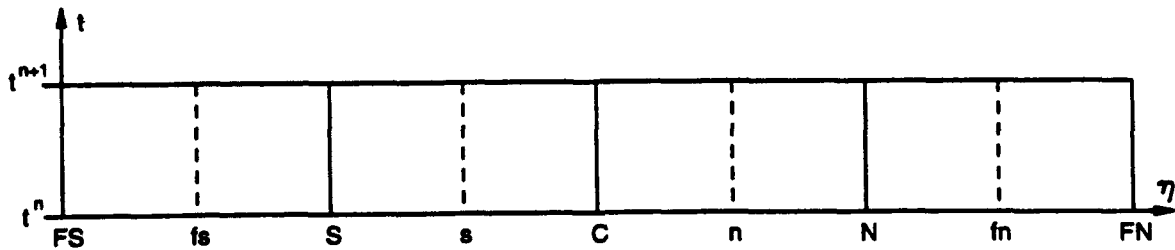


Figure B6.

$$\bar{H}_s = \frac{H_s^{n+1} + H_s^n}{2} \quad \bar{H}_n = \frac{H_n^{n+1} + H_n^n}{2} \quad \bar{H}_c = \frac{H_c^{n+1} + H_c^n}{2}$$

$$\bar{C}_{r_s} = R_0 \frac{\bar{v}_s \Delta t}{\Delta \eta} \quad \bar{C}_{r_n} = R_0 \frac{\bar{v}_n \Delta t}{\Delta \eta}$$

$$\bar{v}_s = \frac{v_s^{n+1} + v_s^n}{2} \quad \bar{v}_n = \frac{v_n^{n+1} + v_n^n}{2}$$

$$\bar{\alpha}_{H_s} = \frac{E_{k_H}}{S_{c_H}} \frac{\bar{D}_{H_s} \Delta t}{\Delta \eta^2} \quad \bar{\alpha}_{H_n} = \frac{E_{k_H}}{S_{c_H}} \frac{\bar{D}_{H_n} \Delta t}{\Delta \eta^2}$$

$$\bar{D}_{H_s} = \frac{D_{H_s}^{n+1} + D_{H_s}^n}{2} \quad \bar{D}_{H_n} = \frac{D_{H_n}^{n+1} + D_{H_n}^n}{2}$$

$$\left(\frac{\partial(\rho C)}{\partial \eta} \right)_s^n = \frac{(\rho C)_c^n - (\rho C)_s^n}{\Delta \eta}$$

$$\left(\frac{\partial^2(\rho C)}{\partial \eta^2} \right)_s^n = \frac{(\rho C)_c^n - 2(\rho C)_s^n + (\rho C)_{fs}^n}{\Delta \eta^2} \quad \text{if } \bar{C}_{r_s} \geq 0$$

$$\left(\frac{\partial^2(\rho C)}{\partial \eta^2} \right)_s^n = \frac{4(\rho C)_c^n - 12(\rho C)_s^n + 8(\rho C)_{B_{fs}}^n}{3\Delta \eta^2} \quad \text{if } \bar{C}_{r_s} \geq 0 \text{ and } fs \text{ (Fig. B6) is a boundary } B_{fs}$$

$$\left(\frac{\partial^2(\rho C)}{\partial \eta^2} \right)_s^n = \frac{(\rho C)_n^n - 2(\rho C)_c^n + (\rho C)_s^n}{\Delta \eta^2} \quad \text{if } \bar{C}_{r_s} < 0$$

$$\left(\frac{\partial^2(\rho C)}{\partial \eta^2} \right)_s^n = \frac{8(\rho C)_{B_n}^n - 12(\rho C)_c^n + 4(\rho C)_s^n}{3\Delta \eta^2} \quad \text{if } \bar{C}_{r_s} > 0 \text{ and } n \text{ (Fig. B6) is a boundary } B_n$$

$$\left(\frac{\partial \tilde{\rho C}}{\partial \xi} \right)_s = \frac{1 - \bar{C}_{r_s}}{2} \left(\frac{\partial(\rho C)}{\partial \xi} \right)_c^n + \frac{1 + \bar{C}_{r_s}}{2} \left(\frac{\partial(\rho C)}{\partial \xi} \right)_s^n \quad \text{if } |\bar{C}_{r_s}| < 1$$

$$\left(\frac{\partial \tilde{\rho C}}{\partial \xi} \right)_s = \frac{3 - \bar{C}_{r_s}}{2} \left(\frac{\partial(\rho C)}{\partial \xi} \right)_s^n - \frac{\bar{C}_{r_s} - 1}{2} \left(\frac{\partial(\rho C)}{\partial \xi} \right)_{FS}^n \quad \text{if } \bar{C}_{r_s} > 1$$

$$\left(\frac{\partial(\tilde{\rho C})}{\partial \xi}\right)_s = (2 - \bar{C}_{r_s}) \left(\frac{\partial(\rho C)}{\partial \xi}\right)_S - (\bar{C}_{r_s} - 1) \left(\frac{\partial(\rho C)}{\partial \xi}\right)_{B_{fs}}^n$$

if $\bar{C}_{r_s} > 1$ and fs (Fig. B6) is a boundary B_{fs}

$$\left(\frac{\partial(\tilde{\rho C})}{\partial \xi}\right)_s = \frac{3 + \bar{C}_{r_s}}{2} \left(\frac{\partial(\rho C)}{\partial \xi}\right)_c - \frac{1 - \bar{C}_{r_s}}{2} \left(\frac{\partial(\rho C)}{\partial \xi}\right)_N^n \quad \text{if } \bar{C}_{r_s} < -1$$

$$\left(\frac{\partial(\tilde{\rho C})}{\partial \xi}\right)_s = (2 + \bar{C}_{r_s}) \left(\frac{\partial(\rho C)}{\partial \xi}\right)_c - (1 + \bar{C}_{r_s}) \left(\frac{\partial(\rho C)}{\partial \xi}\right)_{B_n}^n$$

if $\bar{C}_{r_s} < -1$ and n (Fig. B6) is a boundary B_n

All terms in Eq. (B54) are fully equivalent to the appropriate terms in the discretized ξ -direction equation (Eq. B34)), but reorganized to be ready for coding.

The discretized Eq. (B54) is explicit, meaning that the unknown suspended-sediment concentration is related to the computational point C only. Suspended-sediment concentrations related to neighboring computational points appear in Eq. (B54) explicitly, i.e. as known values. Again, it is useful to point out those elements of the discretized equation that are expressed explicitly in terms of sediment variables by introducing a special notation for them. Therefore, Equation (B54) is rewritten as:

$$\begin{aligned} J_c H_c^\eta (\rho C)_c^\eta - J_c H_c^n (\rho C)_c^n \\ = J_c H_c^\xi (\rho C)_c^\xi - J_c H_c^n (\rho C)_c^n + (\text{adv})_s - (\text{adv})_n + (\text{dif})_n - (\text{dif})_s \end{aligned} \quad (\text{B55})$$

where $(\text{adv})_s$ and $(\text{adv})_n$ stand for advection fluxes across the s-face and n-face of the control volume, respectively, while $(\text{dif})_s$ and $(\text{dif})_n$ stand for diffusion fluxes across the s-face and n-face of the control volume, respectively:

$$(\text{adv})_s = J_s \bar{H}_s \bar{C}_{r_s} \left[\frac{(\rho C)_c^n + (\rho C)_s^n}{2} - \frac{\Delta \eta}{2} \bar{C}_{r_s} \left(\frac{\partial(\rho C)}{\partial \eta}\right)_s^n - \frac{\Delta \eta^2}{6} (1 - \bar{C}_{r_s}^2) \left(\frac{\partial^2(\rho C)}{\partial \eta^2}\right)_s^n \right]$$

$$(\text{adv})_n = J_n \bar{H}_n \bar{C}_{r_n} \left[\frac{(\rho C)_N^n + (\rho C)_c^n}{2} - \frac{\Delta \eta}{2} \bar{C}_{r_n} \left(\frac{\partial(\rho C)}{\partial \eta} \right)_n - \frac{\Delta \eta^2}{6} (1 - \bar{C}_{r_n}^2) \left(\frac{\partial^2(\rho C)}{\partial \eta^2} \right)_n \right]$$

$$(\text{dif})_s = \bar{\alpha}_{H_s} \frac{\bar{H}_c}{J_s} \left\{ g_{11_s} \left[\Delta \eta \left(\frac{\partial(\rho C)}{\partial \eta} \right)_s - \frac{\Delta \eta^2}{2} \bar{C}_{r_s} \left(\frac{\partial^2(\rho C)}{\partial \eta^2} \right)_s \right] - g_{12_s} \Delta \eta \left(\frac{\partial(\tilde{\rho C})}{\partial \xi} \right)_s \right\}$$

$$(\text{dif})_n = \bar{\alpha}_{H_n} \frac{\bar{H}_c}{J_n} \left\{ g_{11_n} \left[\Delta \eta \left(\frac{\partial(\rho C)}{\partial \eta} \right)_n - \frac{\Delta \eta^2}{2} \bar{C}_{r_n} \left(\frac{\partial^2(\rho C)}{\partial \eta^2} \right)_n \right] - g_{12_n} \Delta \eta \left(\frac{\partial(\tilde{\rho C})}{\partial \xi} \right)_n \right\}$$

Boundary Conditions

Boundary conditions for Eq. (B54) (i.e. Eq. (B55)) differ depending on the type of the boundary (impermeable, outflow or inflow). Following the recommendation of Leonard (1979), boundary conditions are specified to be control-volume wall values, rather than node values. Boundary conditions, fully equivalent to those for the ξ -direction equation, are summarized below.

Impermeable boundary at s-face of control volume:

$$(\text{adv})_s = 0 \quad (\text{B56})$$

$$(\text{dif})_s = \bar{\alpha}_{H_s} \frac{\bar{H}_c}{J_s} \left\{ g_{11_s} \Delta \eta \left(\frac{\partial(\tilde{\rho C})}{\partial \eta} \right)_{B_s} - g_{12_s} \Delta \eta \left(\frac{\partial(\tilde{\rho C})}{\partial \xi} \right)_{B_s} \right\} \quad (\text{B57})$$

where:

$$\left(\frac{\partial(\tilde{\rho C})}{\partial \eta} \right)_{B_s} = 0$$

$$\left(\frac{\partial(\tilde{\rho C})}{\partial \xi} \right)_{B_s} = \left(\frac{\partial(\rho C)}{\partial \eta} \right)_n$$

Outflow boundary at s-face of control volume:

$$(\text{adv})_s = J_s \bar{H}_s \bar{C}_{r_s} \left[(\rho C)_{B_s}^n - \frac{\Delta \eta}{2} \bar{C}_{r_s} \left(\frac{\partial(\rho C)}{\partial \eta} \right)_{B_s}^n - \frac{\Delta \eta^2}{2} \left(\frac{1}{4} - \bar{C}_{r_s}^2 \right) \left(\frac{\partial^2(\rho C)}{\partial \eta^2} \right)_{B_s}^n \right] \quad (\text{B58})$$

$$(\text{dif})_s = \bar{\alpha}_{H_s} \frac{\bar{H}_c}{J_s} \left\{ g_{11s} \left[\Delta \eta \left(\frac{\partial(\rho C)}{\partial \eta} \right)_{B_s}^n - \frac{\Delta \eta^2}{2} \bar{C}_{r_s} \left(\frac{\partial^2(\rho C)}{\partial \eta^2} \right)_{B_s}^n \right] - g_{12s} \Delta \eta \left(\frac{\partial(\tilde{\rho C})}{\partial \eta} \right)_{B_s} \right\} \quad (\text{B59})$$

where:

$$\left(\frac{\partial(\tilde{\rho C})}{\partial \xi} \right)_{B_s} = (1 + \bar{C}_{r_s}) \left(\frac{\partial(\rho C)}{\partial \xi} \right)_{B_s}^n - \bar{C}_{r_s} \left(\frac{\partial(\rho C)}{\partial \xi} \right)_c^n \quad \text{for } -1 < \bar{C}_{r_s} < 0$$

$$\left(\frac{\partial(\tilde{\rho C})}{\partial \xi} \right)_{B_s} = \frac{3 + \bar{C}_{r_s}}{2} \left(\frac{\partial(\rho C)}{\partial \xi} \right)_c^n - \frac{1 + \bar{C}_{r_s}}{2} \left(\frac{\partial(\rho C)}{\partial \xi} \right)_N^n \quad \text{for } \bar{C}_{r_s} < -1$$

Inflow boundary at s-face of control volume:

$$(\text{adv})_s = J_s \bar{H}_s \bar{C}_{r_s} \left[(\rho C)_{B_s} - \frac{\Delta \eta^2}{24} \left(\frac{\partial^2(\rho C)}{\partial \eta^2} \right)_{B_s}^n \right] \quad (\text{B60})$$

$$(\text{dif})_s = \bar{\alpha}_{H_s} \frac{\bar{H}_c}{J_s} \left\{ g_{11s} \Delta \eta \left(\frac{\partial(\rho C)}{\partial \eta} \right)_{B_s}^n - g_{12s} \Delta \eta \left(\frac{\partial(\tilde{\rho C})}{\partial \eta} \right)_{B_s} \right\} \quad (\text{B61})$$

where:

$$(\tilde{\rho C})_{B_s} = \frac{(\rho C)_{B_s}^{n+1} + (\rho C)_{B_s}^n}{2}$$

$$\left(\frac{\partial(\tilde{\rho C})}{\partial \xi} \right)_{B_s} = \frac{1}{2} \left[\left(\frac{\partial(\rho C)}{\partial \xi} \right)_{B_s}^{n+1} + \left(\frac{\partial(\rho C)}{\partial \xi} \right)_{B_s}^n \right]$$

and:

$$\left(\frac{\partial(\rho C)}{\partial \eta}\right)_{B_s}^n = \frac{-8(\rho C)_{B_s}^n + 9(\rho C)_c^n - (\rho C)_N^n}{3\Delta\eta}$$

$$\left(\frac{\partial^2(\rho C)}{\partial \eta^2}\right)_{B_s}^n = \frac{4(\rho C)_N^n - 12(\rho C)_c^n + 8(\rho C)_{B_s}^n}{3\Delta\eta^2}$$

with the last two terms being the same for both outflow and inflow boundary conditions.

Impermeable boundary at n-face of control volume:

$$(\text{adv})_n = 0 \quad (\text{B62})$$

$$(\text{dif})_n = \bar{\alpha}_{H_n} \frac{\bar{H}_c}{J_n} \left\{ g_{11_n} \Delta\eta \left(\frac{\partial(\tilde{\rho C})}{\partial \eta}\right)_{B_n} - g_{12_n} \Delta\eta \left(\frac{\partial(\tilde{\rho C})}{\partial \xi}\right)_{B_n} \right\} \quad (\text{B63})$$

where:

$$\left(\frac{\partial(\tilde{\rho C})}{\partial \eta}\right)_{B_n} = 0$$

$$\left(\frac{\partial(\tilde{\rho C})}{\partial \xi}\right)_{B_n} = \left(\frac{\partial(\rho C)}{\partial \xi}\right)_{B_n}^n$$

Outflow boundary at n-face of control volume:

$$(\text{adv})_n = J_n \bar{H}_n \bar{C}_{r_n} \left[(\rho C)_{B_n}^n - \frac{\Delta\eta}{2} \bar{C}_{r_n} \left(\frac{\partial(\rho C)}{\partial \eta}\right)_{B_n}^n - \frac{\Delta\eta^2}{6} \left(\frac{1}{4} - \bar{C}_{r_n}^2\right) \left(\frac{\partial^2(\rho C)}{\partial \eta^2}\right)_{B_n}^n \right] \quad (\text{B64})$$

$$\begin{aligned}
 (\text{dif})_n = \bar{\alpha}_{H_n} \frac{\bar{H}_c}{J_n} \left\{ g_{11_n} \left[\Delta\eta \left(\frac{\partial(\rho C)}{\partial\eta} \right)_{B_n}^n - \frac{\Delta\eta^2}{2} \bar{C}_{r_n} \left(\frac{\partial^2(\rho C)}{\partial\eta^2} \right)_{B_n}^n \right] \right. \\
 \left. - g_{12_n} \Delta\eta \left(\frac{\partial(\tilde{\rho C})}{\partial\xi} \right)_{B_n} \right\}
 \end{aligned} \tag{B65}$$

where:

$$\left(\frac{\partial(\tilde{\rho C})}{\partial\xi} \right)_{B_n} = (1 - \bar{C}_{r_n}) \left(\frac{\partial(\rho C)}{\partial\xi} \right)_{B_n}^n + \bar{C}_{r_n} \left(\frac{\partial(\rho C)}{\partial\xi} \right)_c^n \quad \text{for } 0 < C_{r_n} < 1$$

$$\left(\frac{\partial(\tilde{\rho C})}{\partial\xi} \right)_{B_n} = \frac{3 - \bar{C}_{r_n}}{2} \left(\frac{\partial(\rho C)}{\partial\xi} \right)_c^n + \frac{\bar{C}_{r_n} - 1}{2} \left(\frac{\partial(\rho C)}{\partial\xi} \right)_s^n \quad \text{for } \bar{C}_{r_n} > 1$$

Inflow boundary at n-face of control volume:

$$(\text{adv})_n = J_n \bar{H}_n \bar{C}_{r_n} \left[(\tilde{\rho C})_{B_n} - \frac{\Delta\eta^2}{24} \left(\frac{\partial^2(\rho C)}{\partial\eta^2} \right)_{B_n}^n \right] \tag{B66}$$

$$(\text{dif})_n = \bar{\alpha}_{H_n} \frac{\bar{H}_c}{J_n} \left\{ g_{11_n} \Delta\eta \left(\frac{\partial(\rho C)}{\partial\eta} \right)_{B_n}^n - g_{12_n} \Delta\eta \left(\frac{\partial(\tilde{\rho C})}{\partial\xi} \right)_{B_n} \right\} \tag{B67}$$

where:

$$(\tilde{\rho C})_{B_n} = \frac{(\rho C)_{B_n}^{n+1} + (\rho C)_{B_n}^n}{2}$$

$$\left(\frac{\partial(\tilde{\rho C})}{\partial\xi} \right)_{B_n} = \frac{1}{2} \left[\left(\frac{\partial(\rho C)}{\partial\xi} \right)_{B_n}^{n+1} + \left(\frac{\partial(\rho C)}{\partial\xi} \right)_{B_n}^n \right]$$

and:

$$\left(\frac{\partial^2(\rho C)}{\partial \eta} \right)_{B_n}^n = \frac{8(\rho C)_{B_n}^n - 9(\rho C)_c^n + (\rho C)_S^n}{3\Delta\eta}$$

$$\left(\frac{\partial^2(\rho C)}{\partial \eta^2} \right)_{B_n}^n = \frac{8(\rho C)_{B_n}^n - 12(\rho C)_c^n + 4(\rho C)_S^n}{3\Delta\eta^2}$$

with the last two terms being the same for both outflow and inflow boundary conditions.

σ -direction step

Equation (B4) is integrated over the time step and a control volume built around a main computational point C:

$$\frac{\Delta\sigma}{2} \int_{\frac{\Delta\sigma}{2}} JH^{n+1}(\rho C)^{n+1} dp - \frac{\Delta\sigma}{2} \int_{\frac{\Delta\sigma}{2}} JH^n(\rho C)^n dp = \frac{\Delta\sigma}{2} \int_{\frac{\Delta\sigma}{2}} JH^\eta(\rho C)^\eta dp - \frac{\Delta\sigma}{2} \int_{\frac{\Delta\sigma}{2}} JH^n(\rho C)^n dp$$

(1)

(2)

(1')

(2')

$$+ R_o \int_0^{\Delta t} J_b H_b (\rho C)_b \omega_b d\tau - R_o \int_0^{\Delta t} J_t H_t (\rho C)_t \omega_t d\tau$$

(3)

(4)

$$+ R_{of} \int_0^{\Delta t} J_t (\rho C)_t w_f d\tau - R_{of} \int_0^{\Delta t} J_b (\rho C)_b w_f d\tau$$

(5)

(6)

$$+ \frac{E_{k_v}}{S_{c_v}} \int_0^{\Delta t} \frac{J_t}{H_t} \left(D_v \frac{\partial(\rho C)}{\partial \sigma} \right)_t d\tau - \frac{E_{k_v}}{S_{c_v}} \int_0^{\Delta t} \frac{J_b}{H_b} \left(D_v \frac{\partial(\rho C)}{\partial \sigma} \right)_b d\tau$$

(7)

(8)

(B68)

where: (1) and (2) are local rate-of-change terms due to the action of σ -direction terms added to the combined action of ξ - and η -direction terms; (1') and (2') are local rate-of-change terms due to the action of ξ - and η -direction terms; (3) and (4) are advection terms in the σ direction; (5) and (6) are fall-velocity terms in the σ direction; (7) and (8) are

diffusion terms in the σ direction; τ, p are local coordinates (Fig. B7); subscripts t,b denote top and bottom faces of the control volume built around the main computational point C (Fig. B7); superscript η denotes variables at time $(n+1)$ after the η -direction step; superscript $(n+1)$ defines variables at time $(n+1)$ after the last, i.e. σ -direction, step.

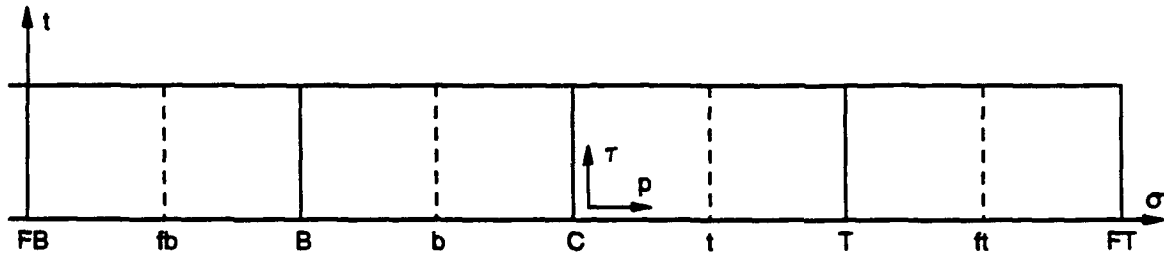


Figure B7.

Taking into account that $J_c (= J_b = J_t)$ does not depend on time and the σ -coordinate direction, that $H_c (= H_b = H_t)$ does not depend on the σ -coordinate direction, and further simplifying the local rate-of-change and advection terms (to make application of the QUICKEST method easier), integral Eq. (B66) now reads:

$$J_c H_c^{n+1} \int_{-\frac{\Delta\sigma}{2}}^{\frac{\Delta\sigma}{2}} (\rho C)^{n+1} dp - J_c H_c^n \int_{-\frac{\Delta\sigma}{2}}^{\frac{\Delta\sigma}{2}} (\rho C)^n dp = J_c H_c^\eta \int_{-\frac{\Delta\sigma}{2}}^{\frac{\Delta\sigma}{2}} (\rho C)^\eta dp - J_c H_c^n \int_{-\frac{\Delta\sigma}{2}}^{\frac{\Delta\sigma}{2}} (\rho C)^\eta dp$$

(1)
(2)
(1')
(2')

$$+ R_o J_c \bar{H}_c \int_0^{\Delta t} (\rho C)_b \omega_b d\tau - R_o J_c \bar{H}_c \int_0^{\Delta t} (\rho C)_t \omega_t d\tau$$

(3)
(4)

$$+ R_{of} J_c \int_0^{\Delta t} (\rho C)_t w_f d\tau - R_{of} J_c \int_0^{\Delta t} (\rho C)_b w_f d\tau$$

$$(5) \qquad (6)$$

$$+ \frac{E_{kv}}{S_{cv}} \int_0^{\Delta t} \frac{1}{H_c} \left(D_v \frac{\partial(\rho C)}{\partial \sigma} \right)_t d\tau - \frac{E_{kv}}{S_{cv}} J_c \int_0^{\Delta t} \frac{1}{H_c} \left(D_v \frac{\partial(\rho C)}{\partial \sigma} \right)_b d\tau$$

$$(7) \qquad (8)$$

(B69)

The local rate-of-change terms (1') and (2') are integrated by assuming that cell-center values are representative of the entire integration interval:

$$J_c H_c^n \int_{-\frac{\Delta \sigma}{2}}^{\frac{\Delta \sigma}{2}} (\rho C)^n dp - J_c H_c^n \int_{-\frac{\Delta \sigma}{2}}^{\frac{\Delta \sigma}{2}} (\rho C)^n dp = \Delta \sigma J_c H_c^n (\rho C)_c^n - \Delta \sigma J_c H_c^n (\rho C)_c^n \quad (B70)$$

The local rate-of-change terms (1) and (2) as well as the advection terms (3) and (4), are discretized by using the same adapted version of the QUICKEST method as in the ζ - and η -direction steps:

$$J_c H_c^{n+1} \int_{-\frac{\Delta \sigma}{2}}^{\frac{\Delta \sigma}{2}} (\rho C)^{n+1} dp - J_c H_c^n \int_{-\frac{\Delta \sigma}{2}}^{\frac{\Delta \sigma}{2}} (\rho C)^n dp \equiv \Delta \sigma \left[J_c H_c^{n+1} (\rho C)_c^{n+1} - J_c H_c^n (\rho C)_c^n \right] \quad (B71)$$

$$+ \Delta \sigma \frac{\Delta \sigma^2}{24} J_c \tilde{H}_c \left[\tilde{C}_{rb} \left(\frac{\partial^2(\rho C)}{\partial \sigma^2} \right)_b^n - \tilde{C}_{ri} \left(\frac{\partial^2(\rho C)}{\partial \sigma^2} \right)_i^n \right]$$

$$R_o J_c \tilde{H}_c \int_0^{\Delta t} (\rho C)_b \omega_b d\tau = R_o J_c \tilde{H}_c \tilde{C}_{rb} \Delta \sigma \left[\frac{(\rho C)_c^n + (\rho C)_b^n}{2} - \frac{\Delta \sigma}{2} \tilde{C}_{rb} \left(\frac{\partial(\rho C)}{\partial \sigma} \right)_b^n \right. \\ \left. - \frac{\Delta \sigma^2}{6} \tilde{C}_{rb} \left(\frac{\partial^2(\rho C)}{\partial \sigma^2} \right)_b^n - \frac{\Delta \sigma^2}{8} \left(\frac{\partial^2(\rho C)}{\partial \sigma^2} \right)_b^n \right] \quad (B72)$$

$$R_0 J_c \bar{H}_c \int_0^{\Delta t} (\rho C)_t \omega_t d\tau = R_0 J_c \bar{H}_c \bar{C}_{r_t} \Delta \sigma \left[\frac{(\rho C)_T^n + (\rho C)_C^n}{2} - \frac{\Delta \sigma}{2} \bar{C}_{r_t} \left(\frac{\partial(\rho C)}{\partial \sigma} \right)_t \right. \\ \left. - \frac{\Delta \sigma^2}{6} \bar{C}_{r_t}^2 \left(\frac{\partial^2(\rho C)}{\partial \sigma^2} \right)_t - \frac{\Delta \sigma^2}{8} \left(\frac{\partial^2(\rho C)}{\partial \sigma^2} \right)_t \right] \quad (B73)$$

where:

$$\bar{C}_{r_t} = R_0 \frac{\bar{\omega}_t \Delta t}{\Delta \sigma}$$

$$\bar{\omega}_t = \frac{\omega_t^{n+1} + \omega_t^n}{2}$$

$$\left(\frac{\partial(\rho C)}{\partial \sigma} \right)_t = \frac{(\rho C)_T^n - (\rho C)_C^n}{\Delta \sigma}$$

$$\left(\frac{\partial^2(\rho C)}{\partial \sigma^2} \right)_t = \frac{(\rho C)_T^n - 2(\rho C)_C^n + (\rho C)_B^n}{\Delta \sigma^2} \quad \text{for } \bar{C}_{r_t} \geq 0$$

$$\left(\frac{\partial^2(\rho C)}{\partial \sigma^2} \right)_t = \frac{(\rho C)_{FT}^n - 2(\rho C)_T^n + (\rho C)_C^n}{\Delta \sigma^2} \quad \text{for } \bar{C}_{r_t} < 0$$

and subscripts T and B denote computational points top and bottom from C, respectively (Fig. B7); subscripts FT and FB denote computational points far top and far bottom from C, respectively.

Special cases of upstream quadratic interpolation occur for points next to boundaries. For point C next to the bed, $k=1$, Fig. B8:

$$\left(\frac{\partial^2(\rho C)}{\partial \sigma^2} \right)_t = 2 \left[\frac{(\rho C)_T^n}{\Delta \sigma_1 (\Delta \sigma_1 + \Delta \sigma_0)} - \frac{(\rho C)_C^n}{\Delta \sigma_1 \Delta \sigma_0} + \frac{(\rho C)_{\sigma_{a+\Delta a}}^n}{\Delta \sigma_0 (\Delta \sigma_1 + \Delta \sigma_0)} \right] \quad \text{for } \bar{C}_{r_t} \geq 0, k=1$$

For point C next to free surface, $k=K-1$, Fig. B9:

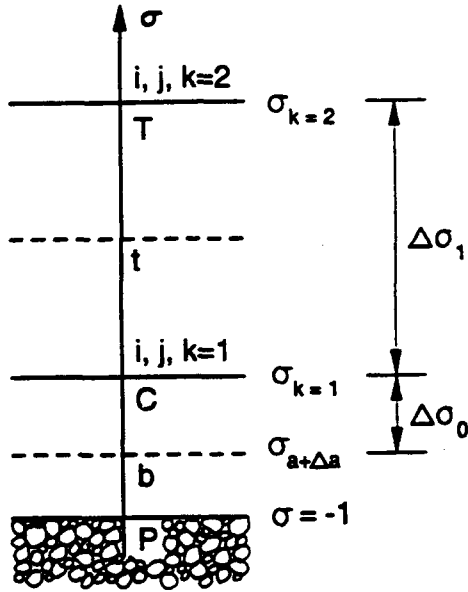


Figure B8.

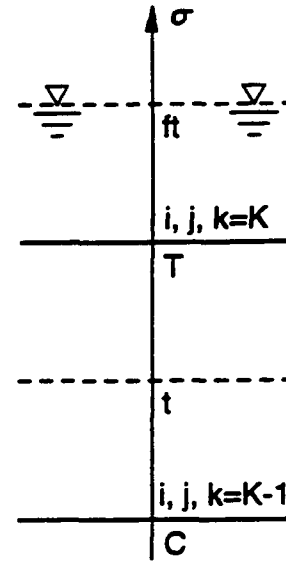


Figure B9.

$$\left(\frac{\partial^2(\rho C)}{\partial \sigma^2} \right)_t = \frac{8(\rho C)_{ft}^n - 12(\rho C)_T^n + 4(\rho C)_C^n}{3\Delta\sigma^2} \quad \text{for } \bar{C}_{r_i} < 0, k = K - 1$$

$$(\rho C)_{ft} = (\rho C)_T$$

When the zero-gradient condition next to the free surface is applied, the last expression reduces to:

$$\left(\frac{\partial^2(\rho C)}{\partial \sigma^2} \right)_t = \frac{-4(\rho C)_T^n + 4(\rho C)_C^n}{3\Delta\sigma^2} \quad \text{for } \bar{C}_{r_i} < 0, k = K - 1$$

Similar terms are easily written for the b-face of the control volume built around the computational point C.

Integration of the fall-velocity terms (5) and (6) (Eq. (B69)) yields:

$$R_{\sigma} J_c \int_0^{\Delta t} (\rho C)_t w_f dt = R_{\sigma_f} J_c w_f \left[\theta (\rho C)_T^{n+1} + (1 - \theta) (\rho C)_T^n \right] \Delta t \quad (B74)$$

$$R_o J_c \int_0^{\Delta t} (\rho C)_b w_f d\tau = R_o J_c w_f \left[\theta (\rho C)_c^{n+1} + (1-\theta) (\rho C)_c^n \right] \Delta t \quad (B75)$$

where θ is a weighting factor. The same result could be obtained by applying an upwind finite-difference scheme.

Integration of the diffusion terms (7) and (8) of Eq. (B69) yields:

$$\begin{aligned} & \frac{E_{k_v}}{S_{c_v}} J_c \int_0^{\Delta t} \frac{1}{H_c} \left(D_v \frac{\partial(\rho C)}{\partial \sigma} \right)_t d\tau \\ &= \frac{E_{k_v}}{S_{c_v}} J_c \left[\theta \frac{D_{v_t}^{n+1}}{H_c^{n+1}} \frac{(\rho C)_T^{n+1} - (\rho C)_c^{n+1}}{\Delta \sigma} + (1-\theta) \frac{D_{v_t}^n}{H_c^n} \frac{(\rho C)_T^n - (\rho C)_c^n}{\Delta \sigma} \right] \Delta t \end{aligned} \quad (B76)$$

$$\begin{aligned} & \frac{E_{k_v}}{S_{c_v}} J_c \int_0^{\Delta t} \frac{1}{H_c} \left(D_v \frac{\partial(\rho C)}{\partial \sigma} \right)_b d\tau \\ &= \frac{E_{k_v}}{S_{c_v}} J_c \left[\theta \frac{D_{v_b}^{n+1}}{H_c^{n+1}} \frac{(\rho C)_c^{n+1} - (\rho C)_B^{n+1}}{\Delta \sigma} + (1-\theta) \frac{D_{v_b}^n}{H_c^n} \frac{(\rho C)_c^n - (\rho C)_B^n}{\Delta \sigma} \right] \Delta t \end{aligned} \quad (B77)$$

The same result could be obtained by applying a time weighted central differencing.

The discretized σ -direction equation now reads:

$$\begin{aligned} & J_c H_c^{n+1} (\rho C)_c^{n+1} - J_c H_c^n (\rho C)_c^n = J_c H_c^\eta (\rho C)^\eta - J_c H_c^n (\rho C)_c^n \\ & + J_c \bar{H}_c \bar{C}_{r_b} \left[\frac{(\rho C)_c^n + (\rho C)_B^n}{2} - \frac{\Delta \sigma}{2} \bar{C}_{r_b} \left(\frac{\partial(\rho C)}{\partial \sigma} \right)_b - \frac{\Delta \sigma^2}{6} (1 - \bar{C}_{r_b}^2) \left(\frac{\partial^2(\rho C)}{\partial \sigma^2} \right)_b \right] \\ & - J_c \bar{H}_c \bar{C}_{r_t} \left[\frac{(\rho C)_T^n + (\rho C)_c^n}{2} - \frac{\Delta \sigma}{2} \bar{C}_{r_t} \left(\frac{\partial(\rho C)}{\partial \sigma} \right)_t - \frac{\Delta \sigma^2}{6} (1 - \bar{C}_{r_t}^2) \left(\frac{\partial^2(\rho C)}{\partial \sigma^2} \right)_t \right] \\ & + R_{o_f} J_c w_f \left[\theta (\rho C)_T^{n+1} + (1-\theta) (\rho C)_T^n \right] \frac{\Delta t}{\Delta \sigma} \end{aligned}$$

$$-R_{of} J_c w_f \left[\theta (\rho C)_c^{n+1} + (1-\theta) (\rho C)_c^n \right] \frac{\Delta t}{\Delta \sigma} \quad (B78)$$

$$+ \frac{E_{k_v}}{S_{c_v}} J_c \left[\theta \frac{D_{v_t}^{n+1}}{H_c^{n+1}} \frac{(\rho C)_T^{n+1} - (\rho C)_c^{n+1}}{\Delta \sigma} + (1-\theta) \frac{D_{v_t}^n}{H_c^n} \frac{(\rho C)_T^n - (\rho C)_c^n}{\Delta \sigma} \right] \frac{\Delta t}{\Delta \sigma}$$

$$- \frac{E_{k_v}}{S_{c_v}} J_c \left[\theta \frac{D_{v_b}^{n+1}}{H_c^{n+1}} \frac{(\rho C)_c^{n+1} - (\rho C)_B^{n+1}}{\Delta \sigma} + (1-\theta) \frac{D_{v_b}^n}{H_c^n} \frac{(\rho C)_c^n - (\rho C)_B^n}{\Delta \sigma} \right] \frac{\Delta t}{\Delta \sigma}$$

The discretized σ -direction equation (Eq. (B78)) is implicit, meaning that the unknown suspended-sediment concentrations are related not only to the computational point C, but also to the neighboring points T and B. Still, it is useful to point out those elements of the discretized equation that are expressed explicitly in terms of sediment variables by introducing a special notation for them. Therefore, Equation (B78) is rewritten as:

$$\begin{aligned} J_c H_c^{n+1} (\rho C)_c^{n+1} - J_c H_c^n (\rho C)_c^n &= J_c H_c^\eta (\rho C)_c^\eta - J_c H_c^n (\rho C)_c^n \\ &+ (\text{adv})_b - (\text{adv})_t \\ &+ R_{of} J_c \theta w_f (\rho C)_T^{n+1} \frac{\Delta t}{\Delta \sigma} + (1-\theta) (\text{fall})_t^n \frac{\Delta t}{\Delta \sigma} \\ &- R_{of} J_c \theta w_f (\rho C)_c^{n+1} \frac{\Delta t}{\Delta \sigma} - (1-\theta) (\text{fall})_b^n \frac{\Delta t}{\Delta \sigma} \\ &+ \frac{E_{k_v}}{S_{c_v}} J_c \theta \frac{D_{v_t}^{n+1}}{H_c^{n+1}} \frac{(\rho C)_T^{n+1} - (\rho C)_c^{n+1}}{\Delta \sigma} \frac{\Delta t}{\Delta \sigma} + (1-\theta) (\text{dif})_t^n \frac{\Delta t}{\Delta \sigma} \\ &- \frac{E_{k_v}}{S_{c_v}} J_c \theta \frac{D_{v_b}^{n+1}}{H_c^{n+1}} \frac{(\rho C)_c^{n+1} - (\rho C)_B^{n+1}}{\Delta \sigma} \frac{\Delta t}{\Delta \sigma} - (1-\theta) (\text{dif})_b^n \frac{\Delta t}{\Delta \sigma} \end{aligned} \quad (B79)$$

where $(\text{adv})_t$ and $(\text{adv})_b$ stand for advection fluxes across the t-face and the b-face of the control volume built around point C, respectively; $(\text{fall})_t^n$ and $(\text{fall})_b^n$ stand for previous-time fall-velocity fluxes across the t-face and the b-face of the control volume built around point

C, respectively; and $(\text{dif})_t^n$ and $(\text{dif})_b^n$ stand for previous-time diffusion fluxes across the t-face and the b-face of control volume built around point C, respectively:

$$(\text{adv})_b = J_c \bar{H}_c \bar{C}_{r_b} \left[\frac{(\rho C)_c^n + (\rho C)_B^n}{2} - \frac{\Delta \sigma}{2} \bar{C}_{r_b} \left(\frac{\partial(\rho C)}{\partial \sigma} \right)_b^n - \frac{\Delta \sigma^2}{6} (1 - \bar{C}_{r_b}^2) \left(\frac{\partial^2(\rho C)}{\partial \sigma^2} \right)_b^n \right]$$

$$(\text{adv})_t = J_c \bar{H}_c \bar{C}_{r_t} \left[\frac{(\rho C)_T^n + (\rho C)_c^n}{2} - \frac{\Delta \sigma}{2} \bar{C}_{r_t} \left(\frac{\partial(\rho C)}{\partial \sigma} \right)_t^n - \frac{\Delta \sigma^2}{6} (1 - \bar{C}_{r_t}^2) \left(\frac{\partial^2(\rho C)}{\partial \sigma^2} \right)_t^n \right]$$

$$(\text{fall})_t^n = R_{of} J_c w_f (\rho C)_T^n$$

$$(\text{fall})_b^n = R_{of} J_c w_f (\rho C)_c^n$$

$$(\text{dif})_t^n = \frac{E_{k_v}}{S_{c_v}} J_c \frac{D_{v_t}^n}{H_c^n} \frac{(\rho C)_T^n - (\rho C)_c^n}{\Delta \sigma}$$

$$(\text{dif})_b^n = \frac{E_{k_v}}{S_{c_v}} J_c \frac{D_{v_b}^n}{H_c^n} \frac{(\rho C)_c^n - (\rho C)_B^n}{\Delta \sigma}$$

Boundary Conditions

The discretized σ -direction equation is different for points next to the bed ($k=1$) and points next to the free surface ($k=K$).

Points Next to the Bed

The advection flux across the b-face of the control volume is equal to zero:

$$(\text{adv})_b = 0 \quad (\text{B80})$$

The fall-velocity flux across the b-face of the control volume actually represents deposition of suspended sediment onto the bed. It uses the near-bed concentration $(\rho C)_{\sigma_a + \Delta a}$, defined as in Eq. (31), i.e. evaluated at a near-bed location $\sigma_a + \Delta a$ by simple linear extrapolation:

$$(\rho C)_b = (\rho C)_{\sigma_a + \Delta\sigma} = (1-c)(\rho C)_T + c(\rho C)_c \quad (\text{B81})$$

where c is an extrapolation coefficient.

The fall-velocity flux across the b-face of the control volume reads:

$$\begin{aligned} R_{of} J_c \int_0^{\Delta t} (\rho C)_b w_f d\tau &= R_{of} J_c w_f \left\{ \theta \left[(1-c)(\rho C)_T^{n+1} + c(\rho C)_c^{n+1} \right] \right. \\ &\quad \left. + (1-\theta) \left[(1-c)(\rho C)_T^n + c(\rho C)_c^n \right] \right\} \Delta t \end{aligned} \quad (\text{B82})$$

The diffusion flux across the b-face of the control volume actually represents erosion, i.e. entrainment of sediment particles from the bed into suspension and has to be modified by the active-layer size fraction to reflect the availability of a particular size class in the active-layer control volume. Furthermore, the derivative is defined as in the 'erosion' source term (Eq. (12)):

$$\left(\frac{\partial(\rho C)}{\partial \sigma} \right)_b = \left(\frac{\partial(\rho C)}{\partial \sigma} \right)_{\sigma_a} = \frac{(\rho C)_{\sigma_a + \Delta\sigma} - (\rho C)_{\sigma_a}}{\Delta\sigma_{\Delta a}} = \frac{(1-c)(\rho C)_T + c(\rho C)_c - (\rho C)_{\sigma_a}}{\Delta\sigma_{\Delta a}} \quad (\text{B83})$$

where $(\rho C)_{\sigma_a + \Delta\sigma}$ is defined as in Eq. (B81), and $(\rho C)_{\sigma_a}$ is near-bed concentration defined by the appropriate empirical relation.

The diffusion flux across the b-face of the control volume, modified by β , reads:

$$\begin{aligned} \frac{E_{kv}}{S_{cv}} J_c \int_0^{\Delta t} \frac{\beta}{H_c} \left(D_v \frac{\partial(\rho C)}{\partial \sigma} \right)_b dt \\ = \frac{E_{kv}}{S_{cv}} J_c \left[\theta \beta^{n+1} \frac{D_v^{n+1}}{H_c^{n+1}} \frac{(1-c)(\rho C)_T^{n+1} + c(\rho C)_c^{n+1} - (\rho C)_{\sigma_a}^{n+1}}{\Delta\sigma_{\Delta a}} \right. \\ \left. + (1-\theta) \beta^n \frac{D_v^n}{H_c^n} \frac{(1-c)(\rho C)_T^n + c(\rho C)_c^n - (\rho C)_{\sigma_a}^n}{\Delta\sigma_{\Delta a}} \right] \Delta t \end{aligned} \quad (\text{B84})$$

The discretized σ -direction equation for a point next to the bed (with a special notation, as in Eq. (B79), used to point out those elements of the discretized equation that are expressed explicitly in terms of sediment variables) reads:

$$\begin{aligned}
& J_c H_c^{n+1} (\rho C)_c^{n+1} - J_c H_c^n (\rho C)_c^n = J_c H_c^n (\rho C)_c^n - J_c H_c^n (\rho C)_c^n \\
& -(\text{adv})_t \\
& + R_{of} J_c \theta w_f (\rho C)_T^{n+1} \frac{\Delta t}{\Delta \sigma} + (1-\theta)(\text{fall})_t^n \frac{\Delta t}{\Delta \sigma} \\
& - R_{of} J_c \theta w_f \left[(1-c)(\rho C)_T^{n+1} + c(\rho C)_c^{n+1} \right] \frac{\Delta t}{\Delta \sigma} - (1-\theta)(\text{fall})_b^n \frac{\Delta t}{\Delta \sigma} \tag{B85} \\
& + \frac{E_{k_v}}{S_{c_v}} J_c \theta \frac{D_{v_t}^{n+1}}{H_c^{n+1}} \frac{(\rho C)_T^{n+1} - (\rho C)_c^{n+1}}{\Delta \sigma} \frac{\Delta t}{\Delta \sigma} + (1-\theta)(\text{dif})_t^n \frac{\Delta t}{\Delta \sigma} \\
& - \frac{E_{k_v}}{S_{c_v}} J_c \theta \beta^{n+1} \frac{D_{v_b}^{n+1}}{H_c^{n+1}} \frac{(1-c)(\rho C)_T^{n+1} + c(\rho C)_c^{n+1} - (\rho C)_{\sigma_a}^{n+1}}{\Delta \sigma_{\Delta a}} \frac{\Delta t}{\Delta \sigma} - (1-\theta)(\text{dif})_b^n \frac{\Delta t}{\Delta \sigma}
\end{aligned}$$

where $(\text{fall})_b^n$ and $(\text{dif})_b^n$ are the same as the 'deposition' and 'erosion' source terms in the discretized mass-conservation equation for active-layer sediment (Eq. (35)) and the global mass-conservation equation for bed sediment (Eq. (34)):

$$\begin{aligned}
(\text{fall})_b^n &= R_{of} J_c w_f \left[(1-c)(\rho C)_T^n + c(\rho C)_c^n \right] = (S_d)_P^n \\
(\text{dif})_b^n &= \frac{E_{k_v}}{S_{c_v}} J_c \beta^n \frac{D_{v_b}^n}{H_c^n} \frac{(1-c)(\rho C)_T^n + c(\rho C)_c^n - (\rho C)_{\sigma_a}^n}{\Delta \sigma_{\Delta a}} = (S_e)_P^n
\end{aligned}$$

and $(\text{adv})_t$, $(\text{fall})_t^n$ and $(\text{dif})_t^n$ are the same as in Eq. (B79).

Point Next to the Free Surface

Advection, fall-velocity, and diffusion fluxes across the free surface (t-face of the control volume) are equal to zero:

$$(\text{adv})_t = 0 \quad (\text{B86})$$

$$R_{o_f} J_c \int_0^{\Delta t} (\rho C)_t w_f dt = 0 \quad (\text{B87})$$

$$\frac{E_{k_v}}{S_{c_v}} J_c \int_0^{\Delta t} \frac{1}{H_c} \left(D_v \frac{\partial(\rho C)}{\partial \sigma} \right)_t d\tau = 0 \quad (\text{B88})$$

The discretized σ -direction equation for a point next to the free surface (with a special notation, as in Eq. (B79), used to point out those elements of the discretized equation that are expressed explicitly in terms of sediment variables) reads:

$$\begin{aligned} J_c H_c^{n+1} (\rho C)_c^{n+1} - J_c H_c^n (\rho C)_c^n &= J_c H_c^\eta (\rho C)_c^\eta - J_c H_c^n (\rho C)_c^n \\ &+ (\text{adv})_b \\ &- R_{o_f} J_c \theta w_f (\rho C)_c^{n+1} \frac{\Delta t}{\Delta \sigma} - (1 - \theta) (\text{fall})_b^n \frac{\Delta t}{\Delta \sigma} \\ &- \frac{E_{k_v}}{S_{c_v}} J_c \theta \frac{D_{v_b}^{n+1}}{H_c^{n+1}} \frac{(\rho C)_c^{n+1} - (\rho C)_b^{n+1}}{\Delta \sigma} \frac{\Delta t}{\Delta \sigma} - (1 - \theta) (\text{dif})_b^n \frac{\Delta t}{\Delta \sigma} \end{aligned} \quad (\text{B89})$$

where $(\text{fall})_b^n$, $(\text{adv})_b$ and $(\text{dif})_b^n$ are the same as in Eq. (B79).

Complete Discretized Mass-Conservation Equation for Suspended Sediment

A complete discretized mass-conservation equation for suspended sediment is obtained by adding the discretized ξ -, η - and σ -direction step equations (Eqs. (B35), (B55) and (B79)):

$$\begin{aligned} J_c H_c^{n+1} (\rho C)_c^{n+1} - J_c H_c^n (\rho C)_c^n &= (\text{adv})_w - (\text{adv})_e + (\text{dif})_e - (\text{dif})_w \\ &+ (\text{adv})_s - (\text{adv})_n + (\text{dif})_n - (\text{dif})_s \\ &+ (\text{adv})_b - (\text{adv})_t \end{aligned}$$

$$\begin{aligned}
& +R_{of} J_c \theta w_f (\rho C)_T^{n+1} \frac{\Delta t}{\Delta \sigma} + (1-\theta)(fall)_i^n \frac{\Delta t}{\Delta \sigma} \\
& -R_{of} J_c \theta w_f (\rho C)_c^{n+1} \frac{\Delta t}{\Delta \sigma} - (1-\theta)(fall)_b^n \frac{\Delta t}{\Delta \sigma} \\
& + \frac{E_{k_v}}{S_{c_v}} J_c \theta \frac{D_{v_i}^{n+1}}{H_c^{n+1}} \frac{(\rho C)_T^{n+1} - (\rho C)_c^{n+1}}{\Delta \sigma} \frac{\Delta t}{\Delta \sigma} + (1-\theta)(dif)_i^n \frac{\Delta t}{\Delta \sigma} \\
& - \frac{E_{k_v}}{S_{c_v}} J_c \theta \frac{D_{v_b}^{n+1}}{H_c^{n+1}} \frac{(\rho C)_c^{n+1} - (\rho C)_B^{n+1}}{\Delta \sigma} \frac{\Delta t}{\Delta \sigma} - (1-\theta)(dif)_b^n \frac{\Delta t}{\Delta \sigma}
\end{aligned} \tag{B90}$$

The discretized mass-conservation equation for suspended sediment (Eq. (B90)) is implicit in the σ direction only, and can be rewritten as:

$$a(\rho C)_B^{n+1} + b(\rho C)_c^{n+1} + c(\rho C)_T^{n+1} = d \tag{B91}$$

where

$$\begin{aligned}
a &= -\frac{E_{k_v}}{S_{c_v}} J_c \theta \frac{D_{v_b}^{n+1}}{H_c^{n+1}} \frac{\Delta t}{\Delta \sigma^2} \\
b &= J_c H_c^{n+1} + \frac{E_{k_v}}{S_{c_v}} J_c \frac{\theta}{H_c^{n+1}} (D_{v_i}^{n+1} + D_{v_b}^{n+1}) \frac{\Delta t}{\Delta \sigma^2} + R_{of} J_c \theta w_f \frac{\Delta t}{\Delta \sigma} \\
c &= -\frac{E_{k_v}}{S_{c_v}} J_c \theta \frac{D_{v_i}^{n+1}}{H_c^{n+1}} \frac{\Delta t}{\Delta \sigma^2} - R_{of} J_c \theta w_f \frac{\Delta t}{\Delta \sigma}
\end{aligned}$$

$$\begin{aligned}
d &= J_c H_c^n (\rho C)_c^n \\
&+ (\text{adv})_w - (\text{adv})_e + (\text{dif})_e - (\text{dif})_w \\
&+ (\text{adv})_s - (\text{adv})_n + (\text{dif})_n - (\text{dif})_s \\
&+ (\text{adv})_b - (\text{adv})_t \\
&+ (1-\theta)(\text{fall})_t^n \frac{\Delta t}{\Delta \sigma} - (1-\theta)(\text{fall})_b^n \frac{\Delta t}{\Delta \sigma} \\
&+ (1-\theta)(\text{dif})_t^n \frac{\Delta t}{\Delta \sigma} - (1-\theta)(\text{dif})_b^n \frac{\Delta t}{\Delta \sigma}
\end{aligned}$$

are known coefficients.

Similarly, by combining the discretized Eqs. (B35), (B55) and (B85), an equation for points next to the bed is obtained in the same form as Eq. (B91) where the appropriate coefficients are:

$$a = 0$$

$$b = J_c H_c^{n+1} + R_{of} J_c \theta w_f c \frac{\Delta t}{\Delta \sigma} + \frac{E_{kv}}{S_{cv}} J_c \frac{\theta}{H_c^{n+1}} \left(\frac{D_{vt}^{n+1}}{\Delta \sigma} + \beta^{n+1} \frac{D_{vb}^{n+1}}{\Delta \sigma_{\Delta a}} c \right) \frac{\Delta t}{\Delta \sigma}$$

$$c = R_{of} J_c \theta w_f \frac{\Delta t}{\Delta \sigma} + R_{of} J_c \theta w_f (1-c) \frac{\Delta t}{\Delta \sigma} - \frac{E_{kv}}{S_{cv}} J_c \frac{\theta}{H_c^{n+1}} \left[\frac{D_{vt}^{n+1}}{\Delta \sigma} - \beta^{n+1} \frac{D_{vb}^{n+1}}{H_c^{n+1}} (1-c) \right] \frac{\Delta t}{\Delta \sigma}$$

$$d = J_c H_c^n (\rho C)^n$$

$$\begin{aligned}
&+ (\text{adv})_w - (\text{adv})_e + (\text{dif})_e - (\text{dif})_w \\
&+ (\text{adv})_s - (\text{adv})_n + (\text{dif})_n - (\text{dif})_s \\
&- (\text{adv})_t \\
&+ (1-\theta)(\text{fall})_t^n \frac{\Delta t}{\Delta \sigma} - (1-\theta)(S_d)_p^n \frac{\Delta t}{\Delta \sigma} \\
&+ (1-\theta)(\text{dif})_t^n \frac{\Delta t}{\Delta \sigma} - (1-\theta)(S_e)_p^n \frac{\Delta t}{\Delta \sigma} \\
&+ \frac{E_{kv}}{S_{cv}} J_c \theta \beta^{n+1} \frac{D_{vb}^{n+1}}{H_c^{n+1}} \frac{(\rho C)_{\sigma a}^{n+1}}{\Delta \sigma_{\Delta a}} \frac{\Delta t}{\Delta \sigma}
\end{aligned}$$

By combining the discretized Eqs. (B35), (B55) and (B89), an equation for points next to the free surface is obtained in the same form as Eq. (B91) where the appropriate coefficients are:

$$a = -\frac{E_{kv}}{S_{cv}} J_c \theta \frac{D_{vb}^{n+1}}{H_c^{n+1}} \frac{\Delta t}{\Delta \sigma^2}$$

$$b = J_c H_c^{n+1} + R_{of} J_c \theta w_f \frac{\Delta t}{\Delta \sigma} + \frac{E_{kv}}{S_{cv}} J_c \theta \frac{D_{vb}^{n+1}}{H_c^{n+1}} \frac{\Delta t}{\Delta \sigma^2}$$

$$c = 0$$

$$d = J_c H_c^n (\rho C)_c^n$$

$$+(\text{adv})_w - (\text{adv})_e + (\text{dif})_e - (\text{dif})_w$$

$$+(\text{adv})_s - (\text{adv})_n + (\text{dif})_n - (\text{dif})_s$$

$$+(\text{adv})_b$$

$$-(1 - \theta)(\text{fall})_b^n \frac{\Delta t}{\Delta \sigma} - (1 - \theta)(\text{dif})_b^n \frac{\Delta t}{\Delta \sigma}$$

APPENDIX C

COEFFICIENTS IN DISCRETIZED GLOBAL MASS-CONSERVATION EQUATION FOR BED SEDIMENT AND MASS-CONSERVATION EQUATIONS FOR ACTIVE-LAYER SEDIMENT

The discretized global mass-conservation equation for bed sediment, Eq. (34), which after linearization is written as Eq. (48), can be rewritten as:

$$a_{1,1}\Delta s_1 + \sum_{kks=1}^{KKS} a_{1,kks+1}\Delta s_{kks+1} = b_1 \quad (C.1)$$

where

$$\begin{aligned} a_{11} &= \frac{\partial F_1}{\partial s_1} = \frac{\partial F_1}{\partial z_b} = \frac{\rho_s(1-p)J}{\Delta t} \\ a_{1,kks+1} &= \frac{\partial F_1}{\partial s_{kks+1}} = \frac{\partial F_1}{\partial \beta_{kks}} = \theta(S_e^t)_{ks}^{n+1} \\ b_1 &= -F_1(\bar{s}^{n+1}) = -\rho_s(1-p)J \frac{m_z^{n+1} - z_b^n}{\Delta t} \\ &\quad - \sum_{ks=1}^{KS} \left[\theta(\text{div}q_b)_{ks}^{n+1} + (1-\theta)(\text{div}q_b)_{ks}^n \right. \\ &\quad \left. + \theta m \beta_{ks}^{n+1} (S_e^t)_{ks}^{n+1} + (1-\theta)(S_e)_{ks}^n \right. \\ &\quad \left. - \theta(S_d)_{ks}^{n+1} - (1-\theta)(S_d)_{ks}^n \right] \end{aligned}$$

Since all variables are evaluated at the same main computational point P, there is no need for a special subscript to denote the computational point. Subscript ks is introduced to denote a sediment size class, while subscript kks denotes a sediment variable. Superscript m denotes the iteration level. All other notation is as previously defined for Eq. (34).

The discretized mass-conservation equation for the ks-th size class of active-layer sediment, Eq. (35), after linearization as shown in Eq. (49), can be rewritten as:

$$a_{ks+1,1}\Delta s_1 + \sum_{kks=1}^{KKS} a_{ks+1,kks+1} = b_{ks+1} \quad (C2)$$

where

$$a_{ks+1,1} = \frac{\partial F_{ks+1}}{\partial s_1} = \frac{\partial F_{ks+1}}{\partial z_b} = \frac{\rho_s(1-p)J}{\Delta t} m \beta_{ks}^{n+1} (E_m)'_{,1} - J(S_F)'_{ks,1}$$

$$a_{ks+1,kks+1} = \frac{\partial F_{ks+1}}{\partial s_{kks+1}} = \frac{\partial F_{ks+1}}{\partial \beta_{kks}} = \frac{\rho_s(1-p)J}{\Delta t} m \beta_{ks}^{n+1} (E_m)'_{,kks+1} - J(S_F)'_{ks,kks+1} \quad ks \neq kks$$

$$a_{ks+1,kks+1} = \frac{\partial F_{ks+1}}{\partial s_{kks+1}} = \frac{\partial F_{ks+1}}{\partial \beta_{kks}} = \frac{\rho_s(1-p)J}{\Delta t} m \beta_{ks}^{n+1} (E_m)'_{,kks+1} - J(S_F)'_{ks,kks+1} \quad ks \neq kks$$

$$b_{ks+1} = -\rho_s(1-p)J \frac{m \beta_{ks}^{n+1} m E_m^{n+1} - \beta_{ks}^n E_m^n}{\Delta t} \\ - \theta(\text{div} q_b)_{ks}^{n+1} - (1-\theta)(\text{div} q_b)_{ks}^n \\ - \theta m \beta_{ks}^{n+1} (S_e^t)_{ks}^{n+1} - (1-\theta)(S_e)_{ks}^n \\ + \theta(S_d)_{ks}^{n+1} + (1-\theta)(S_d)_{ks}^n + J^m (S_F)_{ks}^{n+1}$$

Here $(E_m)'_{,1}$ denotes the derivative of active-layer thickness E_m with respect to sediment variable $s_1 = z_b$; $(E_m)'_{,kks+1}$ denotes the derivative of active-layer thickness E_m with respect to sediment variable $s_{kks+1} = \beta_{kks}$; $(S_F)'_{ks,1}$ represents the derivative of active-layer floor "source" $(S_F)_{ks}$ for the ks -th size-class, with respect to sediment variable $s_1 = z_b$; $(S_F)'_{ks,kks+1}$ represents the derivative of active-layer floor "source" $(S_F)_{ks}$ for the ks -th size-class, with respect to sediment variable $s_{kks+1} = \beta_{kks}$. All other notation is as previously defined.

APPENDIX D: CH3D INPUT DATA GUIDE (May 1992)

This input data guide was developed through analysis of the CH3D code by the authors of this report. Question marks indicate uncertainty in this analysis, and may require consultation with the developers of CH3D.

DUMMY indicates a blank data record (separator).

rec	var	Format (columns)	Variable description and remarks
*MAIN PROGRAM			
Note: Data are read from main input file (file 4 : main.inp)			
Debug-output flags			
	NBUGS		
	NBUGE	5(2I8) (1-80)	Pairs of debug-output flags 5 pairs per record 100 pairs total
*SUBROUTINE CH3DIR			
Note: All data are read from main input file (file 4 : main.inp) except for centered-cell depths (file 12 : dpth.inp) and Manning's roughness coefficients (file 18 : mann.inp)			
Run descriptor			
	DUMMY		
	TITLE	A80 (1-80)	Title of run
Timestep info			
	DUMMY		
	IT1	I8 (1-8)	Starting time-step number (=1)
	IT2	I8 (9-16)	Ending time-step number
	DT	F8.0 (17-24)	Computational time step [s]
	ISTART	I8 (25-32)	=0 Cold start (arrays initialized in CH3DIF)
			>0 Hot start (not operational?)
	ITEST	I8 (33-40)	=0 No diagnostic output =3 Diagnostic output for XC, QXU, XU in subroutine CH3DTR
			=4 Diagnostic output for GIJ,HIJ,DIJK in subroutine CH3DTR
	ITSALT	I8 (41-48)	Number of time steps before salinity and temperature computations are

ISCOM	I8 (49-56)	initiated =0 No sediment computations =1 Sediment computations performed
NTSED0	I8 (57-64)	Number of time steps before sediment computations are initiated
Printout windows		
DUMMY		
WPCRD	I8 (1-8)	>0 Number of printout windows =0 No printout windows
DUMMY		
Following record is repeated WPCRD times Omitted if WPCRD=0		
WXCEL1	I8 (1-8)	Starting printout-window index in KSI direction
WXCEL2	I8 (9-16)	Ending printout-window index in KSI direction
WYCEL1	I8 (17-24)	Starting printout-window index in ETA direction
WYCEL2	I8 (25-32)	Ending printout-window index in ETA direction
WZCEL1	I8 (33-40)	Starting printout-window index in vertical direction
WZCEL2	I8 (41-48)	Ending printout-window index in vertical direction
WPRINT	I8 (49-56)	Printout interval
WPRSTR	I8 (57-64)	Starting time-step number
WPREND	I8 (65-72)	Ending time-step number
WPRVAR	A8 (73-80)	Printout variables E - water-surface fluctuations X - X-direction unit flow rate Y - Y-direction unit flow rate U - X-direction velocity V - Y-direction velocity W - vertical-direction velocity S - salinity T - temperature A - velocity magnitude and direction
Snapshots		
DUMMY		
SNPCRD	I8 (1-8)	>0 Number of snapshots =0 No snapshots
DUMMY		
Following record is repeated SNPCRD times Omitted if SNPCRD=0		
SXCEL1	I8 (1-8)	Starting index in KSI direction
SXCEL2	I8 (9-16)	Ending -----//-----
SYCEL1	I8 (17-24)	Starting index in ETA direction
SYCEL2	I8 (25-32)	Ending -----//-----

SZCEL1	I8 (33-40)	Starting index in vertical direction
SZCEL2	I8 (41-48)	Ending -----//-----
SNPINT	I8 (49-56)	Printout interval
SNPSTR	I8 (57-64)	Starting time-step number
SNPEND	I8 (65-72)	Ending time-step number
SNPVAR	A8 (73-80)	Snapshot variables
Flow rate ranges		
DUMMY		
NRANG	I8 (1-8)	>0 Number of flow-rate ranges =0 No flow-rate ranges Stop if NRANG>NRANGS
DUMMY		
Following record is repeated NRANG times Omitted if NRANG=0		
RANGDR	A1 (8)	Direction of a flow =X Flow is in KSI direction, therefore the range is along an ETA-direction coordinate line =Y Flow is in ETA direction, therefore the range is along a KSI-direction coordinate line
if RANGDR=X:		
RPOS1	I8 (9-16)	I index defining the appropriate ETA-direction range
RPOS2	I8 (17-24)	J1 starting J index of the range
RPOS3	I8 (25-32)	J2 ending J index of the range
RRNAME	A45 (33-77)	Range name
if RANGDR=Y:		
RPOS1	I8 (9-16)	J index defining the appropriate KSI-direction range
RPOS2	I8 (17-24)	I1 starting I index of the range
RPOS3	I8 (25-32)	I2 ending I index of the range
RRNAME	A45 (33-77)	Range name
Initial condition printing flags		
DUMMY		
IGI	I8 (1-8)	=1 Printout arrays such as NS, MS, NR, MR, IROW, IU1, IU2, ISW etc. NBX, NBY 0 No printout
IGH	I8 (9-16)	=1 Printout all depth arrays HS,HU,HV 0 No printout
IGT	I8 (17-24)	=1 Print initial temperature arrays? 0 No printout
IGS	I8 (25-32)	=1 Printout initial surface elevations S,UI,VI 0 No printout
IGU	I8 (33-40)	=1 Printout mass flux and velocity in horizontal direction ??(Sheng) 0 No printout

IGW	I8 (41-48)	=1 Print the initial wind-shear stress 0 No printout
IGC	I8 (49-56)	=1 Print dimensional grid coordinates 0 No printout
IGQ	I8 (57-64)	=1 Print turbulent velocity? (Sheng) 0 No printout
IGP	I8 (65-72)	=1 Save cell-centered depth to file 23 Save Cartesian coordinates of cell centered grid points to file 23 Save NS, MS arrays to file 23 Save FY11, FY12, FY21, FY22 arrays (transform. coeff.) on file 23 for snapshot plot 0 Does not save

Physical constants

DUMMY XREF	F8.0 (1-8)	Reference horizontal grid distance (Maximum horizontal dimension divided by number of cells in that direction in cm)
ZREF	F8.0 (9-16)	Reference depth (Average typical depth in cm)
UREF	F8.0 (17-24)	Reference horizontal velocity (Average velocity in cm/s)
COR	F8.0 (25-32)	Coriolis parameter (1/s) - ref. 'time'
GR	F8.0 (33-40)	Gravitational acceleration (cm/s ²)
ROO	F8.0 (41-48)	Minimum density expected (gr/cm ³)
ROR	F8.0 (49-56)	Reference density (Maximum expected (gr/cm ³))
TO	F8.0 (57-64)	Minimum temperature (Celsius)
TR	F8.0 (65-72)	Reference temperature (Maximum expected (Celsius))
SAR	F8.0 (1-8)	Reference salinity (Max expected) ??
SAO	F8.0 (9-16)	Minimum salinity ??

Water depths read from file 12 (dpth.inp)

DUMMY HS	16F5.0	Water depths (ft) at the center of computational cell along a KSI-coordinate line, 16 values per record, ICELLS values altogether (read from file 12 (dpth.inp))
-------------	--------	--

Previous records are repeated JCELLS times

Manning's roughness coefficients n
(read from file 18 (mann.inp))

DUMMY FMAN	20F4.0	Manning's roughness coefficients n(m-1/3*s??) (divided by 0.001)
---------------	--------	---

at computational points along an
ETA-coordinate line, 20 values per
record, ICELLS values altogether
(read from file 18 (mann.inp))
Previous records are repeated JCELLS times

Time-level weighting coefficients

DUMMY THETA	F8.0 (1-8)	Time-level weighting coefficient
----------------	------------	----------------------------------

Flags for computing inertia and diffusion

DUMMY ITEMP	I8 (1-8)	=2 Compute temperature (use time-varying temperature as river boundary temperature) =1 Compute temperature (use daily equilibrium temperature as river boundary temperature) =0 No computation of temperature <0 Update time-variable equilibrium temperature and coefficient of heat exchange at every time step
ISALT	I8 (9-16)	=1 Compute salinity =0 No computation of salinity
ICC	I8 (17-24)	=1 Compute dissolved species concen. =0 Do not compute concentration
IFI	I8 (25-32)	=1 Compute nonlinear inertia terms in the momentum equation =0 Do not compute inertia terms
IFA	I8 (33-40)	=1 Include one group higher-order lateral diffusion terms ?? =0 Do not include
IFB	I8 (41-48)	=1 Include another group higher-order diffusion terms ?? =0 Do not include
IFC	I8 (49-56)	=1 Include another group higher-order diffusion terms ?? =0 Do not include
IFD	I8 (57-64)	=1 Include diffusion terms in salinity and temperature =0 Do not include

Temperature parameters

DUMMY BVR	F8.0 (1-8)	Reference turbulent thermal eddy diffusivity??
S1	F8.0 (9-16)	Constant in computation of variable vertical eddy viscosity [GA=GX(1+S1*Ri)**FM1] if first-order turbulence model is used
S2	F8.0 (17-24)	Constant in computation of variable

		vertical eddy diffusivity [GB=GX(1+S2*Ri)**FM2] if first- order turbulence model is used
PR	F8.0 (25-32)	Turbulent Prandtl number
PRV	F8.0 (33-40)	Vertical turbulent Prandtl number
TWE	F8.0 (41-48)	Temperature in the epilimnion (for the initial condition)
TWH	F8.0 (49-56)	Temperature in the hypolimnion (for the initial condition)
FKB	F8.0 (57-64)	Vertical grid index of the initial thermocline location (boundary between epilimnion and hypolimnion ??)
TQO	F8.0 (65-72)	Initial surface heat flux TQ (cal/cm/cm/s)
Concentration parameters		
DUMMY		
IVER	I8 (1-8)	=1 Explicit vertical diffusion term for water quality equations ?? =2 Implicit vertical diffusion term for water quality equations ??
ICON	I8 (9-16)	=0 Do not compute advection terms for water quality equations ?? =1 Compute advection terms in conservative form with central differencing =3 Compute advection terms in conservative form with second upwind differencing scheme =4 Compute advection terms in conservative form with combined central and upwind differencing
IUBO	I8 (17-24)	Bottom orbital velocity flag (=0)
IBL	I8 (25-32)	Concentration computation does not have to be performed for the entire domain. Instead, it can be done for a window which covers an area from I=IBL to I=IBR and from J=JBM to J=JBP. The window will change in time.
IBR	I8 (33-40)	
JBM	I8 (41-48)	
JBP	I8 (49-56)	
DUMMY		
CREF	F8.0 (1-8)	Reference species concentration
CMAX	F8.0 (9-16)	Maximum concentration allowed by the code (halts if exceeded)
C0	F8.0 (17-24)	Initial concentration
DUMMY		
ICC1	I8 (1-8)	Initial concentration field may be specified to be zero everywhere in the computational domain except within two windows: the first one
ICC2	I8 (9-16)	
JCC1	I8 (17-24)	
JCC2	I8 (25-32)	

ID1	I8 (33-40)	covers an area from I=ICC1 to I=ICC2
ID2	I8 (41-48)	and from J=JCC1 to J=JCC2
JD1	I8 (49-56)	the second one from I=ID1 to I=ID2
JD2	I8 (57-64)	and from J=JD1 to J=JD2
Turbulent parameters and eddy coefficients		
DUMMY IEXP	I8 (1-8)	Vertical eddy-coefficient flag =0 Constant eddy coefficient (must also set ISPAC(9)=0 ??) =-1 Munk-Anderson type first order turbulence model (unstratified eddy coefficients are determined from mixing length theory) Richardson-number-dependent eddy coefficient with length scale linearly increasing from the bottom and surface =-2 Munk-Anderson type first order turbulence model Richardson-number dependent eddy coefficient with length scale linearly increasing from the bottom to the surface =-3 Second-order turbulence model
IAV	I8 (9-16)	=0 Input parameter AVR is used as reference eddy viscosity =1 Reference eddy viscosity is computed from $AV1 + TXY \cdot AV2$, where TXY is the total wind stress and AV1 and AV2 are input parameters
AVR	F8.0 (17-24)	Reference vertical eddy coef. (cm ² /s)
AV1	F8.0 (25-32)	Background vertical eddy viscosity when wind is zero
AV2	F8.0 (33-40)	If IAV=1 unstratified vertical eddy viscosity is computed from $AV1 + TXY \cdot AV2$
AVM	F8.0 (41-48)	Minimum vertical eddy coef. (cm ² /s)
AVM1	F8.0 (49-56)	Minimum vert. eddy diffusivity (cm ² /s)
AHR	F8.0 (57-64)	Reference horizontal eddy viscosity or diffusivity (cm ² /s)
DUMMY FM1	F8.0 (1-8)	Parameter in Richardson-number dependent eddy viscosity (see definition of S1)
FM2	F8.0 (9-16)	Parameter in Richardson-number dependent eddy diffusivity (see definition of S2)
ZTOP	F8.0 (17-24)	Distance between the top of computational domain and the free surface. Used in computing

SLMIN	F8.0 (25-32)	turbulence length scale (cm) Minimum value of turbulence macroscale (cm)
QQMIN	F8.0 (33-40)	Minimum value of turbulence kinetic energy (gr/cm/s ²)
DUMMY ICUT	I8 (1-8)	=0 Eddy coefficients constant below halocline =1 Eddy coefficients computed below halocline
KSMALL	I8 (9-16)	A non-zero value of KSMALL turns on the smoother for the eddy coeffic.
QCUT	F8.0 (17-24)	Coefficient in second-order turbulence model (0.15-0.25)
GAMAX	F8.0 (25-32)	Max.value of eddy viscosity (cm ² /s)
GBMAX	F8.0 (33-40)	Max. value of eddy diffusivity (cm ² /s)
FZS	F8.0 (41-48)	Turbulence scale is not allowed to exceed the product of FZS and depth
Wind parameters		
DUMMY IWIND	I8 (1-8)	=0 Steady and uniform wind stress specified by TAUX and TAUY =1 Steady and uniform wind speed =2 Steady and space variab. wind stress =3 Steady and space variable wind speed =4 Time variab.and uniform wind stress =5 Time variable and uniform wind speed =6 Time and space variable wind stress =7 Time and space variable wind speed
TAUX(1,1)	F8.0 (9-16)	Uniform wind stress in KSI direction if IWIND=0 Uniform wind speed (m/s) in KSI direction if IWIND=1
TAUY(1,1)	F8.0 (17-24)	Uniform wind stress in ETA direction if IWIND=0 Uniform wind speed (m/s) in ETA direction if IWIND=1
Flags		
(Note different meaning for ISPAC, JSPAC in Sheng's report)		
DUMMY ISPAC(1)	I8 (1-8)	ISPAC(1)=1 Use spatially variable Manning's n in vertically averaged model =0 Use constant Manning's n in vertically averaged model
ISPAC(2)	I8 (9-16)	ISPAC(2)=1 Bottom drag coefficients computed in 3D model =0 Bottom drag coefficients set to CBF(?) in 3D model

ISPAC (3) I8 (17-24)	ISPAC (3)=1 Coriolis ON =0 Coriolis OFF
ISPAC (4) I8 (25-32)	ISPAC (4)=1 Variable bottom roughness height =0 Constant bottom roughness height given by BZ1
ISPAC (5) I8 (33-40)	ISPAC (5-8) Not used
ISPAC (6) I8 (41-48)	Not used
ISPAC (7) I8 (49-56)	Not used
ISPAC (8) I8 (57-64)	Not used
ISPAC (9) I8 (65-72)	ISPAC (9)=0 Constant vertical eddy coefficient =2 Variable vertical eddy coefficient =3 Variable vertical eddy coefficient computed from Kent-Prichard formulation
ISPAC (10) I8 (73-80)	ISPAC (10) Not used
DUMMY	
JSPAC (1) I8 (1-8)	JSPAC (1)=1 Save dimensional Cartesian unit flows UI and VI on a file =0 Does not save
JSPAC (2) I8 (9-16)	JSPAC (2)=1 Save depth-averaged dimensional Cartesian U and V on a file =0 Does not save
JSPAC (3) I8 (17-24)	JSPAC (3)=1 Save dimensional Cartesian 3D u and v at cell faces on a file =0 Does not save
JSPAC (4) I8 (25-32)	JSPAC (4)=1 Save dimensional Cartesian 3D u and v at cell center on a file =0 Does not save
JSPAC (5) I8 (33-40)	JSPAC (5)=1 Save nondimensional cartesian UI an VI =0 Does not save
JSPAC (6) I8 (41-48)	JSPAC (6) Not used
JSPAC (7) I8 (49-56)	Not used
JSPAC (8) I8 (57-64)	Not used
JSPAC (9) I8 (65-72)	Not used
JSPAC (10) I8 (73-80)	Not used
DUMMY	
RSPAC (1) F8.0 (1-8)	RSPAC (1)= Manning's n in c.g.s. units
RSPAC (2) F8.0 (9-16)	RSPAC (2)= Not used
RSPAC (3) F8.0 (17-24)	RSPAC (3)= An infinitesimal number used in checking the convergence to steady state (0.0001)
RSPAC (4) F8.0 (25-32)	RSPAC (4)= An infinitesimal number used in checking the convergence to steady state (0.0001)

RSPAC(5)	F8.0 (33-40)	RSPAC(5)= Not used
RSPAC(6)	F8.0 (41-48)	RSPAC(6)= Not used
RSPAC(7)	F8.0 (49-56)	RSPAC(7)= Depth below which the bottom friction coefficient follows a ramp function (see subs CH2DXY, CH3DXYZ)
RSPAC(8)	F8.0 (57-64)	RSPAC(8)= Not used
RSPAC(9)	F8.0 (65-72)	RSPAC(9)= Coefficient for the spatial smoother (0.25)
RSPAC(10)	F8.0 (73-80)	RSPAC(10)= Coefficient for the curvature check of the spatial smoother (4)

Depth flags and constants

DUMMY		
IBTM	I8 (1-8)	=4 Depths are read in subroutine CH3DIR <4 Other options for reading depth see subroutine CH3DIH
HADD	F8.0 (9-16)	Constant datum added to the depth at all locations (=0.0)
NMIN	F8.0 (17-24)	Minimum depth =0 No adjustment of the depth data >0 Depth cannot be less than HMIN H=max(H,NMIN)
H1	F8.0 (25-32)	Depth along one boundary
H2	F8.0 (33-40)	Depth along the opposing boundary
SSSO	F8.0 (41-48)	Initial water-surface elevation relative to initial water depth
DUMMY		
ISMALL	I8 (1-8)	=1 Scaling factor in reference surface elevation computations (sub CH3DND)
ISF	I8 (9-16)	=0 Do not compute current at the free surface =1 Compute free-surface current from linear formula
ITB	I8 (17-24)	=1 Linear bottom friction for internal mode =2 (or >1) Quadratic bottom friction for internal mode
ZREFBN	F8.0 (25-32)	Reference height above bottom (cm)
CTB	F8.0 (33-40)	Constant bottom drag coefficient (typical value of 0.003)
BZ1	F8.0 (41-48)	Bottom roughness height (cm)
ZREFTN	F8.0 (49-56)	Reference height at the top
TZ1	F8.0 (57-64)	Constant surface roughness height

Variable mapping for computational grid

DUMMY		
XMAP	F8.0 (1-8)	Factor that scales the (x,y) coordinates created by grid generation codes to the real world

		(Mapping ratio between physical domain and computational domain)
ALXREF	F8.0 (9-16)	Reference length in the X direction of the computational domain ??
ALYREF	F8.0 (17-24)	Reference length in the Y direction of the computational domain ??
Transformation parameters		
DUMMY ITRAN	I8 (1-8)	=0 Compute grid coordinates for equidistant Cartesian grid =1 Read grid coordinates (file created by WESCOR?) (grid with spline evaluated transformation coefficients ??) =2 Read grid coordinates and corner depths (file created by WESCORA?) (grid with numerically evaluated transformation coefficients ??)
IBD	I8 (9-16)	Spline boundary conditions ??
Timebreaks for storing snapshot data		
DUMMY ITBRK	10I8	Time- step numbers at which information is written to files for snapshot plots Ten values maximum
Timefile gage stations		
Current stations		
DUMMY NSTA	I8 (1-8)	Number of stations where information is saved for time series plots of currents (major flow data) Stop if NSTA>NSTATS
NFREQ	I8 (9-16)	Time-step number frequency for saving current information
NSTART	I8 (17-24)	Beginning time-step number for saving current information
DUMMY		Following record is repeated NSTA times Omitted if NSTA=0
IST	I4 (1-4)	Coordinate (I,J) of a station where
JST	I4 (5-8)	currents are saved
STATID	A48 (9-56)	Station descriptor
Tide stations		
DUMMY NSTAS	I8 (1-8)	Number of stations where water-surface

		elevations are saved for time series plots
NFREQS	I8 (9-16)	Stop if NSTAS>NSTATS Time-step number frequency for saving surface elevations
NSTRTS	I8 (17-24)	Beginning time-step number for saving water-surface elevations
DUMMY		
		Following record is repeated NSTAS times Omitted if NSTAS=0
ISTS	I4 (1-4)	Coordinate (I,J) of a station where
JSTS	I4 (5-8)	water-surface elevations are saved
STATS	A48 (9-56)	Station descriptor
		Salinity and temperature gaging stations
DUMMY		
MSTA	I8 (1-8)	Number of stations where salinity, temperature, etc., are saved for time series plots
MFREQ	I8 (9-16)	Stop if MSTAS>NSTATS Time-step number frequency for saving information
MSTART	I8 (17-24)	Beginning time-step number for saving information
DUMMY		
		Following record is repeated MSTAS times Omitted if MSTAS=0
ISTSA	I4 (1-4)	Coordinate (I,J) of a station where
JSTSA	I4 (5-8)	salinities etc. are saved
STATSA	A48 (9-56)	Station descriptor
		River information
DUMMY		
NRIVER	I8 (1-8)	Number of river-type boundaries (assigned inflow) NRIVER=0 No river-type boundaries <0 River inflows are steady >0 Time variable inflows read from file 13: rivr.inp in subroutine CH3DRI,CH3DRV Stop if abs(NRIVER)>NRIVERS
		If NRIVER=0, use the following records:
DUMMY		
DUMMY		
		If NRIVER>0, use the following records:
DUMMY		
IJRDIR	I8 (1-8)	=1 River boundary is on left (west) =2 River boundary is on bottom (south) =3 River boundary is on right (east) =4 River boundary is on top (north)

IJRROW	I8 (9-16)	Index of the row (J) or column (I) of the river boundary
IJRSTR	F8.0 (17-24)	Starting I or J index of the river boundary
IJREND	F8.0 (25-32)	Ending I or J index of the river boundary
		Previous record is repeated NRIVER times
		If NRIVER<0, use the following records:
DUMMY		
IJRDIR	I8 (1-8)	=1 River boundary is on left (west) =2 River boundary is on bottom (south) =3 River boundary is on right (east) =4 River boundary is on top (north)
IJRROW	I8 (9-16)	Index of the row (J) or column (I) of the river boundary
IJRSTR	F8.0 (17-24)	Starting I or J index of the river boundary
IJREND	F8.0 (25-32)	Ending I or J index of the river boundary
I	I8 (1-8)	Coordinate (I,J) of a cell (vertical)
J	I8 (9-16)	where QRIVER is prescribed
QRIVER	F8.0 (17-24)	Steady river inflow (cfs)
		Previous record is repeated for each cell, from IJRSTR to IJREND, along a specific river boundary defined by IJRDIR
		Procedure is repeated abs(NRIVER) times
		Thin-wall barriers
DUMMY		
NBAR	I8 (1-8)	Number of interior barriers
		Stop if NBAR>NBARRS
NBARU	I8 (9-16)	
KU	I8 (17-24)	
NBARV	I8 (25-32)	
KV	I8 (33-40)	
DUMMY		
		If NBAR=0 following record is omitted
		Otherwise, record is repeated NBAR times
IJBDIR	I8 (1-8)	=1 barrier is horizontal (KSI direction) =2 barrier is vertical (ETA direction)
IJBROW	I8 (9-16)	Index of row (J) or column (I) of interior barrier
IJBSTR	F8.0 (17-24)	Starting I or J index of interior barrier
IJBEND	F8.0 (25-32)	Ending I or J index of interior barrier
		If NBARU=0 following record is omitted
		Otherwise, record is repeated NBARU times
		Initially BARU(I,J,K)=1.0 for all I,J,K
I	I8 (1-8)	I, J point where BARU(I,J,K)=0.0

J	I8 (9-16)	for K=1,KU If NBARV=0 following record is omitted Otherwise, record is repeated NBARV times Initially BARV(I,J,K)=1.0 for all I,J,K
I	I8 (1-8)	I,J point where BARV(I,J,K)=0.0
J	I8 (9-16)	for K=1,KV

Tidal boundary conditions

DUMMY		
TIDFNO	I8 (1-8)	Number of tidal-elevation tables entered as an input
TIDBND	I8 (9-16)	Number of tidal elevation boundaries

DUMMY		
TIDSTR	10I8 (1-80)	If TIDFNO=0 following record is omitted The entry number in each tidal-elevation table corresponding to the starting time of the simulation From 1 to TIDFNO, maximum 10 values

DUMMY		
IJDIR	I8 (1-8)	If TIDBND=0 following record is omitted Otherwise, record is repeated TIDBND times =1 Tidal boundary is on left (west) =2 Tidal boundary is on bottom (south) =3 Tidal boundary is on right (east) =4 Tidal boundary is on top (north)
IJROW	I8 (9-16)	Index of row (J) or column (I) of the tidal boundary
IJSTRT	I8 (17-24)	Starting I or J of the tidal boundary
IJEND	I8 (25-32)	Ending I or J of the tidal boundary
TIDTYP	A8 (33-40)	='CONSTANT' Constant tidal elevation between IJSTRT and IJEND ='INTERP' Linear interpolation of tidal elevation at IJSTR and IJEND
TIDFN1	I8 (41-48)	Number of the tidal-elevation table for CONSTANT or INTERP type of boundaries
TIDFN2	I8 (49-56)	Number of second tidal-elevation table used for interpolation on INTERP type boundary

*SUBROUTINE CH3DTR

Note: Data are read from file 15 : grid.inp

If ITRAN=1 read following records:

FILENM	A80 (1-80)	Data-file descriptor
NX	I12 (1-12)	Number of cell-centered grid points along a KSI-direction coord. line
NY	I12 (13-24)	Number of cell-centered grid points along an ETA-direction coord. line
XCT	unformatted	Cartesian X coordinates of cell-centered grid points, created by the grid generation code WESCOR Coordinates are read along a KSI-direction coordinate lines, starting at the first KSI line (ETA=1) IC1*JC1 points altogether
YCT	unformatted	Cartesian Y coordinates of cell-centered grid points, created by the grid generation code WESCOR Coordinates are read along a KSI-direction coordinate lines, starting at the first KSI line (ETA=1) IC1*JC1 points altogether

If ITRAN=2 read following records:

FILENM	A80 (1-80)	Data-file descriptor
NX	unformatted	Number of cell-centered grid points along a KSI-direction coord. line
NY	unformatted	Number of cell-centered grid points along an ETA-direction coord. line
XCT	unformatted	Cartesian X coordinate of a cell-centered grid point, created by the grid generation code WESCORA
YCT	unformatted	Cartesian Y coordinate of a cell-centered grid point, created by the grid generation code WESCORA
HC	unformatted	Corner-point depth
LSLIT	unformatted	

Previous record is read point by point along KSI-coordinate lines, starting at the first KSI line (ETA=1)
NX*NY (IC1*JC1) points altogether

Cartesian X and Y coordinates, created by the grid generation codes WESCOR or WESCORA, are first multiplied by XMAP to scale them to the real world, and then divided by XREF to make them nondimensional

*SUBROUTINE BJINTR

Note: Data are read from file 4: main.inp

DUMMY

I unformatted
J unformatted

Point (I,J) where the cell-centered
depth HS has been set to zero

DUMMY

I unformatted
J unformatted

Point (I,J) where the U-face
depth HU has been set to zero

DUMMY

I unformatted
J unformatted

Point (I,J) where the V-face
depth HV has been set to zero

DUMMY

I unformatted
J unformatted
RDEPTH unformatted

Point (I,J) where the cell-centered
depth HS has been reset to
the given value RDEPTH (ft)

DUMMY

I unformatted
J unformatted
AREAM unformatted

Point (I,J) where the storage area
has been assigned a non-zero
value AREAM (m2)

*IWIND<2, following records read in CH3DWS, CH3DWT are omitted

*SUBROUTINE CH3DWS, ENTRY CH3DWT

Note: Wind data are read from file 14: wind.inp

IWIND=2: (steady and space variable ??? wind stress)

|TX1(1,1)| F8.0 (1-8) | X-direction component of wind stress
|TY1(1,1)| F8.0 (9-16) | Y-direction component of wind stress

Subroutine CH3DWS is called, prior to the main computational time loop,
to read wind-stress components
and to assign them to all computational points

IWIND=3: (steady and space variable wind speed)
 Same as for IWIND=2, except that TX1,TY1 are pairs of X- and Y-direction components of wind speed

IWIND=4: (time-variable and uniform wind stress)
 File 14 (wind.inp) contains wind stress time table

IDAY1	I5 (1-5)	Day and hour defining the first time level in the time table
IHOURL	I5 (6-10)	
WNDX1		Pairs of X- and Y-direction components of time-varying wind stress
WNDY1	6F10.0 (21-80)	Total of NWINDS pairs

Previous record is repeated until the last time level in the time table exceeds the end-of-computation time

Subroutine CH3DWS is called, prior to the main computational time loop, to read wind-stress components for the first two time levels (called time levels 1 and 2, defined by IDAY1,IHOURL and IDAY2,IHOURL) in a wind stress time table and to evaluate initial wind stress by interpolation, between time levels 1 and 2 read from the time table

Entry CH3DWT is called, during the main computational loop, to update the wind-stress components i.e. to read the next time level from the wind stress time table if the current computational time exceeds the time level 2, last read from the table

IWIND=5: (time-variable and uniform wind speed)
 File 14 (wind.inp) contains wind speed time table
 Same as for IWIND=4, except that WNDX,WNDY are pairs of X- and Y-direction components of time-varying wind speed

IWIND=6: (time and space ??? variable wind stress)
 File 14 (wind.inp) contains wind stress time table

IDAY1	I5 (1-5)	Day and hour defining the first time level in the time table
IHOURL	I5 (6-10)	
TX1(1,1)	F8.0 (1-8)	X-direction component of time-varying wind stress
TY1(1,1)	F8.0 (9-16)	Y-direction component of time-varying wind stress

Previous two records are repeated until the last time level in the time table exceeds the end-of-computation time

Subroutine CH3DWS is called, prior to the main computational time loop, to read wind-stress components for the first two time levels (called time levels 1 and 2, defined by IDAY1,IHOURL and IDAY2,IHOURL) in a wind stress time table and to evaluate initial wind stress by interpolation, between time levels 1 and 2 read from the time table and to assign them to all computational points ???

Entry CH3DWT is called, during the main computational loop, to update the wind-stress components i.e. to read the next time level from the wind stress time table if the current computational time exceeds the time level 2, last read from the table

if IWIND=7: (time and space variable wind speed)
 File 14 (wind.inp) contains wind speed time table
 Same as for IWIND=6, except that TX1,TY1 are pairs of X- and
 Y-direction components of time-varying wind speed

*ITEMP=0, records read in CH3DTK are omitted
 *ITEMP.GE.0.OR.NRIVER.EQ.0 records read in CH3DTB are omitted
 *SUBROUTINE CH3DTK, ENTRY CH3DTB

Note: Time-varying equilibrium temperature (TEP) and
 time-varying coefficient of surface heat exchange (TEK)
 are read from file 19: heat.inp

IDAYT1	I5 (1-5)	Day and hour defining the first time
IHRT1	I5 (6-10)	level in the TEP/TEK time table
TEP1	F10.0 (11-20)	Equilibrium temperature (Celsius)
TEK1	E12.5 (21-32)	Coefficient of surface heat exchange (cm3/s3)

Previous record is repeated until the last time level
 in the time table exceeds the end-of-computation time

Subroutine CH3DTK is called, prior to the main computational time loop,
 to read TEP and TEK for the first two time levels (called
 time levels 1 and 2, defined by IDAYT1,IHRT1 and IDAYT2,IHRT2) in
 a TEP/TEK time table

Entry CH3DTB is called, during the main computational loop, to update
 TEP and TEK, i.e. to read the next time level from
 the TEP/TEK time table if the current computational time
 exceeds the time level 2, last read from the table
 to evaluate TEP and TEK by interpolation, between time
 levels 1 and 2 read from the time table
 and to assign them to all computational points

*NRIVER=0, no river boundaries
 *NRIVER<0, records read in CH3DRI are omitted
 (steady QRIVER read in CH3DIR)
 *SUBROUTINE CH3DRI, ENTRY CH3DRV

Note: Time-varying river inflows are read from file 13: rivr.inp

Following records are repeated until the last time level
 in the time table exceeds the end-of-computation time

IDAYA	I8 (1-8)	Day and hour defining the time
IHOURA	I8 (9-16)	level in the river inflow time table
I	I8 (1-8)	Coordinate (I,J) of a cell (vertical)

J	I8 (9-16)		where the river inflow is prescribed
QRIVRA	F8.0 (17-24)		Boundary river inflow (cfs)
			Previous record is repeated for each cell, from
			IJRSTR to IJREND, along a specific river boundary
			defined by IJRDIR, IJRROW
			The same is done for each of NRIVER river boundaries

Subroutine CH3DRI is called, prior to the main computational time loop, to read boundary river inflows for the first two time levels (called time levels A and B, defined by IDAYA, IHOURA and IDAYB, IHOURE) in a river inflow time table

Entry CH3DRV is called, during the main computational loop, to update boundary river inflow, i.e. to read the next time level from the river inflow time table if the current computational time exceeds the time level B, last read from the table and to evaluate boundary river inflows by interpolation, between time levels A and B read from the time table

*SUBROUTINE CH3DTI, ENTRY CH3DTD

Note: Tidal-elevation time tables read from file 16: tide.inp

TIDTIT	A80 (1-80)		Tidal-data descriptor
IMO0	I2 (1-2)		Reference month, day, year, hour and minute defining reference time level for the data read in the tide elevations time table
IDY0	I3 (4-6)		
IYR0	I3 (7-9)		
IHR0	I2 (11-12)		
IMN0	I2 (13-14)		
IMO	I2 (1-2)		Month, day, year, hour and minute defining time level in the tidal elevations time table
IDY	I3 (4-6)		
IYR	I3 (7-9)		
IHR	I2 (11-12)		
IMN	I2 (13-14)		
TIDELV	8F8.0 (17-80)		Tidal elevations
			Total of TIDFNO elevations
			Previous record is repeated until the last time level in the time table exceeds the end-of-computation time

Subroutine CH3DTI is called, prior to the main computational time loop, to read complete tidal-elevation time table

Entry CH3DRV is called, during the main computational loop, to load tidal elevations at boundaries, by interpolating between points in tidal-elevations time table

*ISALT.NE.-2, records read in CH3DSAI, CH3DSAV are omitted

*SUBROUTINE CH3DSAI, ENTRY CH3DSAV

Note: Time table containing vertical salinity and temperature profiles along tidal boundaries are read from file 76: tidesate.inp

Following records are repeated until the last time level in the time table exceeds the end-of-computation time

IDAYS1	I5 (1-5)	Day and hour defining the time level in the time table containing vertical salinity and temperature profiles along tidal boundaries
IHRS1	I5 (6-10)	
I	I5 (1-5)	Coordinate (I,J) of a cell (vertical) on a tidal boundary where the vertical salinity profile is prescribed
J	I5 (6-10)	
SA1	11F5.0 (11-65)	Vertical salinity profile Salinities are prescribed at all points along the vertical direction, point-by-point, starting from the point at the bed
I	I5 (1-5)	Coordinate (I,J) of a cell (vertical) on a tidal boundary where the vertical temperature profile is prescribed
J	I5 (6-10)	
TE1	11F5.0 (11-65)	Vertical temperature profile Temperatures are prescribed at all points along the vertical direction, point-by-point, starting from the point at the bed

Previous two records are repeated for each cell, from IJSTRT to IJEND, along a specific tidal boundary defined by IJDIR and IJROW

The same is done for each of TIDBND=IJLINE tidal boundaries

Subroutine CH3DSAI is called, prior to the main computational time loop, to read tidal-boundary salinities and temperatures for the first two time levels (called time levels 1 and 2, defined by IDAYS1,IHRS1 and IDAYS2,IHRS2) in the time table containing vertical salinity and temperature profiles along tidal boundaries

Entry CH3DSAV is called, during the main computational loop, to update tidal-boundary salinities and temperatures, i.e. to read the next time level from the time table containing vertical salinity and temperature profiles along tidal boundaries if the current computational time exceeds the time level 2, last read from the table and to evaluate tidal-boundary salinities and temperatures by interpolation, between time levels 1 and 2 read from the time table

*NRIVER.EQ.0.OR.ISALT.NE.-2, records read in CH3DTEI,CH3DTEV are omitted
*SUBROUTINE CH3DTEI, ENTRY CH3DTEV

Note: Vertical temperature profiles along river-type boundaries are read from file 78: rivrte.inp

IDYTE1	I5 (1-5)	Day and hour defining time level
IHRTE1	I5 (6-10)	in the time table containing vertical temperature profiles along river boundaries
I	I5 (1-5)	Coordinate (I,J) of a cell (vertical) on a river boundary where the vertical temperature profile is prescribed
J	I5 (6-10)	
TE3	11F5.0 (11-65)	Vertical temperature profile Temperatures are prescribed at all points along the vertical direction, point-by-point, starting from the point at the bed

Previous record is repeated for each cell, from IJRSTR to IJREND, along a specific river boundary defined by IJRDIR and IJRROW
The same is done for each of abs(NRIVER) river boundaries

NRIVER<0:

Subroutine CH3DTEI is called, prior to the main computational time loop, to read constant vertical temperature profiles along river boundaries
Time table with vertical temperature profiles along river boundaries contains only one time level

NRIVER>0

Subroutine CH3DTEI is called, prior to the main computational time loop, to read river-boundary temperatures for the first two time levels (called time levels 1 and 2, defined by IDYTE1,IHRTE1 and IDYTE2,IHRTE2) in the time table containing vertical temperature profiles along river boundaries
Entry CH3DTEV is called, during the main computational loop, to update river-boundary temperatures, i.e. to read the next time level from the time table containing vertical temperature profiles along river boundaries if the current computational time exceeds the time level 2, last read from the table and to evaluate river-boundary temperatures by interpolation, between time levels 1 and 2 read from the time table

1	5	-1		
1	6	-1		
1	7	-1		
1	8	-1		
1	9	-1		
1	10	-1		
1	11	-1		
1	12	-1		
1	13	-1		
1	14	-1		
1	15	-1		
1	16	-1		
1	17	-1		
51	3	1	1	1
51	4	1	1	1
51	5	1	1	1
51	6	1	1	1
51	7	1	1	2
51	8	1	1	2
51	9	1	1	2
51	10	1	1	2
51	11	1	1	2
51	12	1	1	2
51	13	1	1	2
51	14	1	1	3
51	15	1	1	3
51	16	1	1	3
-51	17	1	1	3
0	0			
	1	0.0	0.5	0.5
1	.000250	.000025		0.0
	.000250	.000035		0.0
	.000250	.000045		0.0
	.000250	.000065		0.0
	.000250	.000085		0.0
	.000250	.000110		0.0
	.000250	.000140		0.0
	.000250	.000180		0.0
	.000250	.000225		0.0
	.000250	.000280		0.0
2	.000250	.000015		0.0
	.000250	.000020		0.0
	.000250	.000025		0.0
	.000250	.000035		0.0
	.000250	.000055		0.0
	.000250	.000075		0.0
	.000250	.000100		0.0
	.000250	.000130		0.0
	.000250	.000165		0.0
	.000250	.000220		0.0
3	.000250	.000000		0.0
	.000250	.000000		0.0
	.000250	.000005		0.0
	.000250	.000010		0.0

	.000250	.000015	0.0
	.000250	.000020	0.0
	.000250	.000030	0.0
	.000250	.000045	0.0
	.000250	.000065	0.0
	.000250	.000090	0.0
30	0		
	1	0.0	0.5
	1	.000250	.000025
		.000250	.000035
		.000250	.000045
		.000250	.000065
		.000250	.000085
		.000250	.000110
		.000250	.000140
		.000250	.000180
		.000250	.000225
		.000250	.000280
	2	.000250	.000015
		.000250	.000020
		.000250	.000025
		.000250	.000035
		.000250	.000055
		.000250	.000075
		.000250	.000100
		.000250	.000130
		.000250	.000165
		.000250	.000220
	3	.000250	.000000
		.000250	.000000
		.000250	.000005
		.000250	.000010
		.000250	.000015
		.000250	.000020
		.000250	.000030
		.000250	.000045
		.000250	.000065
		.000250	.000090

REPORT DOCUMENTATION PAGE

Form Approved
OMB No. 0704-0188

Public reporting burden for this collection of information is estimated to average 1 hour per response, including the time for reviewing instructions, searching existing data sources, gathering and maintaining the data needed, and completing and reviewing the collection of information. Send comments regarding this burden estimate or any other aspect of this collection of information, including suggestions for reducing this burden, to Washington Headquarters Services, Directorate for Information Operations and Reports, 1215 Jefferson Davis Highway, Suite 1204, Arlington, VA 22202-4302, and to the Office of Management and Budget, Paperwork Reduction Project (0704-0188), Washington, DC 20503.

1. AGENCY USE ONLY (Leave blank)		2. REPORT DATE August 1994	3. REPORT TYPE AND DATES COVERED Final report	
4. TITLE AND SUBTITLE Three-Dimensional Numerical Simulation of Mobile-Bed Hydrodynamics			5. FUNDING NUMBERS	
6. AUTHOR(S) Miodrag Spasojevic, Forrest M. Holly, Jr.				
7. PERFORMING ORGANIZATION NAME(S) AND ADDRESS(ES) Iowa Institute of Hydraulic Research The University of Iowa Iowa City, IA 52242			8. PERFORMING ORGANIZATION REPORT NUMBER IIHR Technical Report No. 367	
9. SPONSORING / MONITORING AGENCY NAME(S) AND ADDRESS(ES) U.S. Army Engineer District, New Orleans P.O. Box 60267, New Orleans, LA 70160-0267 U.S. Army Engineer Waterways Experiment Station 3909 Halls Ferry Road, Vicksburg, MS 39180-6199			10. SPONSORING / MONITORING AGENCY REPORT NUMBER Contract Report HL-94-2	
11. SUPPLEMENTARY NOTES Available from the National Technical Information Service, 5285 Port Royal Road, Springfield, VA 22161.				
12a. DISTRIBUTION / AVAILABILITY STATEMENT Approved for public release; distribution is unlimited.			12b. DISTRIBUTION CODE	
13. ABSTRACT (Maximum 200 words) This report describes the theoretical principles of three-dimensional sediment transport and bed evolution processes and numerical solution of the appropriate governing equations. It also includes technical documentation and user's instructions for the sediment-operations program module developed as an integral part of the CH3D-WES code. The generalized CH3D-WES code provides numerical simulation of three-dimensional unsteady water flow, sediment transport, and bed evolution in natural watercourses. Sediment mixtures are represented through a suitable and unlimited number of discrete size classes, any of which may be subject to either suspended load or bed load transport (or both) depending on prevailing local hydrodynamic conditions. The governing dimensionless sediment equations are SIGMA-stretched in the vertical direction and transformed into general (nonorthogonal) curvilinear coordinates in the other two directions. The generalized CH3D-WES code includes the feedback between the flow field and changes in bed elevation, bed-surface size distribution, and the density of the mixture containing water and suspended sediment. <p style="text-align: right;">(Continued)</p>				
14. SUBJECT TERMS See reverse.			15. NUMBER OF PAGES 163	
			16. PRICE CODE	
17. SECURITY CLASSIFICATION OF REPORT UNCLASSIFIED	18. SECURITY CLASSIFICATION OF THIS PAGE UNCLASSIFIED	19. SECURITY CLASSIFICATION OF ABSTRACT	20. LIMITATION OF ABSTRACT	

15. (Concluded).

This report contains detailed descriptions of the sediment-operations program module, memory and time requirements, and an input-data guide for the module.

The new mobile-bed numerical procedures are tested by applying the CH3D-WES code with its new sediment-operations program module to a natural prototype case: the Mississippi River at the Old River Control Structure complex.

14. (Concluded).

**Alluvial channels
Bed load transport
Numerical modeling**

**Sedimentation
Suspended sediment transport**